UNIVERSITY OF ALBERTA

Fluid Flow and Geochemistry of the Mississippian Aquifers in the Williston Basin, Canada-U.S.A.

by

Gavin Kenneth Soren Jensen

A thesis submitted to the Faculty of Graduate Studies and Research in partial fulfillment of the requirements for the degree of Master of Science.

Department of Earth and Atmospheric Sciences

Edmonton, Alberta

Fall, 2007

Your file Votre référence
ISBN: 978-0-494-33266-5
Our file Notre référence
ISBN: 978-0-494-33266-5

For Gwen Jensen, who scarified so much so that I could have the freedom to dream.

Abstract

Water samples collected from 114 producing wells in Mississippian aquifers across the Williston Basin. Results reveal large variations in geochemical and isotopic compositions basin wide. Results show: i) formation waters have distinct chemical fingerprints; ii) large variations in isotopic compositions indicate variable flow pathways within the aquifers; iii) portions of the aquifers host formation waters with a composition similar to original Mississippian seawater. Two separate flow regimes are present in the Mississippian aquifers. One flow regime originates from present-day meteoric water that evolved into a saline brine by halite dissolution and subsequent mixing with a residual brine. The other flow regime originates from a large scale fluid flux occurring at the end of the Cretaceous, that evolved into a saline brine via halite dissolution. These new geochemical data indicate the Mississippian flow system is not a simple regional groundwater flow system, rather highly-variable across the basin.

Acknowledgements

Ben Rostron has given me the opportunity to explore the possibilities of petroleum hydrogeology. I would like to thank him for his patience, understanding, and teaching throughout my master's degree as well as my undergraduate thesis project. I am grateful for the opportunities to attend numerous conferences in particular the 2006 AAPG International Conference in Perth, Australia. I am appreciative for his mentoring especially during the time while I was a research assistant. My time as a graduate student has provided me with the foundation to build a successful career in geosciences and I would like to thank Ben Rostron for his guidance.

I would like to thank the members of the committee Karlis Muehlenbachs, John Duke, and Carl Mendoza, for their time in reviewing my thesis. I am thankful for the memories of field sampling with John Duke and Ben Rostron. I would like to thank John Duke for his tireless efforts to educate me in the field of analytical chemistry. I am thankful to Carl Mendoza for his availability to impromptu questions. As well as increasing my knowledge in hydrogeology by means of instructing the most challenging classes I endured during my education.

Sharing many courses, conferences and discussions with the members of the hydro lab has made my master's project a memorable experience. In particular I would like to express my gratitude to Daniele Palombi for his contagious enthusiasm towards geology and for always having time for "just one quick question."

Other members of the hydro group who always had time for questions and discussions include: Daniel Khan, Joe Riddel, and Brian Smerdon. I would like to thank

Brian Smerdon for his commitment to remembering and respecting the past of hydrogeology.

I would like to thank the following companies who granted permission to sample their wells. The data contained within this thesis would not exist without the cooperation of the operators of the following companies: Duce Oil, Arc Energy Trust, Zargon Energy, Acclaim Energy, Athena Oil and Gas, Condor Petroleum, Nance Petroleum, Eagle Operating, Northrock Energy, Prospective Oil and Gas, Helis Oil, Journey Operating, Simoil, Westport Oil and Gas, Citation Oil and Gas, Wascana Energy, Ballantyne Oil, Anadarko, Nexen, Headington Oil and Husky Oil.

Friends and family that have supported me throughout my educational career include:

Jim Struthers and Chéri Blain have always had an open door for unwinding, laundry and a free home cooked dinner whenever it was needed.

My brother, Derek Jensen has always encouraged my continuing education, as well as to have a bottle of wine whenever it was required.

My mother, Gwen Jensen has devoted her life to raising Derek and I to the best of her ability by sacrificing so much of her life so that Derek and I could have the privilege to pursue our dreams. We are both wholeheartedly grateful for all of the opportunities we have had throughout our lives.

My wife, Lindsey Jensen for her support when I needed it and a push when I required it. As well as for her boundless sense of adventure in life, and also for her ability to always put a smile on face and to make me laugh.

Table of Contents

List of Figures

Chapter 1 Introduction

1.1. Introduction

For decades scientists have investigated the composition and distribution of subsurface formation waters in sedimentary basins (Chebotarev, 1955; Clayton et al., 1966; Collins, 1975; Tóth, 1984; Hanor 1994; Lowenstein et al., 2003). Composition of formation waters, in particular brines, in sedimentary basins are of important scientific interest because of the information fluid compositions can potentially provide on the geochemical, hydrological, thermal and tectonic evolution of the earth's crust (Hanor, 1988).

Questions regarding the occurrence, distribution, and evolution of basinal brines in sedimentary basins has been studied for decades e.g. Clayton et al. (1966), Hanor (1994), Lowenstein et al. (2003) and many others. However, many questions remain especially at the large (basin) scale: 1) what are the source(s) of the basinal fluids? (meteoric versus seawater); 2) what geochemical reactions influence the composition of the major and minor elements? 3) how has hydrogeology (driving forces, rates and directions of flow) influenced the hydrochemistry of the basin (Hanor, 1994)?

Formation waters record the cumulative effects of the events and processes that have occurred throughout a basin's history. Thus, mapping present day hydrochemistry can tell a great deal about a basin's history. For example:

i) Conservative hydrochemical tracers present can be used to elucidate the origin and evolution of basinal brines (halite dissolution versus evaporite seawater) (Carpenter, 1978; MacCaffrey et al., 1987; Walter et al., 1990).

ii) Water types and hydrochemical patterns provide qualitative information and support for understanding the hydrogeology of a basin (i.e. rates, direction, and flow regimes) (Tóth, 1984).

iii) Formation water compositions can provide an insight into numerous applied problems with the hydrocarbon industry, including aspects of exploration and production (Hanor, 1994; Rostron et al., 1998).

One example of a geochemically well-studied basin is the Williston Basin (Canada-USA). The Williston Basin represents one of the largest basin-scale flow systems in the world (Hannon, 1987) and is an ideal setting (Downey et al., 1987; Bachu and Hitchon, 1996; Gerhard et al., 1982) to use hydrochemistry to unravel the cumulative diagenetic and hydraulic processes that have taken place during the evolution of a basin.

1.2. Motivation

This study deals with formation fluids of Mississippian-aged strata in the Williston Basin. Mississippian-aged strata contain 75% or more of the proven oil reserves in the Williston Basin (Kent, 1984), with cumulative production of 1,500+ MMBO, since 1951 (Kent, 1987). A large body of previous research has demonstrated a link between hydrogeology and petroleum migration and accumulation in basins (e.g. Hubbert, 1953; Tóth, 1980; Downey, 1984; Bachu and Hitchon, 1996). Thus, hydrogeology is expected to have an influence on petroleum migration and accumulation in this basin.

There has not been a systematic study of the formation waters in the Williston Basin investigating the main oil producing zone (Mississippian) on a basin scale. Problems with

Mississippian aquifer correlation across state / provincial boundaries as well an international boundary (Canada-U.S.A.), has resulted in inconsistent geologic nomenclature within the Mississippian strata in the Williston Basin. Difficulties with lateral geologic nomenclature and separating the Mississippian units, has resulted in previous hydrogeological studies of Mississippian strata in the Williston Basin grouping all Mississippian strata into a single aquifer, the Madison (Downey, 1984; Gerhard et al., 1982; Carlson and Anderson, 1965; LeFever, 1998; Bachu and Hitchon, 1996).

There is new research that indicates the Mississippian aquifers need to be separated:

1. Recently, detailed consistent cross-border geological and hydrogeological mapping (Cambrian-Cretaceous) was conducted for the IEA GHG Weyburn CO_2 monitoring and storage project (Kent et al., 2004), encompassing portions of Saskatchewan, North Dakota and Montana.
2. Kent et al., (2004) mapped individual Mississippian members in an area spanning the Canada-US border.
3. Results (Khan, 2006) show that the individual Mississippian units are hydrochemically distinct from one another.
4. Mapping for the Weyburn CO_2 project provided a consistent geologic framework of the Mississippian units facilitating further detailed hydrochemical study of the individual aquifers (Kent et al., 2004).

1.3. Study Objectives

The primary objective of this thesis is to understand the major ion and stable isotope geochemistry of the formation waters present in specific Mississippian aquifers in the

centre of the Williston Basin. Three aquifers representing the main hydrocarbon units in the basin were chosen; the Midale Beds (Charles Formation), the overlying Ratcliffe Beds (Charles Formation), and underlying Frobisher Beds (Mission Canyon).

This project was conducted in four stages: i) geologic mapping of the three individual Mississippian aquifers in the study area; ii) using the newly developed hydrostratigraphic framework, to assign producing wells to aquifers; and iii) acquiring stable isotopic compositions and hydrochemical data of the formation waters in the individual aquifers; iv) analysis of the results in the overall context of the Williston Basin hydrochemistry and hydrogeology.

This thesis consists of six chapters. Chapter Two provides the geological and hydrochemical background for the Williston Basin. Chapter Three provides methodology to the geological mapping, sample collection and geochemical analyses. Chapter Four contains hydrochemical results from the 128 wells were sampled for this study. Chapter Five provides interpretations and implications of the results. Chapter Six provides the conclusions of the study.

Chapter 2 The Williston Basin

2.1. Williston Basin

The study area is situated within the Williston Basin, a 520,000 km^2 subcircular intracratonic sedimentary basin covering parts of North Dakota, South Dakota, Montana, Saskatchewan, and Manitoba (Figure 2.1). The Williston Basin is centred in northwestern North Dakota and straddles the Canada-U.S.A. border. Spatially, the basin ranges from approximately 98.5^0 W to 108.5^0 W longitude and 45^0 N to 51.5^0 N latitude (Brown and Brown, 1987).

The basin is bounded on the west and southwest by regions of continental crust, and Tertiary-aged uplifts. To the north and east it is bounded by an erosional edge with the Precambrian Shield (Sloss, 1987). To the northwest it is connected to the Alberta Basin by the Bow Island arch and Meadow Lake escarpments (Mossop and Shetsen, 1994).

Present day structural features in the basin are a result of the Laramide Orogeny (Gerhard et al., 1987). Major structural features that surround the basin include the Black Hills uplift to the southwest, the Transcontinental arch to the south and southeast, and the Central Montana uplift, and Sweetgrass Arch to the west (Figure 2.1).

2.1.1. Regional Geology

The geology of the Williston Basin has been extensively studied, e.g. Carlson and Anderson (1965), Peterson and MacCary, (1987), Mossop and Shetsen, (1994), and many others. A summary of the geology, in relation to hydrochemistry, will be presented here.

The Williston Basin contains sediments of Phanerozoic age and attains a maximum thickness of approximately 4800 metres (Figure 2.2) at the basin centre in the locality of

104^0 W longitude, 47.7^0 N latitude (Figure 2.1) (Gerhard et al., 1982). Paleozoic strata consist predominately of carbonate and evaporitic sediments while the Mesozoic strata constitute a section of siliclastic rocks (Figure 2.3). The boundary separating the Paleozoic units from the Mesozoic units has been placed at the top of the Bakken Formation (Carlson, 1967).

2.1.2. Regional Hydrogeology

The Williston Basin is one of the largest and well-studied aquifer systems in North America (Hannon, 1987). The current flow model for the Williston Basin proposes that formation waters migrate from the south-southwest to north-northeast across the basin (Downey, 1984; Bachu and Hitchon, 1996). The main driving force is a topographic elevation difference of approximately 1000 m across the basin, resulting from the Laramide Orogeny (Bachu and Hitchon, 1996). Fresh formation waters are thought to recharge at the southwestern uplifts of the basin and then are driven downwards towards the basin centre, as indicated by fresh formation water in that portion of the basin (Downey, 1984). Subsequently, the fresher infiltrating waters are thought to migrate to the north, northeast. Finally, formation waters discharge at outcrops and subcrops in the northern basin flank, along the unconformity with the Canadian Shield (Downey et al., 1987).

2.1.3. Regional Hydrochemistry

The origin, evolution, and migration of formation waters in the Williston Basin has been the focus of recent research. Previous hydrochemical research in the Williston Basin has concentrated on the Palaeozoic strata (i.e. Rostron et al., 1998; Benn and Rostron, 1998; Iampen, 2003).

A primary source of data for hydrochemical studies in the Williston Basin has been DST data, in some cases supplemented with a small number of wellhead samples have been used. Two interpretations have developed on the origin of brine salinity in the Williston Basin; 1) brine salinity is derived from halite dissolution and evaporative concentration (Kreis et al., 1991; Bernatsky, 1998; Lefever, 1998; Iampen, 2003). 2) researchers interpreting salinity derived by only halite dissolution (Wittrup and Kyser, 1990; Chipley and Kyser, 1991; Busby et al., 1995; Bachu and Hitchon, 1996).

Only two studies (Benn and Rostron, 1998; and Iampen, 2003) have encompassed the entire basin and involved the majority of major and minor ions. Both of these studies (Benn and Rostron, 1998; and Iampen, 2003), investigated pre-Mississippian aquifers, one using DST data (Benn and Rostron, 1998), the other (Iampen, 2003) involved sampling wellheads to obtain chemistry data. With the exception of these two studies all previous hydrogeochemical research has been restricted by political boundaries and focused on present-day flow systems in parcels of the Williston Basin.

Results from the aforementioned studies show three end-member water types present in the Williston Basin. The first water type found is a brackish water with a total dissolved solids (TDS) of < 50,000 mg/L predominantly Ca-Mg-SO_4 in composition located in northeastern Montana and southwestern Saskatchewan. The second end-

member is a Na-Cl type ranging from 100,000-300,000 mg/L TDS is found in northern North Dakota and south eastern Saskatchewan. The third type is a Ca-Na-Cl brine with Ca as the dominant cation having a TDS > 300,000 mg/L, located near the basin center. Only one study (Iampen, 2003), has been able to utilize high quality reproducible Br data (Duke and Rostron, in press), which elucidates the origin of formation waters. In turn, determining that a residual evaporated seawater brine comprised of Ca-Na-Cl waters was present at the basin centre, as well as defining mixing trends between the three end-member brines via Na-Cl-Br systematics (Iampen, 2003).

There has not been a basin wide study, which utilizes oxygen, and hydrogen isotopes and halogen systematics involving the Mississippian strata of the Williston Basin.

2.2. Mississippian Hydrogeology and Hydrochemistry

Problems with Mississippian aquifer correlations across state / provincial boundaries as well as an international boundary (Canada-U.S.A.), has resulted in inconsistent geologic nomenclature within the Mississippian strata of the Williston Basin. This inconsistency with geologic lateral equivalents has resulted in previous geological studies of Mississippian strata in the Williston Basin grouping all Mississippian strata into a single aquifer, the Madison (Figure 2.4) (Carlson and Anderson, 1965; Gerhard et al., 1982; Downey et al., 1987; Bachu and Hitchon, 1996; LeFever, 1998). Results from Khan (2006) indicate that the seven individual Mississippian units (Figure 2.4), that were hydraulically subdivided are hydrochemically distinct from one another, thereby justifying the Mississippian units should be mapped as separate units.

The current proposed flow model for the Mississippian aquifers suggests that formation waters migrate from the south-southwest to north-northeast across the basin (Downey, 1984; Bachu and Hitchon, 1996) (Figure 2.5). The formation waters are thought to migrate to the north and south around the TDS > 250,000 mg/L brine, present at the basin centre (Downey et al., 1987; Lefever, 1998). Then finally continue onto the northeast basin flank where the Mississippian succession subcrops.

2.3. Study Area

For this thesis the study area was defined by 47^0N to 50^0N latitude, and from 100.5^0W to 106.5^0W longitude (Figure 2.6). The study area was chosen to encompass the extent of currently producing Mississippian wells in the Williston Basin.

2.3.1. Mississippian Geology of the Study

Mississippian strata in the Williston Basin are generally composed of carbonate rocks that are interbedded with evaporite and anhydrite layers (Kent, 1999). There are repeated packages of alternating carbonates and anhydrites throughout most of the Mississippian section within the Williston Basin. This succession is considered to have been deposited in a marine environment reflecting a shallow ramp depositional model under conditions of limited accommodation space (Kent, 1984; Kent et al., 2004) Mississippian strata attain its maximum thickness at approximately 850 metres (Downey, 1984), at the basin centre and reach its minimum thickness around the basin margin due to erosional truncation. The division separating the pre-Mississippian and Mississippian strata has been placed at the top of the Bakken Formation (Carlson, 1967) (Figure 2.3).

Mississippian aquifers, examined in this study belong to the Madison Group which includes (in ascending stratigraphic order), Frobisher Beds (Mission Canyon Formation), Midale Beds (Charles Formation), and the Ratcliffe Beds (Charles Formation) (Figure 2.3).

The lowermost unit examined in the study were the Frobisher Beds which consist of thick accumulations of coated grainstones, packstones, and wackepackstones interbedded with lime mudstones (Kent et al., 2004). The Frobisher Beds contain abundant occurrence of skeletal fragments mainly calcareous algae, other particles include fragments of brachiopod and ostracod valves, rugose horn coral thecae, crinoid columnals, ooids, peloids and pisolites. Carbonate rocks of the Frobisher Beds are in contact with the overlying Frobisher Evaporite, and are disconformable with the overlying Midale Beds (Kent 2001; Kent and Nimegeers, 2002; Nimegeers and Qing, 2002).

Next in the section are the Midale Beds which are comprised of alternating wackestone, wackepackstone and packstone, and grainstones (Kent, 1999). Carbonate rocks of the lower most Midale Beds lie on an exposure surface signifying the top of the Frobisher Evaporite. Rocks of the Midale Beds contain non-skeletal allochems, ooids, calcareous algae, brachiopod and ostracod-valve fragments and crinoid columnals (Kent et al., 2004).

Above that are the Ratcliffe Beds which are conformably deposited on the underlying Midale Evaporite, or on the Midale Beds when the evaporite layer is absent (Kent, 1984). The Ratcliffe Beds have a mixed assemblage of rock types ranging from coated wackestones and lime mudstones to packstones (Kent et al., 2004). An important marker

bed is the Green Point Anhydrite which occurs 40 to 60 m above the top of the Ratcliffe Beds (Kent et al., 2004), this unit is a regionally extensive anhydrite layer. The overlying Poplar Beds are the uppermost Mississippian strata in the basin. The sub-Mesozoic unconformity overlies the Poplar Beds.

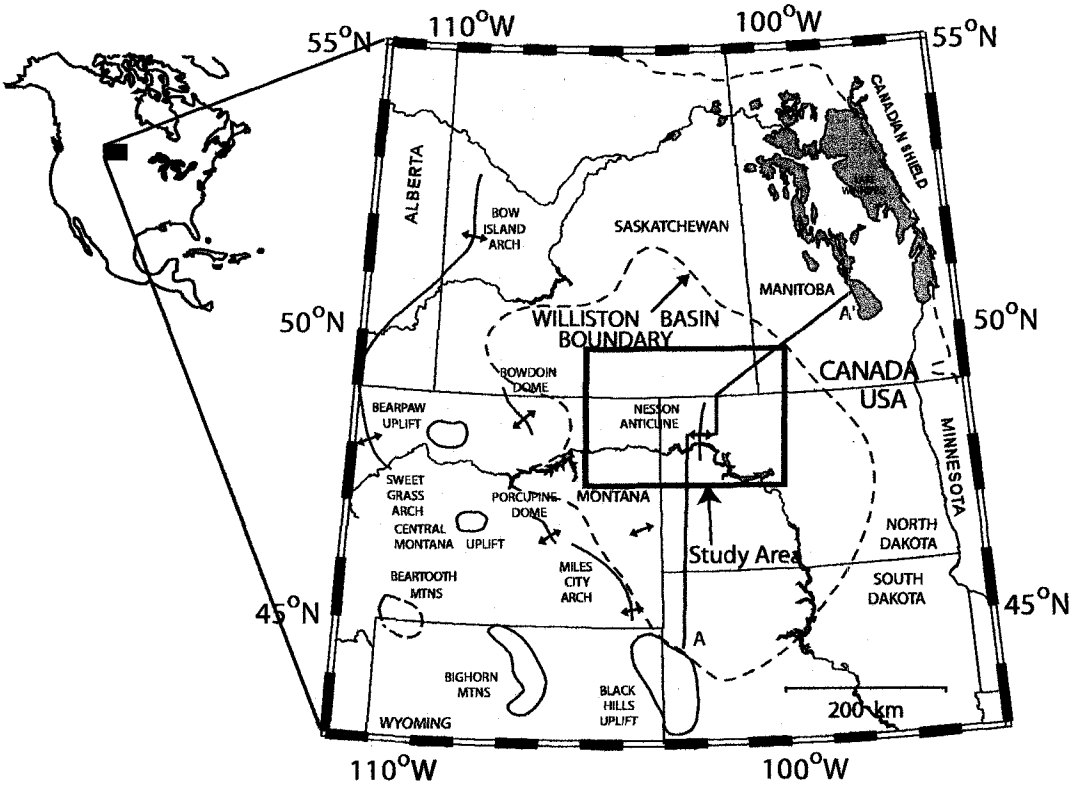

Figure 2.1. Location map of the Williston Basin outlining its major structural features. Basin boundary after Laird, 1952, (modified after Benn and Rostron, 1998).

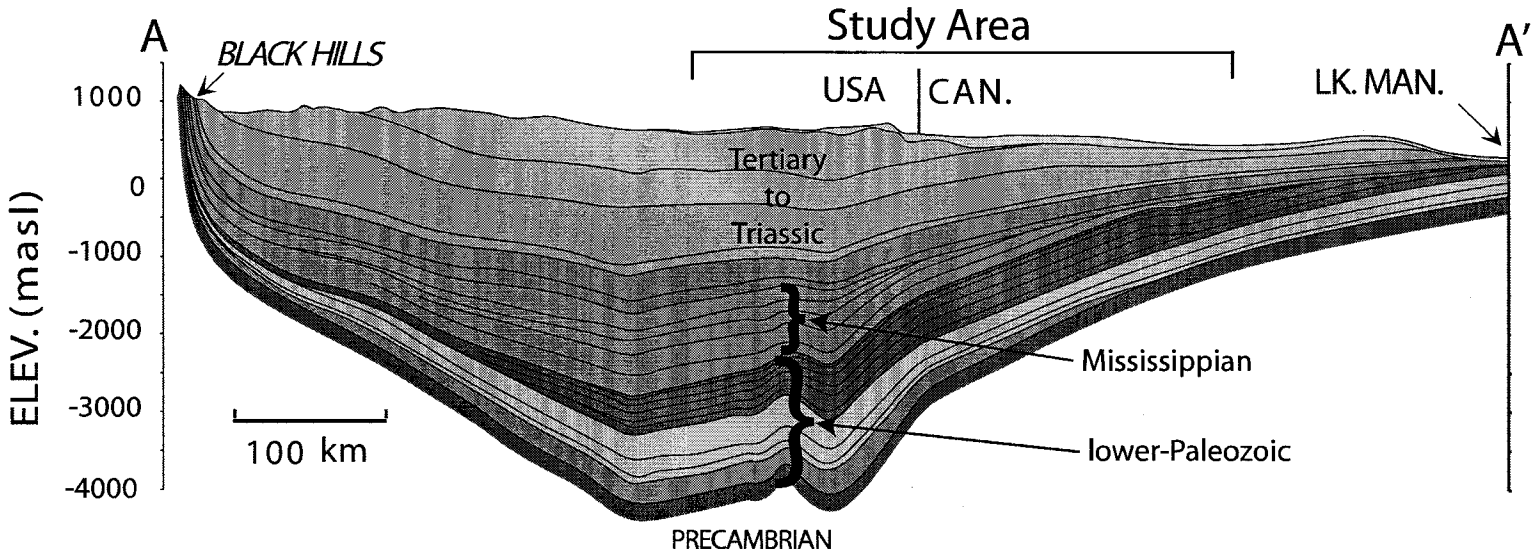

Figure 2.2. Schematic cross-section from A-A'. Modified after Benn and Rostron, 1997. Location of cross-section shown on Figure 2.1

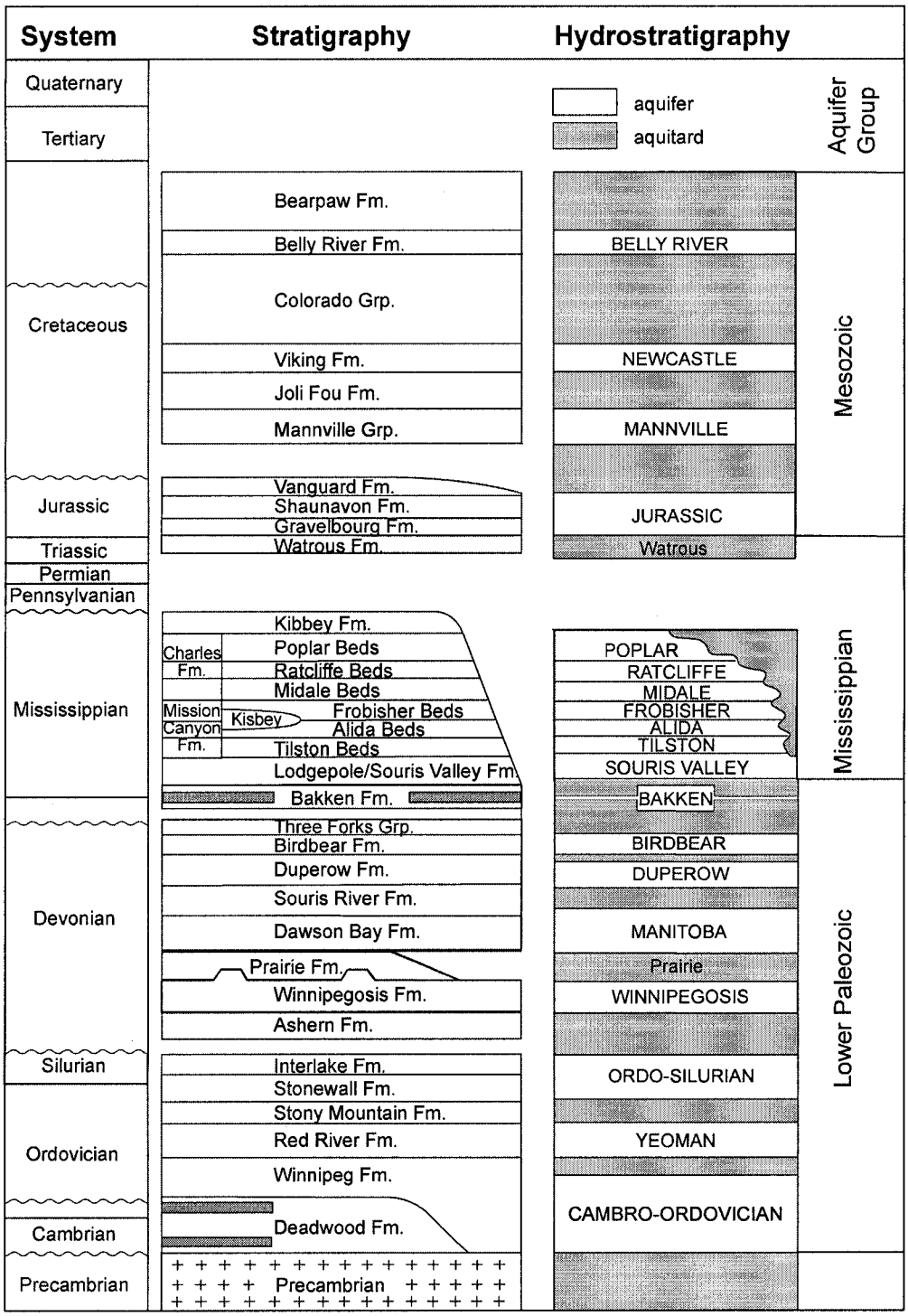

Figure 2.3. Stratigraphic and hydrostratigraphic units of the Williston Basin. Modified from Kent et al., 2004

<table>
<tr><th>USA</th><th>Canada</th><th>Previous Work*</th><th>This study</th></tr>
<tr><td>Ratcliffe Beds</td><td>Ratcliffe Beds</td><td rowspan="12">Madison</td><td rowspan="3">Ratcliffe Beds</td></tr>
<tr><td>Midale Evaporite</td><td>Midale Evaporite</td></tr>
<tr><td>Midale Beds</td><td>Midale Beds</td><td rowspan="3">Midale Beds</td></tr>
<tr><td>Nesson Limestone</td><td rowspan="2">Frobisher Evaporite</td></tr>
<tr><td>Frobisher Evaporite</td></tr>
<tr><td>State “A” Marker</td><td></td><td rowspan="4">Frobisher Beds</td></tr>
<tr><td>Bluell Beds</td><td rowspan="3">Frobisher Beds</td></tr>
<tr><td>Sherwood Beds</td></tr>
<tr><td>Mohall Beds</td><td rowspan="2">Alida Beds</td></tr>
<tr><td>Glenburn Beds</td><td>Alida Beds</td></tr>
</table>

Figure 2.4. Mississippian stratigraphic equivalent problem across the Canada-USA border.
*(Downey, 1984; Bachu and Hitchon, 1996).

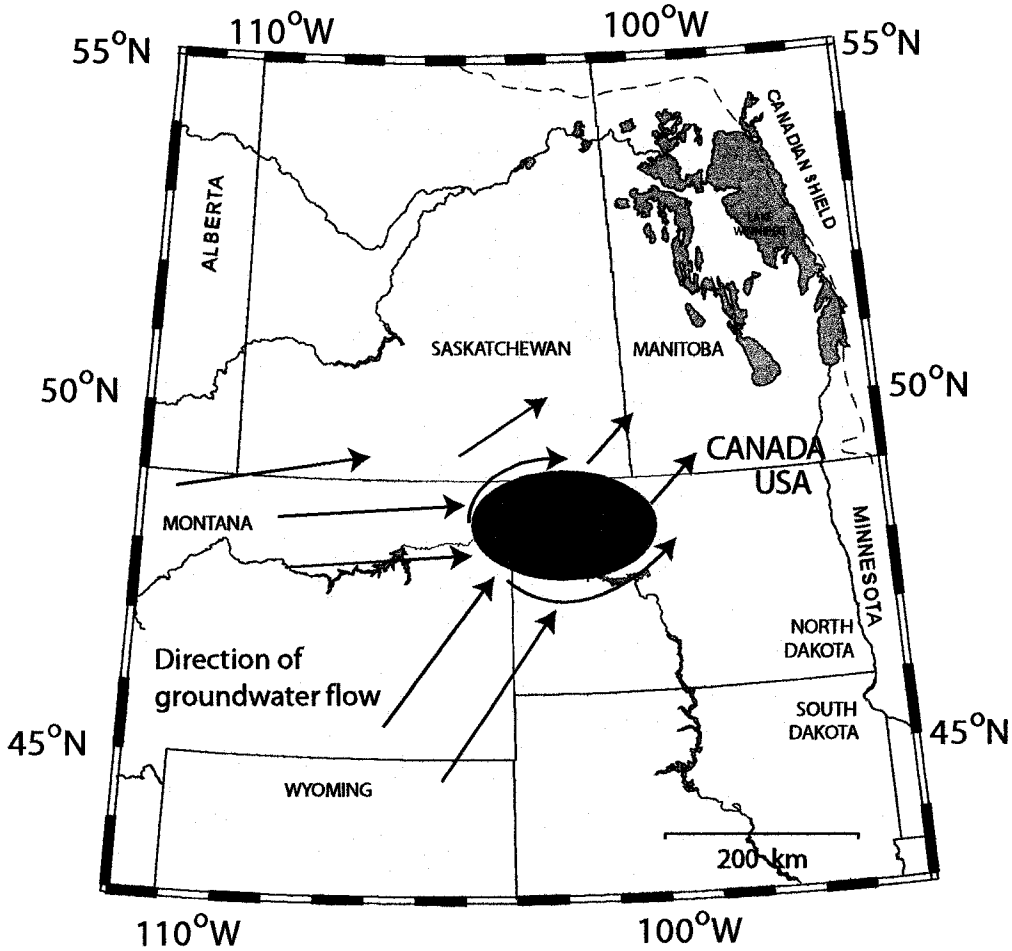

Figure 2.5. Proposed flow model for the Mississippian aquifers in the Williston Basin. Modified from Downey, 1984; Lefever, 1998. Red area indicates TDS > 100, 000 mg/L.

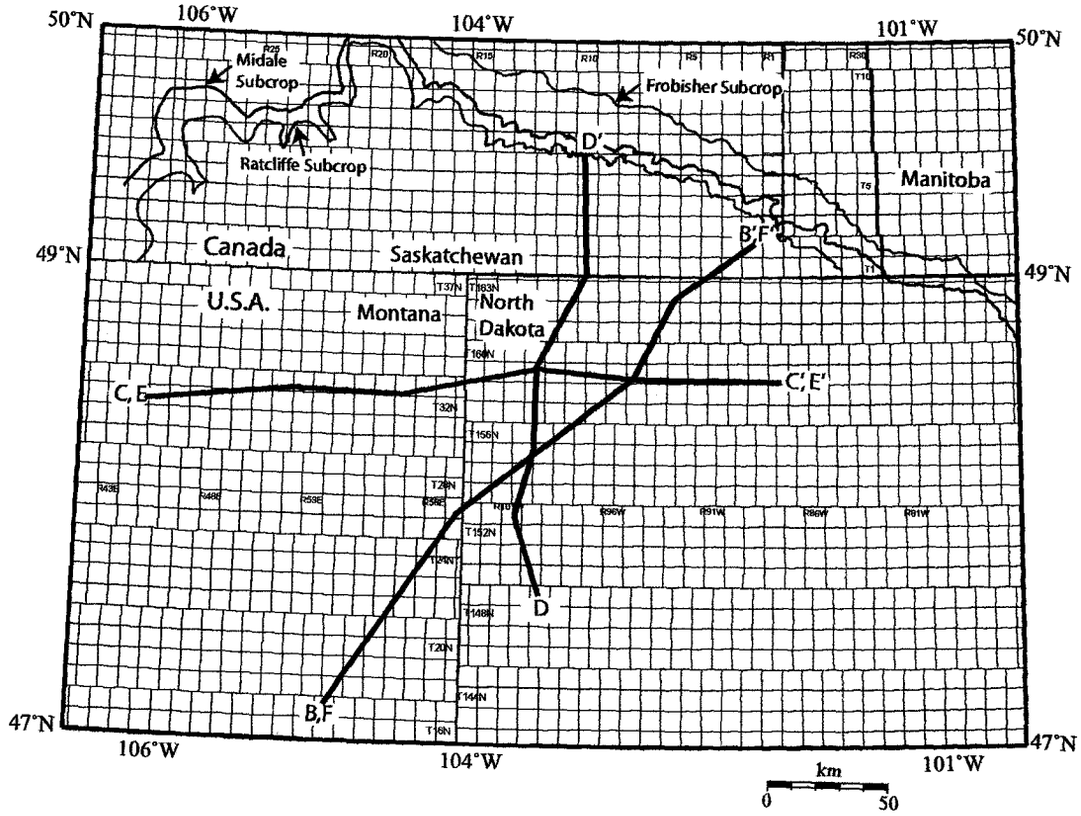

Figure 2.6. Study area within the Williston Basin. Mississippian subcrops for the three aquifers examined in this study are labelled. Lines of section are for structural and stratigraphic cross-sections.

Chapter 3 Methods

3.1. Methodology

The four stages of this thesis include: i) geologic mapping of the three individual Mississippian aquifers in the study area; ii) using the new hydrostratigraphic framework, to assign producing wells to aquifers; and iii) acquiring stable isotopic compositions and hydrochemical data of the formation waters in the individual aquifers; iv) analysis of the results in the overall context of the Williston Basin hydrochemistry and hydrogeology. The primary objective was to understand the geochemistry of the formation waters present in select Mississippian aquifers in the Williston Basin however, the geological mapping had to be completed before sampling could commence. Results of the geological mapping will be presented in Chapter Four.

Using the newly developed geologic framework as discussed in Chapter Two, data for this thesis project were collected during July-August in 2003, 2004 and 2005 (Figure 4.1), and were supplemented with data that were collected from 1999 to 2002 as part of the Williston Basin brine sampling project (Rostron et al., 1999). The procedure for selecting wells, collecting samples and chemical analysis of those samples is described below.

3.2. Sampling (1) - Well Selection

Obtaining the hydrochemistry of formation waters was achieved through collection of pristine samples from currently producing wells. First, currently producing wells in each hydrostratigraphic unit were identified. A list of producing wells was created using standard petroleum on-line databases: Accumap, and Geo webworks, (Canada); North

Dakota Industrial Commission (www.ndic.com) and Montana Board of Oil and Gas (www.bogc.dnrc.state.mt.us) for North Dakota and Montana, respectively.

Second, the precise production interval for each well was determined using the newly developed stratigraphic framework for the Mississippian (discussed in Chapter 4). This step enabled the creation of three lists of producing wells in the Frobisher, Midale, and Ratcliffe aquifers across the study area.

Third, for each aquifer poor sampling candidates were removed from the list. Wells were deemed unsuitable if there was any enhanced recovery or other field operations taking place that would affect the samples (i.e., CO_2 flooding, water flooding, co-mingled production, water disposal, etc.). Wells were also deemed unsuitable if they had a very low water cut (i.e. <30%), unless the well was a "key" well located spatially in a priority area (i.e., to extend areal coverage). Every attempt was made to sample wells in triplets (three samples, same aquifer, and close proximity) to increase confidence in the dataset.

Fourth and finally, the well owner/operator was contacted to request permission to obtain a well-head sample (only one company refused) and confirm producing formation. In addition, at that time the operators were asked to confirm that there was no water-flood present and fresh water "wash" treatment of well bore was not being used to reduce salt build-up.

3.3. Sampling (2) - Sampling Technique

In the field, each well was sampled based on the protocol from Lico et al., 1982, modified for this study:

1. If well production chemicals (e.g. demulsifier or corrosion inhibitor, etc.) were being used on the well they were turned off for periods of 15 minutes to 60 minutes prior to sampling. Control samples were taken to determine if production chemicals affected the produced formation waters hydrochemistry and none were noted. Samples (oil and water) were taken directly from the well-head into 8 or 12 L high-density, polyethylene jugs. Wells with lower water cuts were sampled with 12 L jugs to compensate for the lower water cut.
2. Samples were allowed to stand so that the oil and water could gravity separate inside the collection container. This took 5 minutes to 2 days, however most of the samples were separated, filtered and bottled within 2 hours of collection.
3. Water samples were pre-filtered to remove visible oil sheen by pouring the sample through a funnel packed with glass wool. Usually 2-4 passes were required to remove all visible oil.
4. Water samples were filtered through disposable 0.45 μm polyethylsulfane (Durapore brand) filters. This filter pore size was used to remove any colloids/organics that were present. Filter sizes were either 90 or 142 mm in diameter and were attached to hand-operated vacuum pump and machine run pressure pump, respectively. Suction rates of 30-50 cm Hg were maintained.
5. Filtered samples were then split for analysis:

A) Splits for isotopic analysis were taken in non-coated, non-additive Becton-Dickinson brand 10mL vacutainers from the first 500mL filtered.

B) If sufficient sample was available (i.e., greater than 1000 mL of filtered sample) then field pH and temperature were determined to a 10^{-2} and 10^{-1} precision. A temperature

corrected VWR Scientific Model 2000 portable pH meter with an Ag/Cl gel-filled electrode was used to determine pH to a 10^{-2} precision. Density was measured to a 10^{-4} precision using Fisher brand, 325 mm specific gravity hydrometers.

C) Samples for anion determination were untreated, tightly sealed, and stored in a dark space for analysis.

D) The samples for cation analysis were acidified to a pH < 1, with triple distilled 2.8N HNO_3 acid which was added in the amount of 1% of the cation spilt volume (e.g., using 1 mL of acid per 100 mL of sample).

3.4. Sampling (3) - Chemical Analyses

Specific element analysis was achieved by numerous methods, due to the high ionic strength of the formation waters. Major ions, trace metals and alkalinity were analyzed using Inductively Coupled Plasma Optical Emission Spectroscopy (ICP-OES), Inductively Coupled Plasma Mass Spectroscopy (ICP-MS), and titration techniques at a commercial lab (Norwest Laboratories, Edmonton, Alberta). Reproducibility issues using the ICP-OES technique for the elements Na, and Br in highly saline oilfield brines necessitated the use of a recently developed analytical technique, Epithermal Neutron Activation Analysis (ENAA) (Duke and Rostron, in press). For all analyses duplicate samples were run to ensure quality control in the analyses (1 duplicate for every 10 samples).

3.4.1. Inductively Coupled Plasma Mass Spectroscopy

Cations, particularly trace metals (Ca, Mg, K, Fe, Mn, Li, Be, Ba, Sr, Al, Co, Cr, As, Si, Bi, Cu, Zn, Ni, Tl, Se, Pb, Cd, Mo, Ag, Ti, U, V) were measured using an ICP-emission spectrometer using APHA 3120 B standards. Samples had to be diluted, to detect elements in samples with such varying concentration. Dilution factors ranged from 100 to 500 times. An aliquot of the diluted sample was aspirated, neubulized and transferred into the plasma through an injector tube for concentration analysis. Analytical uncertainties reported by the lab were at the parts per million (ppm) to parts per billion (ppb) level (depending on sensitivity and dilution).

3.4.2. Epithermal Neutron Activation Analysis

A recently developed analytical technique, (ENAA) (Duke and Rostron, in press) for the analysis of highly saline brines was used to determine Cl, Na, and Br concentrations. This method has the advantage that it does not require dilution of the sample, thus eliminating reproducibility problems associated with ICP-OES. Samples were irradiated and analyzed at the SLOWPOKE nuclear reactor, University of Alberta. Released gamma rays at specific frequencies were used to identify each element. Intensity of the gamma rays detected was used to determine the concentration of each element.

For the analysis, an aliquot of brine measuring 250 μL is pipetted into a polyethylene micro-centrifuge tube. Tubes are individually placed in the central cavity of a B_4C shield and irradiated at a nominal thermal neutron flux of 1×10^{11} n cm^{-2} s^{-1} for 360 seconds (6 mins). After irradiation, samples are allowed to decay for 10-15 minutes, and removed from the B_4C shield. Samples were then placed in front of a gamma-ray detector at a

sample-detector distance of 5 mm. After the timed decay period (10-15 min) samples were counted for 360 seconds (6 mins) using a 41% hyperpure Ge detector inside a 10 cm lead cave. Analytical uncertainty for the elements were at the parts per million (ppm) to parts per billion (ppb) level.

3.4.3. Continuous Flow Mass Spectroscopy

Oxygen and hydrogen stable isotopes were determined at the Stable Isotope Lab, University of Saskatchewan, using a continuous flow (CF) Delta plus XL isotope ratio mass spectrometer. Isotopic values were reported in delta (δ) notation as $^{18}O/^{16}O$ and D/H relative to Vienna Standard Mean Ocean Water (VSMOW). Isotopic measurements have an uncertainty of ± 3‰ and ± 0.3‰ for δD and $\delta^{18}O$, respectively.

Chapter 4 Results

4.1. Mississippian Geological Mapping

The starting point for the geological mapping conducted in this project was the geologic framework established for the IEA GHG Weyburn CO_2 monitoring and storage project (Kent et al., 2004). Using that detailed geologic mapping of the Mississippian strata, this project was able to extend their mapping further south in Montana and North Dakota. Geologic mapping from Kent et al. (2004), enabled a regional scale analysis of the Mississippian strata in the Williston Basin, with consistent geologic picks (Figure 4.1).

Five Mississippian stratigraphic tops were picked for this study. In ascending order they are: 1) Base of the Frobisher Beds (i.e., top of the Kisbey/Alida Beds), 2) Top of the Frobisher Beds, 3) Top of the Midale Beds, 4) Top of the Ratcliffe Beds, and 5) Top of the Green Point Anhydrite. These tops were consistently picked on approximately 500 geophysical logs from across the basin. Formation tops were picked by a combination of gamma ray and density porosity logs. The reference geophysical logs for a borehole from NESW-36-159N-100W (Figure 4.1) along cross section A-A', was selected to represent typical Charles and Mission Canyon Formations in the Williston Basin (Figure 4.1).

The Frobisher Beds were picked as follows: the base of the Frobisher Beds is marked by a response on a gamma ray log of approximately 60 API (2540 m on Figure 4.1) that precedes three sharp localized (vertically 5 m) increases in porosity ("pulses") to the left on the density/ neutron logs. This "pulse" indicates an increase in porosity marking the begining of the Frobisher Beds and the top of the Alida Beds. Above the base of the Frobisher Beds, the gamma ray responses throughout the Frobisher Beds vary from 10-50

API: in the lower portion of the Frobisher Beds (2540-2515 m on Figure 4.1) the gamma ray remains relatively constant from 30-50 API. In contrast, gamma responses of 10-30 API (2515-2500 m on Figure 4.1) mark the upper portion of the Frobisher Beds. The top of the Frobisher Beds, in most wells, is identified by the Frobisher Evaporite (at 2500 m on Figure 4.1), which is marked by a typical evaporite signature of low gamma (10 API). When the Frobisher Evaporite was not present, a gamma response of 50 API (not shown) was observed.

Picking the Midale Beds was slightly more complicated than the underlying Frobisher Beds as traditionally the Midale Beds have been divided into the lower ("Vuggy") and upper ("Marly") based on geophysical logs and petrophysical properties (Fuzesy, 1983). Recently, it has become evident that these descriptive terms are limited to the Midale subcrop trend of producing oil pools in Saskatchewan (Kent et al., 2004). Thus the formation names upper Midale and lower Midale have recently been substituted for "Marly" and "Vuggy", respectively (Kent et al., 2004). In the type log (Figure 4.1), the lower Midale (2500-2495 m on Figure 4.1) is characterized by a clean gamma response of 10 API and accompanied with a porosity "pulse". A gamma response of 20-40 API (2495 m on Figure 4.1) marks the upper Midale Beds. Above that the gamma response of the upper Midale (2495-2480 m on Figure 4.1) grades from 10 API to 40 API, with numerous porosity "pulses" (2488 m on Figure 4.1). A change in lithology to the Midale Evaporite defines the top of the Midale Beds (2480 m on Figure 4.1). In some wells the Midale Evaporite was not present. When this occurred a gamma log signature of 10 API, over 2-3 metres was observed to mark the top of the Midale Beds (not shown).

The final unit in the section is the Ratcliffe Beds that are relatively easy to distinguish due a distinct marker, the Oungre Evaporite (2430 m on Figure 4.1). Throughout the Ratcliffe Beds, the gamma ray activity ranges from 10-40 API (2480-2420 m on Figure 4.1). The Ratcliffe top is marked by a 10 API pulse in the gamma log for 5 metres (2420 m on Figure 4.1).

In addition, the Green Point Anhydrite was picked to assist with the mapping and provide a regional datum. The Green Point Anhydrite is typically 5-8m thick (2380m on Figure 4.1) with a distinctive gamma-ray (10 API). All stratigraphic cross sections used the Green Point Anhydrite as the datum due to its wide areal extent and time equivalent nature.

4.2. Results of Mississippian Geologic Mapping

The 500 wells mapped here, in combination with the geologic mapping from the IEA Weyburn CO_2 project, provides a basin wide geological framework of the Mississippian aquifers. Isopach and structural elevation maps were produced for the Frobisher, Midale and Ratcliffe Beds (Figures 4.2.-4.7).

Formation thicknesses range from 0 m to over 90 m for each of the three aquifers mapped (Figures 4.2, 4.3, 4.4). All three formations are thickest in the basin centre and thin towards the north-northeast associated with their subcrop edge (Figures 4.2, 4.3, 4.4). Localized variations are present in each aquifer due to deposition and erosion (Kent, 1984; Kent, 1987; Kent et al., 2004).

Subsea elevations were calculated for each pick by subtracting the measured depth of the formation top from the Kelly Bushing (KB) elevation. Structure elevations range

from -600 to -2300 m (Figures 4.5, 4.6, 4.7). Structure elevation maps also display similar trends for each formation. These trends reflect the overall structure of a bowl shaped basin (Sloss, 1987) with the deepest subsea elevations correlating with the basin center (Figures 4.5, 4.6, 4.7). Major structural features (i.e., Nesson Anticline, Figure 2.1) cause variations in structural elevations across the study area (Figures 4.5, 4.6, 4.7).

These overall features are further illustrated by examination of stratigraphic and structural cross-sections. In general, these cross-sections illustrate an increase in thickness and a decrease in subsea elevation south towards the basin centre and a decrease in thickness and an increase in subsea elevation north along the subcrop (Figure 4.8 & 4.9). Variations in the aforementioned trends are also present. For example, a thickening in the Frobisher Beds towards the northeast (Figure 4.8; Well: 15-29-1-W2) is present. This characteristic is also observed on the isopach map of the Frobisher (Figure 4.2). A large structural variation is observed along a south to north orientation (Figure 4.10 & 4.12), resulting from deposition of a shallow shore face in the north and a deepening of the basin towards the south (Sloss, 1987). Structurally the basin displays a deepening in an east-west trend (Figure 4.11), as a result of the Laramide Orogeny (Gerhard et al., 1982). A major structural feature of the basin, the Nesson Anticline, is evident in Figure 4.10 (Well NENE-33-159N-100W).

4.3. Well Sampling

As described in Chapter 3, the newly developed geological framework was used to select wells within the Mississippian aquifers for sampling. Samples were collected directly from the producing well-head.

In total 127 well-head samples were collected for this study. There were 13 suspect samples (Appendix D) removed from the dataset analysis because they were deemed unrepresentative formation waters based on oxygen isotope fingerprinting using $\delta^{18}O < -10‰$ (SMOW) (Rostron and Holmden, 2000). Results for the remaining 114 samples provide the hydrochemistry of Mississippian formation waters found in the Williston Basin (Table 4.1).

Sampling results include: major ions, TDS, charge balance and isotopes of hydrogen and oxygen (Table 4.1). Land locations, sample date, well name, API number, perforation interval, well type, depth corresponding to sample locations, and temperatures, along with minor elements other than Br, and Sr are provided in Appendix A, B, C.

Of the 114 samples, 49 are from the Midale Beds, 37 from the Frobisher Beds, and 28 from the Ratcliffe Beds (Figure 4.13). Sample depths range from 1000 m to 3065 m (Table 4.1), and all three aquifers span the range of sample depths (Table 4.1).

Charge balance error (CBE) is an assessment of the quality of the analytical analysis (Freeze and Cherry, 1979). The charge balance error is calculated based on the principle of electrical neutrality of liquid solutions, which assumes all solutions are electrically neutral (Freeze and Cherry, 1979).

$$(\text{CBE})\ \%\ \text{Error} = \frac{\Sigma\, zM_c - \Sigma\, zM_a}{\Sigma\, zM_c + \Sigma\, zM_a} \times 100$$

where z: the absolute value of the valence of each ion; M_c: the molality of each cation; and M_a; the molality of each anion.

Charge balance error ranges from 0.1% to 4.1%, the majority are less than 3% and samples that have a charge balance error greater than 3% have only been analyzed for Cl, Na, Br. An acceptable standard of charge balance error is <5%.

4.3.1. Total Dissolved Solids

The total dissolved solids content of a sample represents an overview of a groundwater flow system and can be used to estimate general hydrogeochemical interactions of the pore fluids with the geologic framework (Chebotarev, 1955; Tóth, 1984). Formation waters with TDS > 100,000 mg/L have been classified as brines (Carpenter, 1978), while formation waters with TDS between 30,000 mg/L and 100,000 mg/L are termed brackish waters. Formation waters with TDS < 30,000 mg/L are termed fresh waters.

TDS values of the samples range from 84,000 mg/L to 330,000 mg/L, with the majority of the samples having a TDS greater than 200,000 mg/L (Table 4.1). There are consistent patterns of TDS observed within all three Mississippian aquifers. First, lowest TDS values are found in the western and eastern portions of the basin (Figures 4.14, 4.15, 4.16). Second, TDS increases from the W-SW and from the E-SE until a longitude of 102^0W (Figures 4.14, 4.15, 4.16). Third, generally the highest TDS occurs in the center of the basin (Figures 4.14, 4.15, 4.16). A weak correlation with depth and TDS is evident in all three aquifers (Figure 4.17 a,b,c).

Temperatures range from 41^0C to 107^0C (Table 4.1). Temperature values were either measured while sampling (Chapter 3) or obtained from a drill stem test reports (DST) (Table 4.1). Temperature generally increases linearly with depth (Figure 4.18 a,b,c).

4.3.2. Major and Minor Ion Chemistry

The major ions that are analysed for formation water in sedimentary basins are: Na^{+}, Ca^{+2}, K^{+}, and Mg^{+2}, Cl^{-}, SO_4^{-2}, and HCO_3^{-}. In this study an additional seventeen other minor ions were obtained. For clarity, the valance for the ions will be removed for the remainder of the thesis.

For anions, three major ions dominate the dataset; Cl, SO_4 and HCO_3; one trace anion of importance is Br, which is present in appreciable quantities (Table 4.1). Chloride is the dominant anion (Cl > 90%) in the dataset (Figure 4.19). Chloride values range from 11,000 mg/L to 204,400 mg/L (Figure 4.20 a,b,c). Chloride values increase directly with TDS, at a linear rate (Figure 4.20 a,b,c) and all three formation have similar trends. Bromide compositions range from 50 mg/L to 1000 mg/L and display a linear increase at low TDS then an exponential increase as TDS approaches 250,000 mg/L (Figure 4.21 a,b,c). Sulphate concentrations vary from 90 mg/L to 2260 mg/L and exhibit decreasing values with increasing TDS in all three aquifers (Figure 4.23 a,b,c). Bicarbonate ranges from 79 mg/L to 588 mg/L in all three aquifers and displays no correlation with TDS (Figure 4.24 a,b,c).

For cations, there are four major ions that dominate the dataset; Na, Ca, Mg, and K; one trace cation of importance is Sr. Sodium values range from 4,900 mg/L to 115,200 mg/L (Figure 4.25 a,b,c). Sodium is the dominant cation (Na > 80%) in the dataset (Figure 4.19). Sodium displays a linear correlation with TDS (Figure 4.25 a,b,c), however as TDS approaches 250,000 mg/L the data begins to diverge from the trend (Figure 4.25 a,b,c). This is observed in all three formations. Calcium concentrations range from 1,310

mg/L to 41,800 mg/L (Figure 4.26 a,b,c). Calcium increases linearly with TDS in all three aquifers, up to approximately 225,000-250,000 mg/L TDS past that, there is an exponential increase in Ca versus TDS (Figure 4.26 a,b,c). Magnesium values range from 300 mg/L to 4300 mg/L, magnesium values for all three formations exhibit a linear increase at low TDS then scatters when TDS approaches 250,000 mg/L (Figure 4.27 a,b,c). Potassium values ranges from 320 mg/L to 6670 mg/L, all three formations display similar patterns of increasing potassium with increasing TDS (Figure 4.28 a,b,c). Sr compositions vary from 32 mg/L to 2770 mg/L and demonstrate a linear increase when TDS < 250,000 mg/L then an exponential increase when TDS > 250,000 mg/L (Figure 4.22 a,b,c).

4.4. Classification of Formation Waters in the Williston Basin

In general, previous authors have found three types of formation waters in the pre-Mississippian aquifers of the Williston Basin based on their compositional hydrochemistry (Iampen, 2003; Khan, 2006). Type 1 waters are dominantly Ca-SO_4 with a TDS < 100,000 mg/L. Type 2 waters are predominantly Na-Cl waters with a TDS ranging between 100,000 to 300,000 mg/L. Type 3 are Ca-Cl waters having a TDS > 300,000 mg/L (Iampen, 2003; Khan, 2006).

All the formation waters in the dataset can be grouped as Type 2, Na-Cl waters (Figure 4.19), based on the previous classification of formation waters in the Williston Basin (Iampen, 2003; Khan, 2006).

4.5. Oxygen and Hydrogen Isotopes

These data are the first detailed isotopic measurements of formation waters from individual Mississippian aquifers in the Williston Basin. Oxygen isotope ($\delta^{18}O$) compositions range from -8.15 to +12.64 (SMOW), for all three aquifers (Figure 4.29 a,b,c). $\delta^{18}O$ compositions display a poor negative exponential trend with increasing depths (Figure 4.29 a,b,c). Spatially, within each aquifer the most enriched oxygen values occur south of the basin centre and along the Nesson anticline (Figures 4.30, 4.31, 4.32). Generally, TDS increases linearly with $\delta^{18}O$ (Figure 4.33 a,b,c).

Deuterium (δD) compositions range from -106.0 to -5.3 (SMOW). Deuterium displays similar trends as $\delta^{18}O$ with TDS (Figure 4.34 a,b,c) and depth (Figure 4.35 a,b,c). Spatially, the most enriched deuterium compositions (not shown) occur in the same location as the enriched $\delta^{18}O$ compositions (Figure 4.30, 4.31, 4.32), south of the basin centre and along the Nesson Anticline.

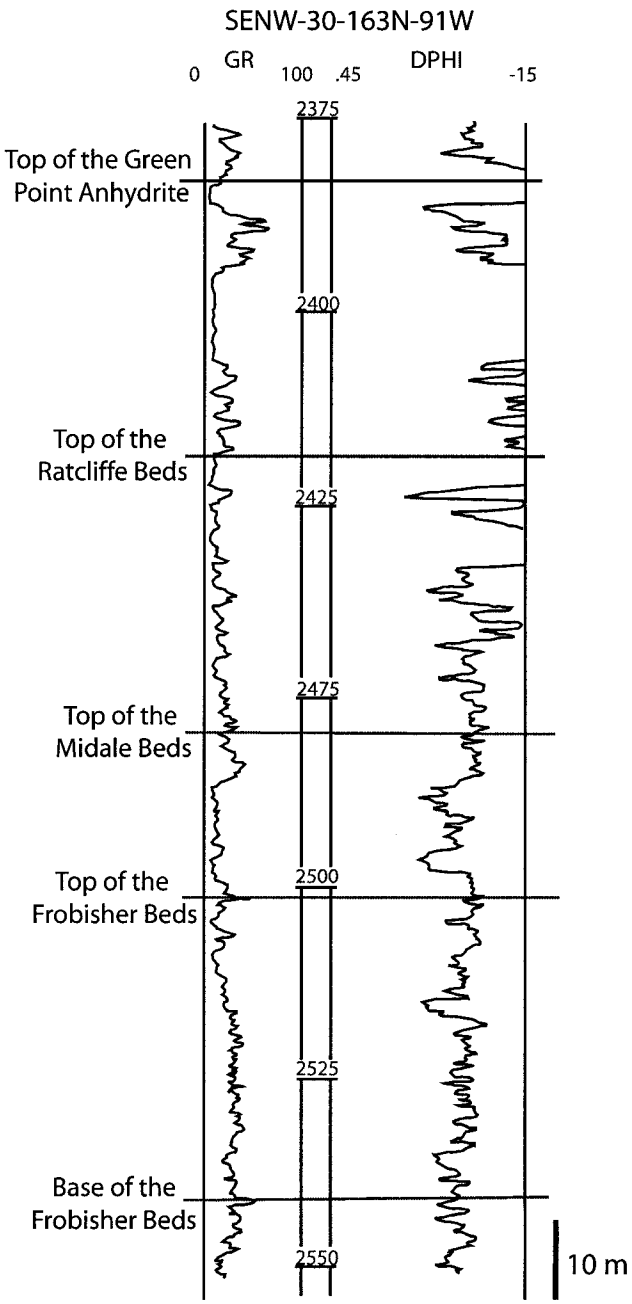

Figure 4.1. Reference geophysical well logs used in this study.

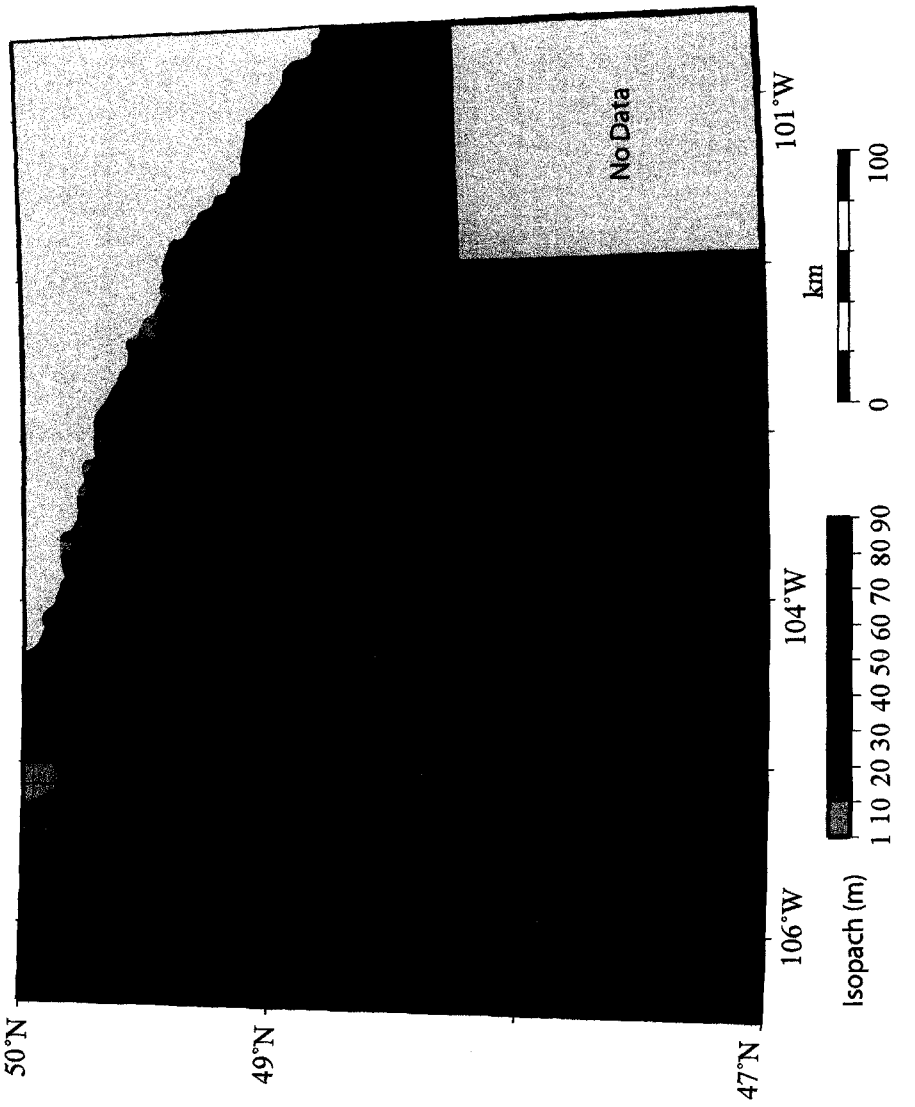

Figure 4.2. Isopach map of the Frobisher Beds.

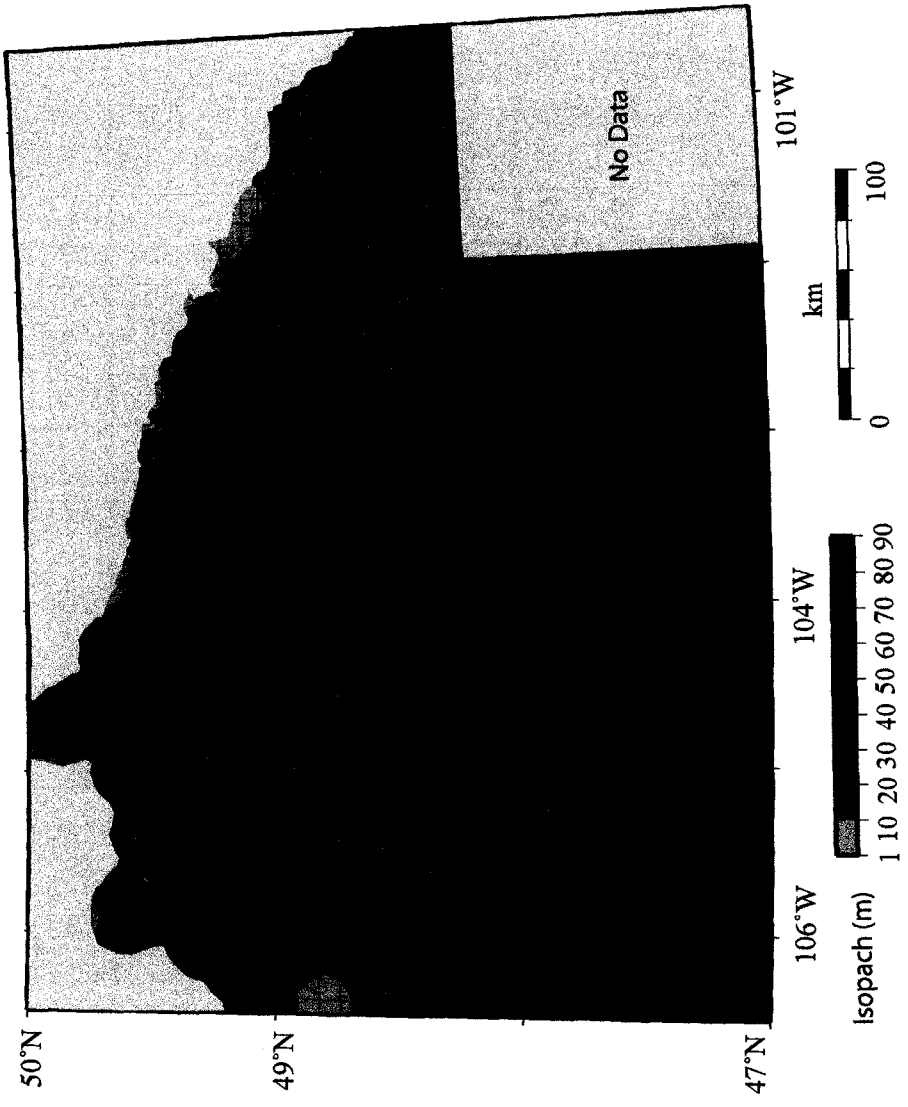

Figure 4.3. Isopach map of the Midale Beds.

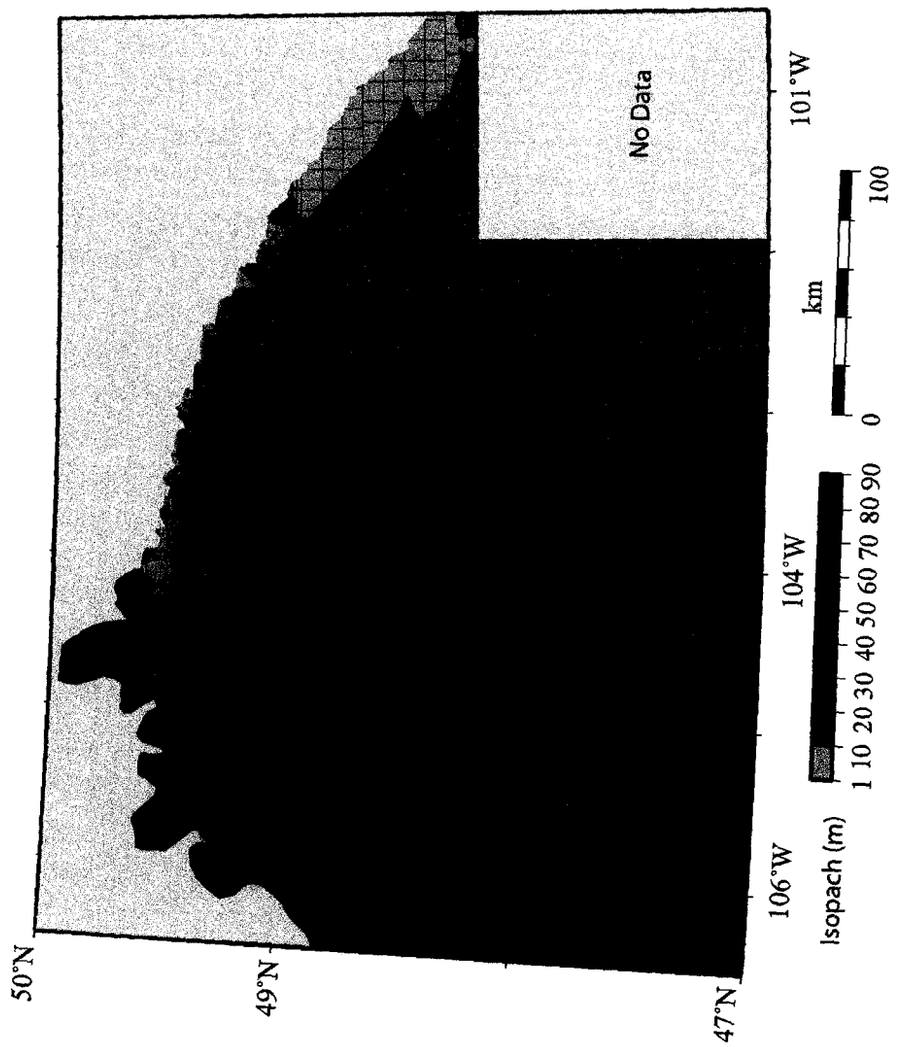

Figure 4.4. Isopach map of the Ratcliffe Beds.

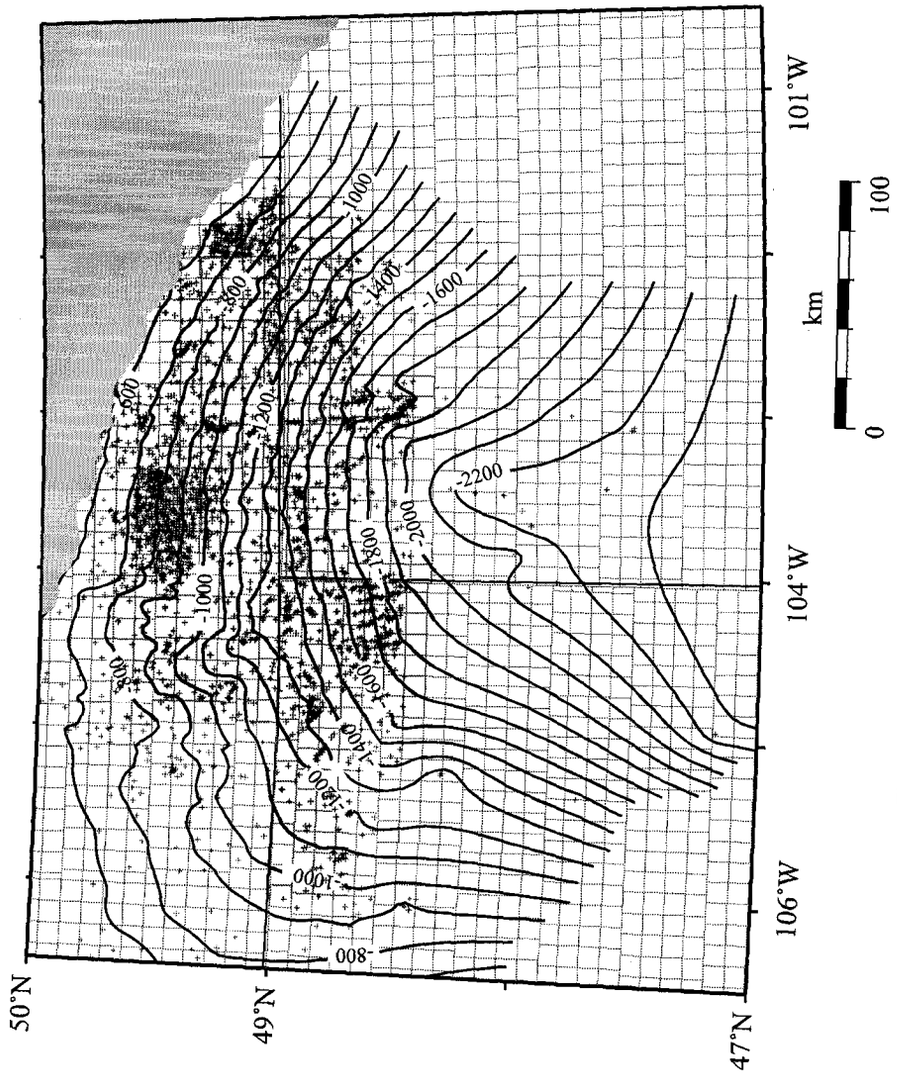

Figure 4.5. Subsea map of the Frobisher Beds.

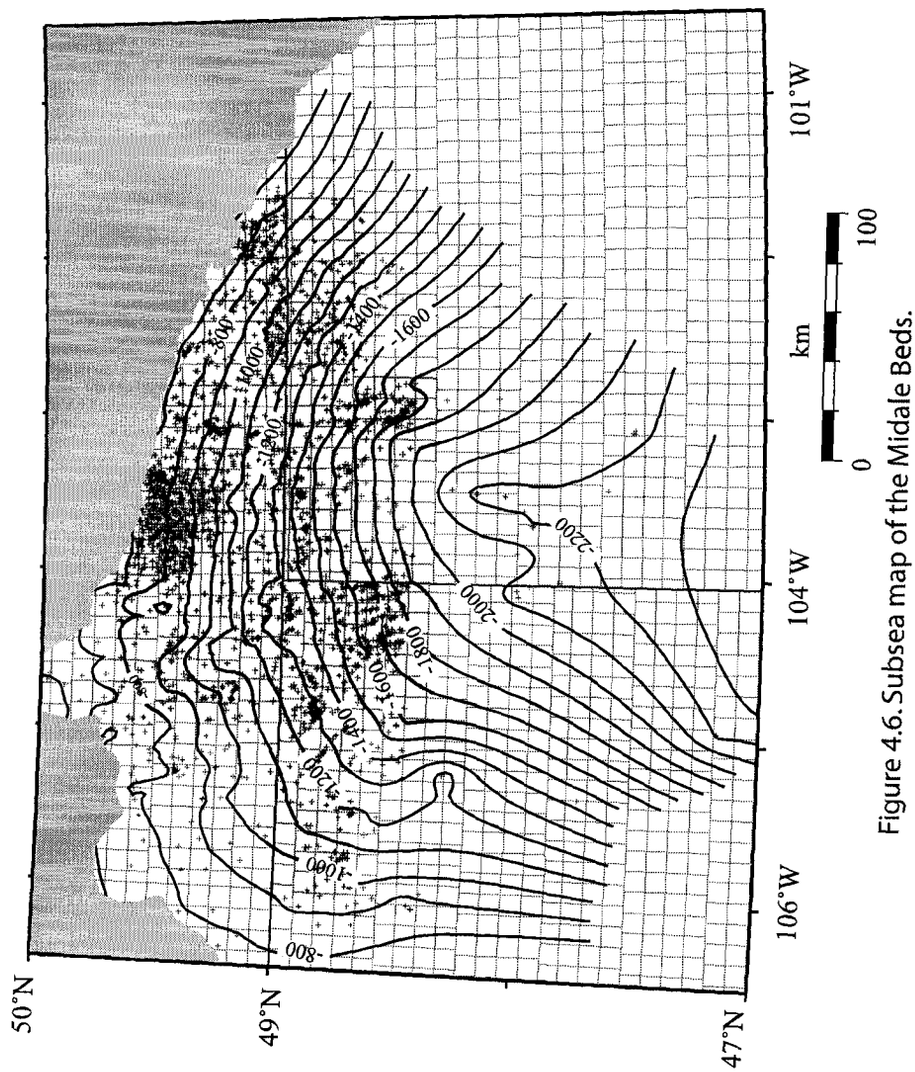

Figure 4.6. Subsea map of the Midale Beds.

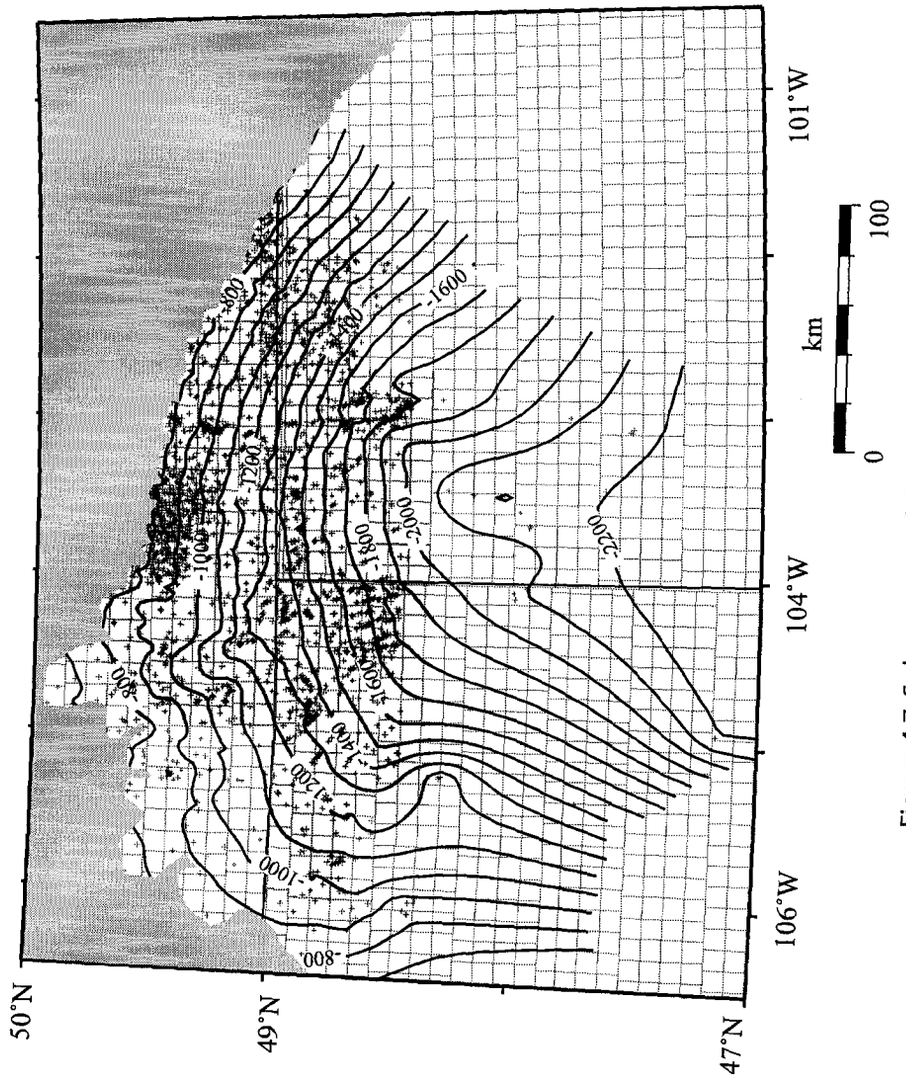

Figure 4.7. Subsea map of the Ratcliffe Beds.

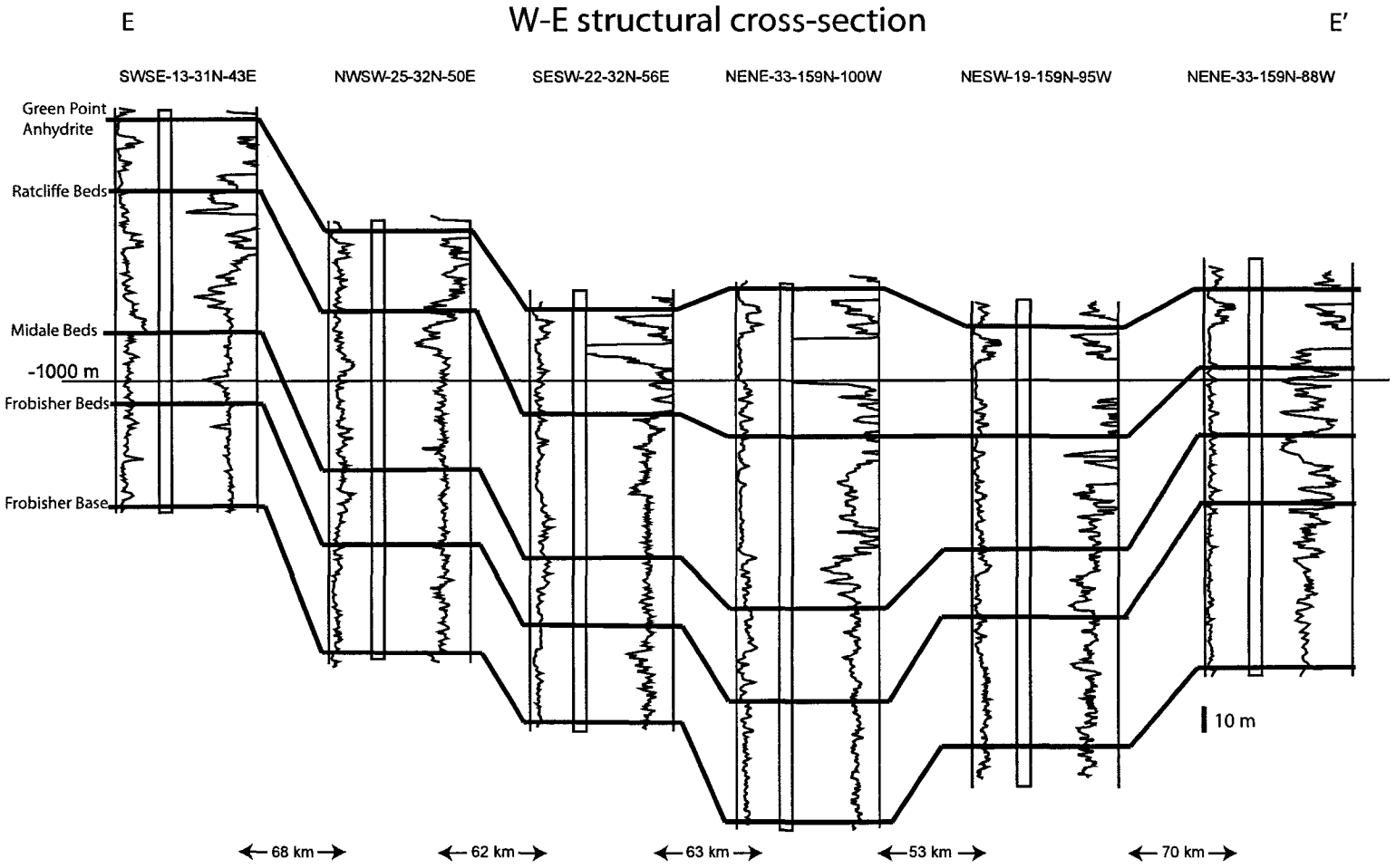

Figure 4.11. W-E trending structural cross-section (not to scale) E-E' (see Figure 2.6 for the line of section). 1000 metres subsea is the datum. Left trace is gamma log and right trace is density neutron log.

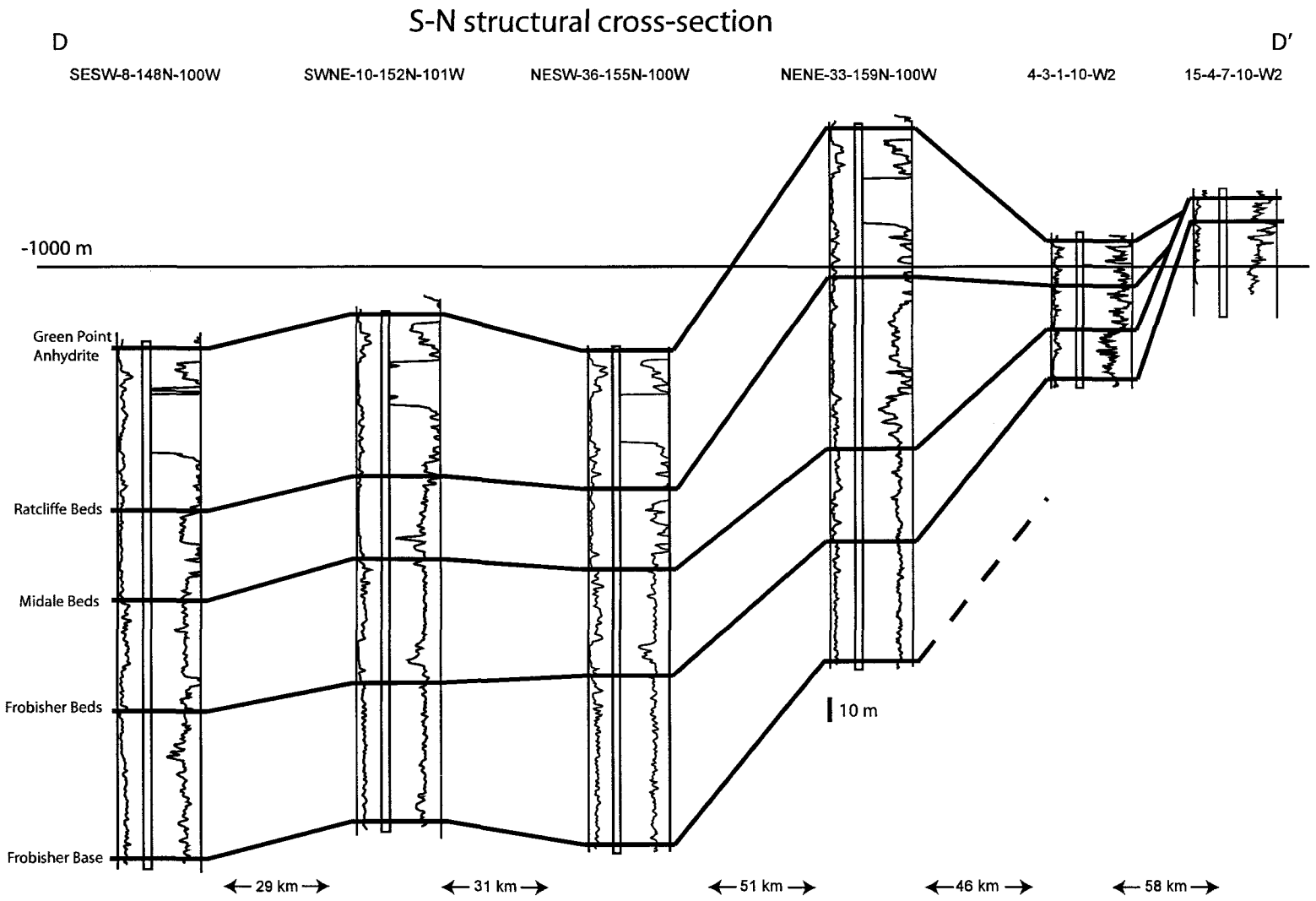

Figure 4.10. S-N trending structural cross-section (not to scale) D-D' (see Figure 2.6 for line of section). 1000 metres subsea is the datum. Left trace is gamma log and right trace is density neutron log.

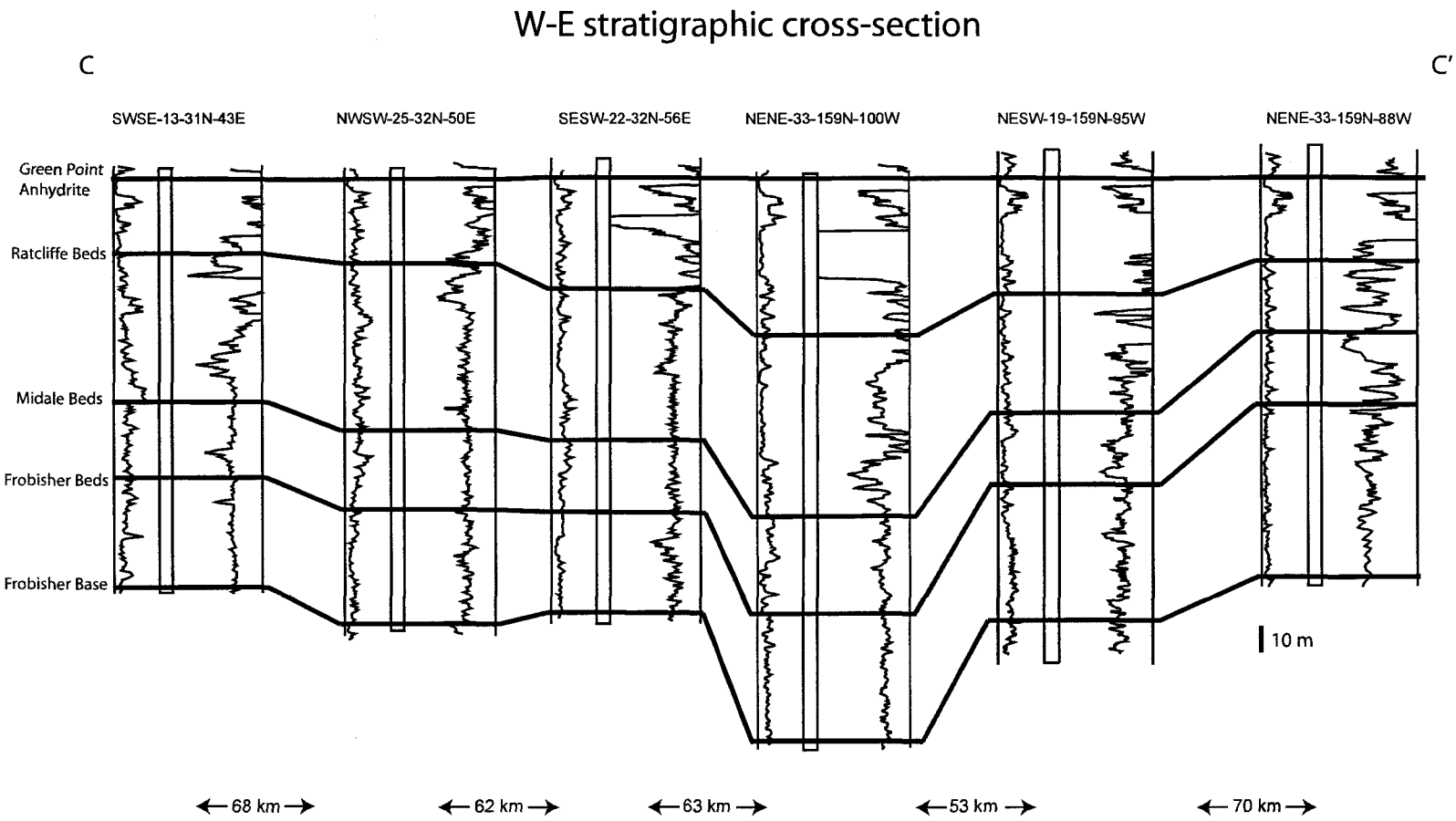

Figure 4.9. W-E trending stratigraphic cross-section (not to scale) C-C' (see Figure 2.6 for the line of section). Green Point Anhydite is the datum. Left trace is gamma log and the right trace is density neutron log.

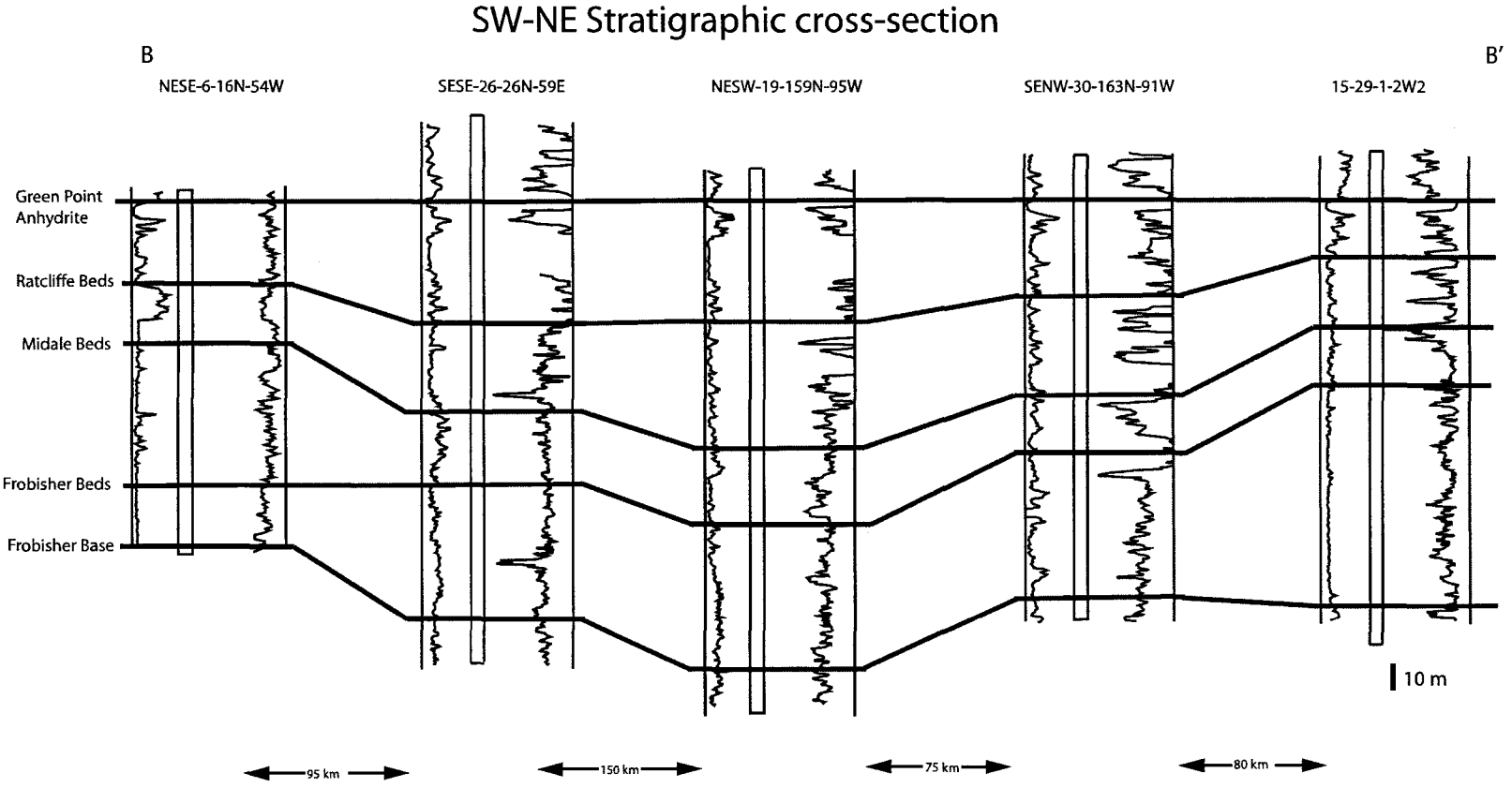

Figure 4.8. SW-NE trending stratigraphic cross-section (not to scale) B-B' (see Figure 2.6 for the line of section). Green Point Anhydrite is the datum. Left trace is gamma log and right trace is density neutron log.

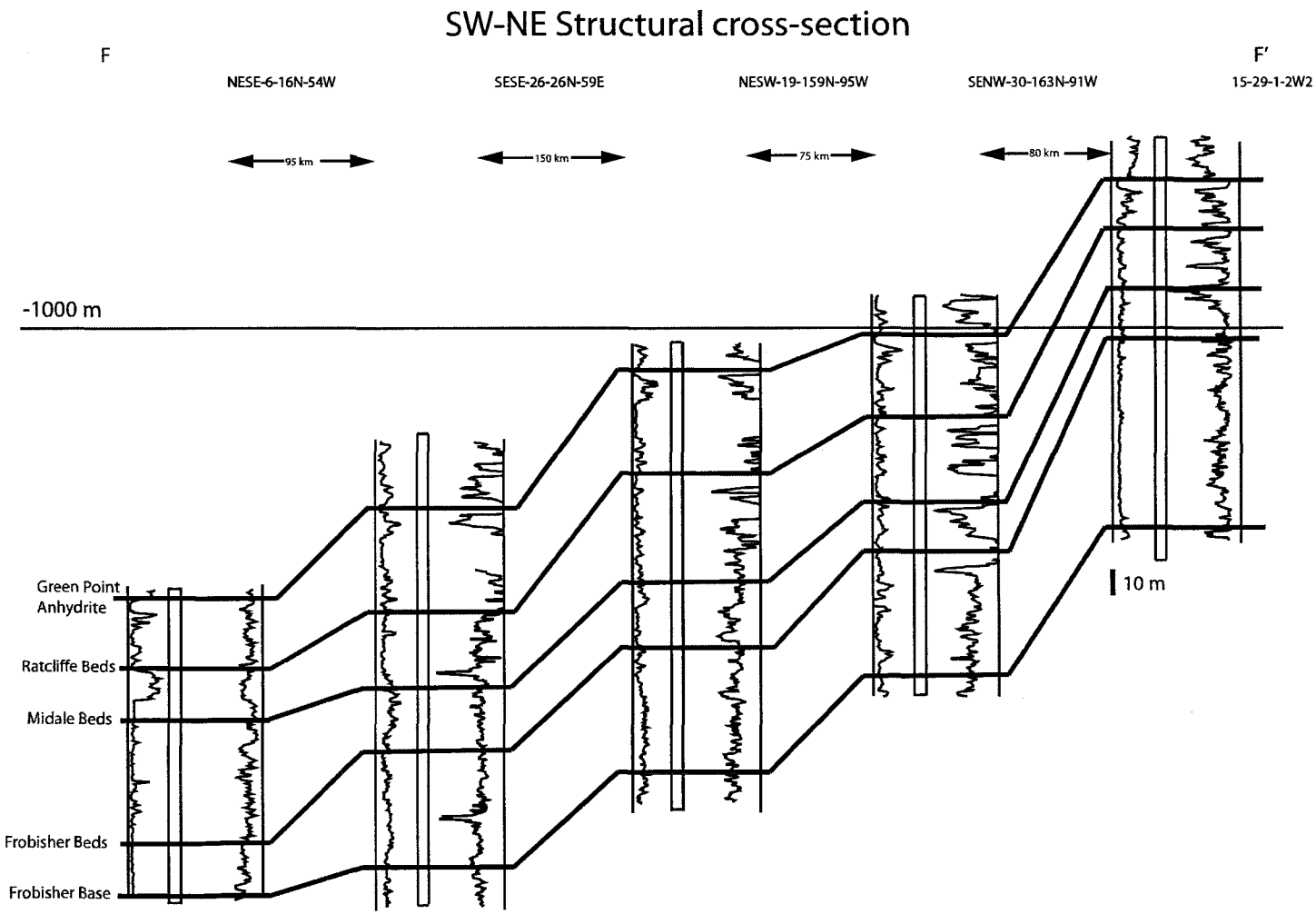

Figure 4.12. SW-NE trending structural cross-section (not to scale) F-F' (see Figure 2.6 for the line of section) 1000 metres subsea is the datum. Left trace is gamma log and right trace is density neutron log.

Table 4.1. Hydrochemistry results for major and minor ions

Sample ID	Formation	Na	Ca	Mg	K	Cl	SO4*	HCO3	Sr	Br	B	TDS	$\delta^{18}O$ ‰	δD ‰	% Charge Balance
03- 201	Midale	65200	2240	489	1720	105400	941	195	83	138	169	177000	2.6	-47	1.5
03- 203	Midale	64800	2150	448	1630	102800	837	194	74	143	159	173000	2.2	-47	2.3
03- 206	Midale	40300	1560	425	350	60600	2200	128	38	50	32.6	106000	-5.6	-75	3.5
03- 207	Midale	103400	8070	1760	5600	184700	278	205	327	440	213	305000	8.3	-16	0.3
03- 208	Midale	100800	5010	1200	1820	165900	305	150	192	319	136	276000	6.7	-17	1.7
03- 209	Midale	103300	6660	1400	4830	181400	259	216	200	410	165	299000	8.8	-18	-0.1
03- 210	Midale	101900	4260	1140	822	170000	320	190	160	318	124	280000	5.8	-21	0.3
03- 211	Midale	44400	1310	300	430	66100	2260	162	32	66	42.8	115000	-3.6	-68	3.3
03- 213	Midale	96800	4250	1030	3690	164700	430	120	149	275	144	272000	6.9	-21	-0.1
03- 216	Midale	67100	3990	913	2020	114000	579	243	140	207	193	189000	1.4	-61	1.1
03- 217	Midale	110600	5170	1010	3120	178200	367	317	193	297	175	299000	7.4	-18	2.3
03- 218	Midale	103400	4700	1140	3240	171700	311	134	171	300	139	285000	7.5	-19	1.0
03- 219	Midale	104700	4700	1140	3200	175200	296	<5	156	295	125	290000	7.9	-20	0.5
03- 220	Midale	102300	4790	1150	3300	171600	313	128	167	326	133	284000	8.1	-18	0.6
03- 221	Midale	106500	4670	1140	3220	181300	294	104	153	304	116	298000	8.0	-19	-0.5
03- 222	Midale	96610	6780	1660	4450	169700	242	232	224	415	176	281000	7.4	-17	0.5
03- 230	Midale	105400	8720	1610	4570	189500	150	271	360	472	228	311000	9.1	-14	-0.1
03- 232	Midale	112000	3930	802	2280	187200	222	121	180	334	177	307000	5.4	-26	-0.4
03- 234	Midale	102700	10500	1530	4260	186300	135	204	670	534	251	307000	7.8	-24	0.4
03- 235	Midale	99200	11100	1650	4870	183600	114	180	667	543	277	302000	10.4	-13	0.3
03- 238	Midale	115100	5030	1120	2550	187000	228	207	190	332	166	312000	8.4	-15	1.7
03- 241	Midale	110400	6030	1300	2660	190100	160	153	258	350	190	312000	7.9	-13	-0.3
03- 242	Midale	115200	5850	1230	2750	191400	155	125	249	341	182	318000	7.9	-16	1.2
03- 243	Midale	108800	5740	1220	2660	185400	179	112	250	333	188	305000	7.2	-18	0.1
03- 244	Midale	100700	12100	1850	5010	185300	90	130	742	615	247	307000	10.7	-13	1.1
03- 245	Midale	115100	5170	1080	2840	191800	189	nd	220	339	158	317000	8.1	-15	0.5
03- 246	Midale	94600	12000	1530	4810	180700	93	123	807	633	272	296000	10.2	-14	-0.5
03- 249	Midale	113100	5580	1010	4280	194200	158	136	292	413	306	320000	9.5	-15	0.0
03- 250	Midale	102800	11900	1480	4830	189300	96	164	704	588	277	312100	9.7	-14	0.6
03- 251	Midale	98710	11900	1490	4480	183800	90	152	820	603	264	302000	10.2	-13	0.3
03- 253	Midale	105200	2530	584	2310	169400	590	415	81	286	157	282000	6.3	-22	0.6
03- 258	Midale	101500	11200	1720	4910	191202	93	122	712	610	244	312000	9.6	-13	-0.7
04- 101	Midale	33800	2310	590	670	56000	1300	156	51	144	38	95100	-2.8	-66	1.6
04- 105	Midale	97700	7750	2000	5260	175800	250	179	230	439	154	290000	9.2	-16	0.1
04- 110	Midale	111100	7110	1500	3870	190600	250	229	270	345	174	316000	9.1	-14	0.7
04- 114	Midale	nd	nd	nd	nd	nd	nd	nd	nd	nd	nd	nd	6.9	-5	nd

* [SO4] is calculated from [total S] by factor 96.06/32.06. This assumes all S exists as SO4, and may slightly overestimate SO4 concentrations.
concentrations in mg/L, nd = not determined.

Table 4.1. Hydrochemistry results for major and minor ions

Sample ID	Formation	Na	Ca	Mg	K	Cl	SO4*	HCO3	Sr	Br	B	TDS	$\delta^{18}O$ ‰	δD ‰	% Charge Balance
04- 115	Midale	100900	nd	nd	nd	167000	nd	nd	nd	288	nd	nd	6.6	-18	-3.6
04- 117	Midale	56000	3650	1200	660	90600	1500	156	54	121	46	154000	-3.1	-66	2.9
04- 118	Midale	55900	3100	890	590	90200	1400	120	62	108	47	152000	-3.0	-68	2.1
05- 103	Midale	89400	14200	1600	4680	175000	<100	121	1040	635	301	287000	10.2	-34	0.1
05- 104	Midale	93000	11200	1200	4790	172900	<100	136	824	642	325	285000	10.4	-31	0.4
05- 107	Midale	86300	12100	1300	4480	162900	<100	115	885	538	280	269000	5.8	-48	0.8
05- 110	Midale	90900	16800	1500	5000	182600	300	588	1420	651	373	300000	11.7	-27	0.1
05- 115	Midale	77500	24300	1700	4830	168900	<100	79	940	545	266	279000	5.0	-44	1.8
05- 117	Midale	100000	13800	1400	4460	181900	<100	114	1000	601	340	304000	11.0	-19	2.3
05- 124	Midale	69200	41800	4300	5480	204400	<100	113	2770	1002	211	329000	8.0	-38	-0.6
05- 138	Midale	46300	2200	400	830	72700	560	240	93	126	173	124000	-2.9	-84	3.7
05- 140	Midale	102300	11400	1200	4940	189900	<100	155	838	539	306	312000	10.7	-15	-0.1
05- 144	Midale	nd	nd	nd	nd	nd	nd	nd	nd	nd	nd	nd	4.0	-46	nd
03- 202	Frobisher	36900	2330	577	600	60100	1110	101	64	153	43.6	102000	-3.3	-64	2.1
03- 204	Frobisher	38600	1960	493	710	62800	1340	132	55	155	56	106000	-2.9	-63	1.4
03- 205	Frobisher	39900	1880	441	740	63700	1400	139	51	152	59.8	108000	-2.8	-65	2.0
03- 212	Frobisher	43000	2920	790	320	70000	1260	152	70	109	35	119000	-5.5	-76	2.4
03- 215	Frobisher	65900	3980	876	2050	111900	589	260	140	202	187	186000	0.3	-66	1.1
03- 223	Frobisher	96100	6640	1800	4300	166500	307	298	189	397	165	277000	6.6	-23	1.1
03- 229	Frobisher	114700	n.d.	n.d.	n.d.	195400	n.d.	n.d.	n.d.	397	n.d.	310000	5.0	-41	n.d.
03- 239	Frobisher	111700	4980	1110	2580	190700	191	246	203	346	174	312000	8.5	-13	-0.7
03- 240	Frobisher	97200	4930	1060	2310	157800	167	119	176	309	150	264000	8.6	-13	2.3
03- 252	Frobisher	87700	5400	1320	3680	153600	240	202	180	359	153	253000	4.2	-35	-0.1
03- 254	Frobisher	97700	2280	581	2120	157600	681	382	72	268	140	262000	4.8	-27	0.4
03- 255	Frobisher	105200	8230	1660	4650	187500	156	158	321	489	239	309000	9.4	-14	0.2
04- 109	Frobisher	108400	8910	1800	6670	187000	310	186	248	415	161	314000	10.0	-11	2.3
05- 101	Frobisher	109500	8440	1500	3900	188000	<100	146	470	433	228	313000	8.8	-21	1.6
05- 102	Frobisher	108400	8620	1500	3900	193400	100	144	453	424	222	317000	9.0	-19	-0.2
05- 112	Frobisher	92600	16800	1600	5180	179500	680	580	1380	645	328	299000	12.6	-12	1.5
05- 114	Frobisher	85600	14600	1400	5000	169700	200	375	1160	626	421	279000	12.2	-12	0.3
05- 116	Frobisher	100800	16200	1400	5230	198500	<100	140	1420	614	427	325000	12.4	-14	-0.1
05- 118	Frobisher	79600	10400	1200	4380	148000	<100	159	709	493	238	245000	7.7	-27	1.1
05- 119	Frobisher	87400	10600	1200	4380	163000	<100	143	741	464	268	268000	7.7	-27	0.3
05- 128	Frobisher	100500	n.d.	n.d.	n.d.	195200	n.d.	n.d.	n.d.	644	n.d.	296000	12.3	-19	n.d.
05- 129	Frobisher	105700	n.d.	n.d.	n.d.	196700	n.d.	n.d.	n.d.	614	n.d.	303000	10.7	-26	n.d.
05- 133	Frobisher	38200	2500	530	1000	61800	780	239	43	105	82.1	105000	-5.0	-92	3.2
05- 137	Frobisher	38900	2000	430	700	64500	680	192	73	105	189	108000	-6.2	-98	1.7
00- 181	Frobisher	103000	5170	1290	3720	176900	268	n.d.	159	422	155	291000	7.7	-22	-2.2
00- 182	Frobisher	103000	5170	1270	3690	180400	264	n.d.	159	427	155	295000	7.5	-22	-3.2
00- 183	Frobisher	99300	5070	1250	3590	172400	279	n.d.	155	408	151	283000	7.1	-24	-2.7

* [SO4] is calculated from [total S] by factor 96.06/32.06. This assumes all S exists as SO4, and may slightly overestimate SO4 concentrations.
Concentrations in mg/L, nd = not determined.

Table 4.1. Hydrochemistry results for major and minor ions

Sample ID	Formation	Na	Ca	Mg	K	Cl	SO4*	HCO3	Sr	Br	B	TDS	$\delta^{18}O$ ‰	δD ‰	% Charge Balance
00- 184	Frobisher	105300	5150	1300	3800	181500	259	n.d.	163	425	155	298000	7.40	-21.7	-2.5
00- 169	Frobisher	75000	3320	788	2030	128600	532	n.d.	102	254	173	211000	1.60	-61.9	-2.4
00- 170	Frobisher	71000	3310	778	1980	120400	525	n.d.	100	248	173	198000	1.70	-61.3	-1.8
00- 171	Frobisher	73900	3350	790	2020	124300	524	n.d.	102	255	174	205000	1.80	-60.7	-1.3
00- 172	Frobisher	71700	3380	800	2070	120900	526	n.d.	104	253	177	200000	1.70	-60.6	-1.3
00- 173	Frobisher	73100	3270	752	1980	123700	513	n.d.	100	253	169	204000	1.60	-62.2	-1.6
99- 102	Frobisher	51000	2690	658	1090	87600	1060	n.d.	72	168	112	145000	-4.00	-76.0	-2.2
99- 104	Frobisher	58000	2010	654	670	94500	1370	n.d.	59	169	75.9	157000	-2.70	-60.0	-1.2
03- 009	Frobisher	n.d.	n.d.	n.d.	n.d.	n.d.	n.d.	n.d.	n.d.	n.d.	n.d.	n.d.	-4.26	-89.0	n.d.
03- 011	Frobisher	n.d.	n.d.	n.d.	n.d.	n.d.	n.d.	n.d.	n.d.	n.d.	n.d.	n.d.	-4.38	-89.2	n.d.
00- 164	Frobisher	92500	3990	1210	1710	157300	479	n.d.	106	330	122	258000	3.60	-39.9	-2.2
00- 161	Frobisher	87700	3570	1070	1370	146200	554	n.d.	90	286	124	241000	3.60	-39.6	-1.3
03- 129	Frobisher	87700	5030	1590	2050	146900	580	133	132	312	145	245000	3.04	-38.8	-0.6
03- 130	Frobisher	88000	5380	1720	2210	150100	674	165	140	305	160	249000	3.99	-38.3	-1.3
03- 145	Frobisher	85900	4690	1530	2240	144000	540	178	150	309	196	240000	4.14	-38.9	-0.7
03- 146	Frobisher	87100	4490	1490	2080	143400	597	<5	127	297	175	240000	3.91	-40.2	0.1
03- 224	Ratcliffe	47900	1510	417	974	72700	1320	537	46	141	170	126000	3.13	-52.9	4.1
03- 225	Ratcliffe	58500	3860	1000	965	99000	691	97	99	162	48	164000	-0.32	-52.5	0.9
03- 226	Ratcliffe	61100	3820	1080	996	103000	660	119	105	167	58	171000	-1.32	-61.6	1.1
03- 227	Ratcliffe	57195	3880	991	874	97300	723	102	100	161	45	161000	-0.80	-56.8	0.7
03- 237	Ratcliffe	112000	5570	1240	2570	187200	182	143	205	334	163	310000	7.57	-15.5	0.7
03- 247	Ratcliffe	98800	12700	1610	4740	184800	96	158	868	620	261	305000	10.28	-12.5	0.6
03- 248	Ratcliffe	98400	12200	1840	5070	187000	97	149	763	607	260	307000	10.57	-11.9	-0.2
03- 256	Ratcliffe	97800	6580	1350	2500	166900	221	224	256	309	219	277000	5.24	-25.9	1.1
03- 259	Ratcliffe	107100	6470	1400	2440	180200	165	204	268	332	233	299000	4.75	-22.5	1.3
04- 103	Ratcliffe	n.d.	n.d.	n.d.	n.d.	n.d.	n.d.	n.d.	n.d.	n.d.	n.d.	n.d.	2.39	-45.5	n.d.
04- 104	Ratcliffe	58200	4020	860	990	96300	800	113	112	142	56	162000	-1.13	-56.3	2.0
05- 106	Ratcliffe	104100	n.d.	n.d.	n.d.	197500	n.d.	n.d.	n.d.	569	n.d.	302000	10.20	-22.7	n.d.
05- 109	Ratcliffe	111000	11100	1100	4880	198100	<100	106	841	499	383	328000	11.09	-21.2	1.1
05- 111	Ratcliffe	104200	15600	1800	5260	199100	<100	96	1050	564	297	328000	9.21	-40.5	0.7
05- 121	Ratcliffe	102900	11600	1300	5340	188200	200	147	754	530	235	311000	9.99	-13.4	0.6
05- 122	Ratcliffe	99600	10100	1300	5090	180000	<100	243	667	481	229	298000	9.97	-10.7	0.7
05- 123	Ratcliffe	108300	11600	1200	5320	193300	<100	153	774	560	209	322000	10.60	-11.6	1.3
05- 127	Ratcliffe	100600	10900	1100	4990	186400	<100	146	842	662	465	306000	11.25	-23.3	0.2
05- 130	Ratcliffe	91400	n.d.	n.d.	n.d.	165600	n.d.	n.d.	n.d.	484	n.d.	258000	5.78	-39.0	-8.2
05- 131	Ratcliffe	58900	2800	600	1100	94900	470	168	125	166	248	160000	2.68	-57.3	2.9
05- 135	Ratcliffe	71800	4550	740	1900	121300	300	200	206	220	249	201000	6.22	-39.1	1.4
05- 136	Ratcliffe	30600	1600	300	610	50100	510	409	66	87	112	84000	-8.15	-106.6	1.8

* [SO4] is calculated from [total S] by factor 96.06/32.06. This assumes all S exists as SO4, and may slightly overestimate SO4 concentrations.
Concentrations in mg/L, nd = not determined.

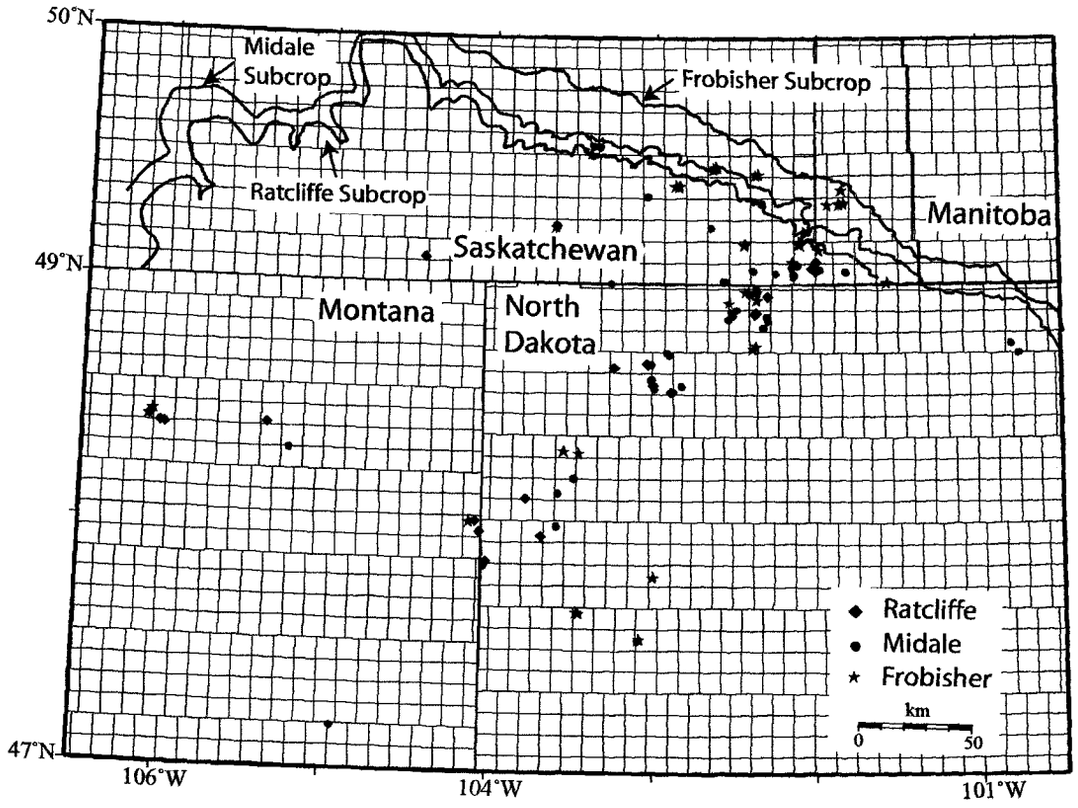

Figure 4.13. Well-head location of samples collected for this study. Subcrops from Kent et al., 2004

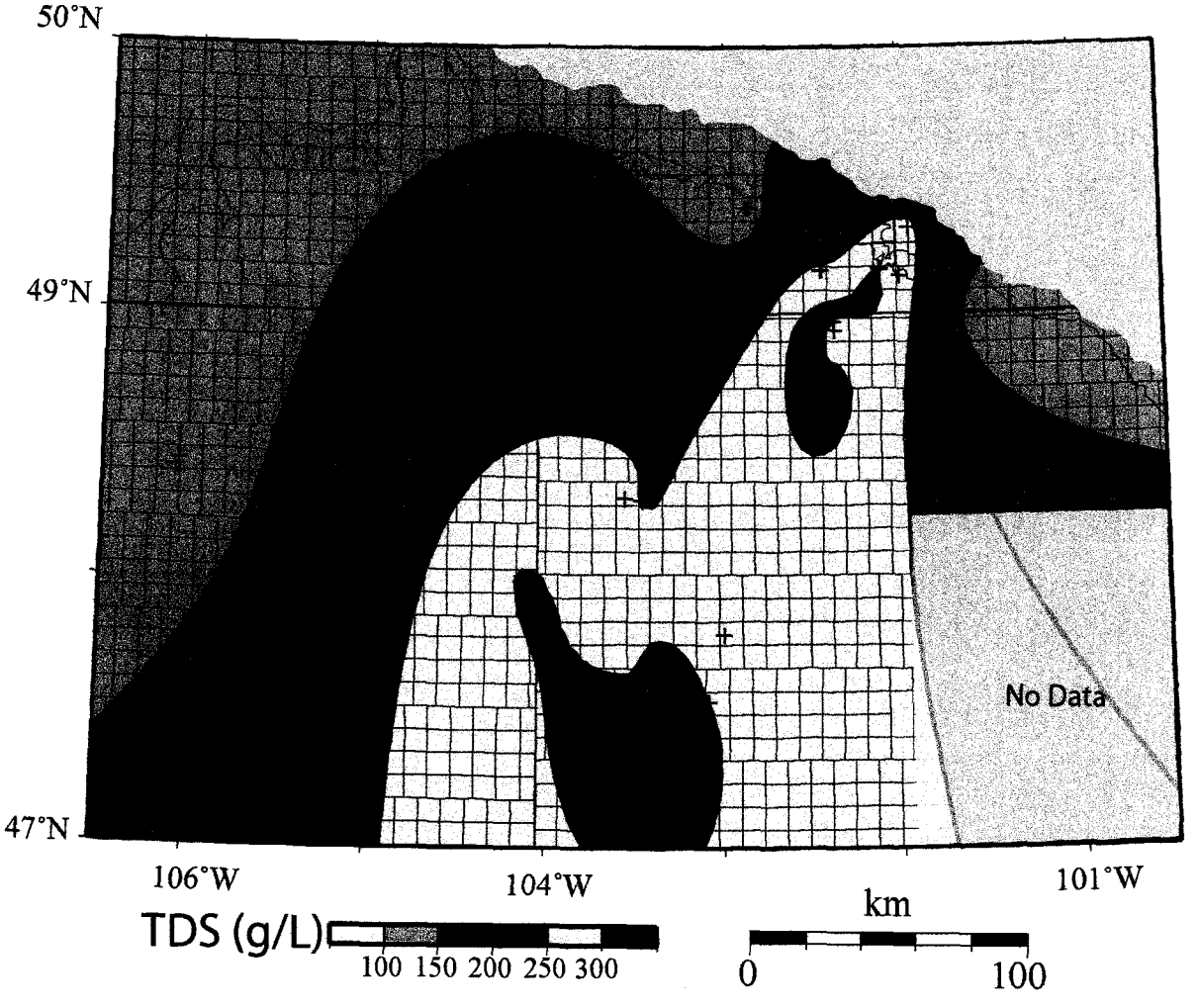

Figure 4.14. Total Dissolved Solids (TDS) map of the Frobisher Beds.

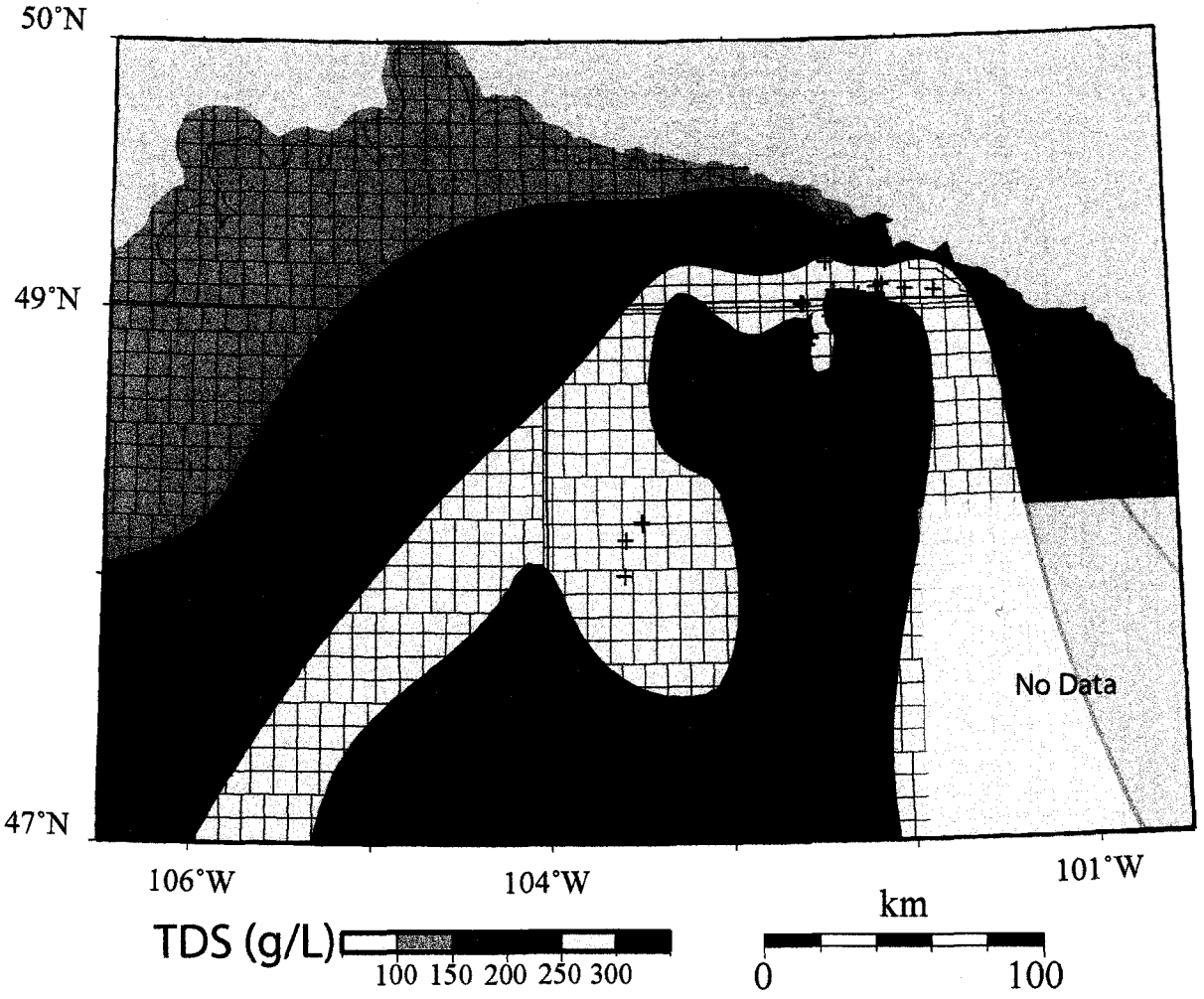

Figure 4.15. Total Dissolved Solids (TDS) map of the Midale Beds.

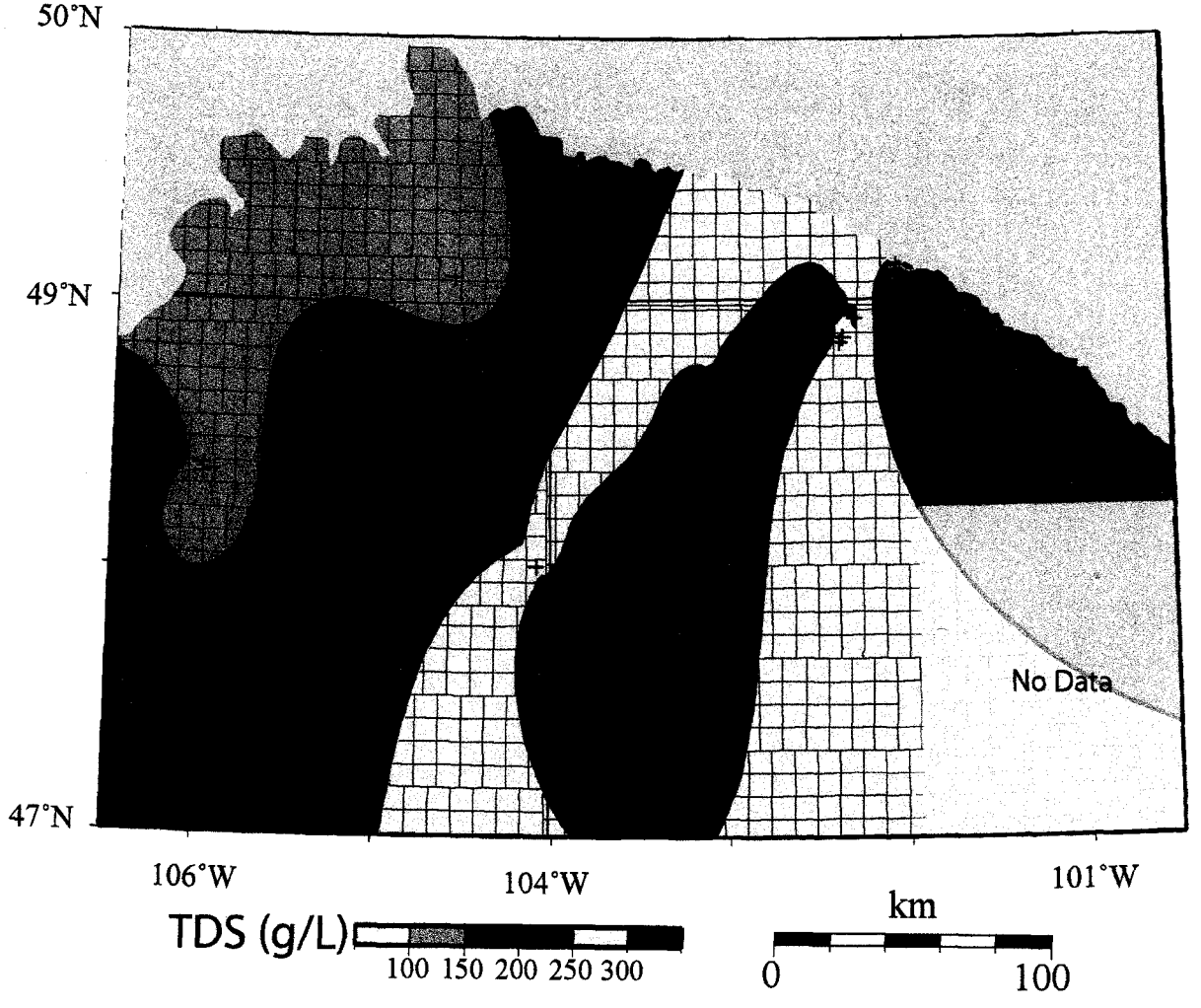

Figure 4.16. Total Dissolved Solids (TDS) map of the Ratcliffe Beds.

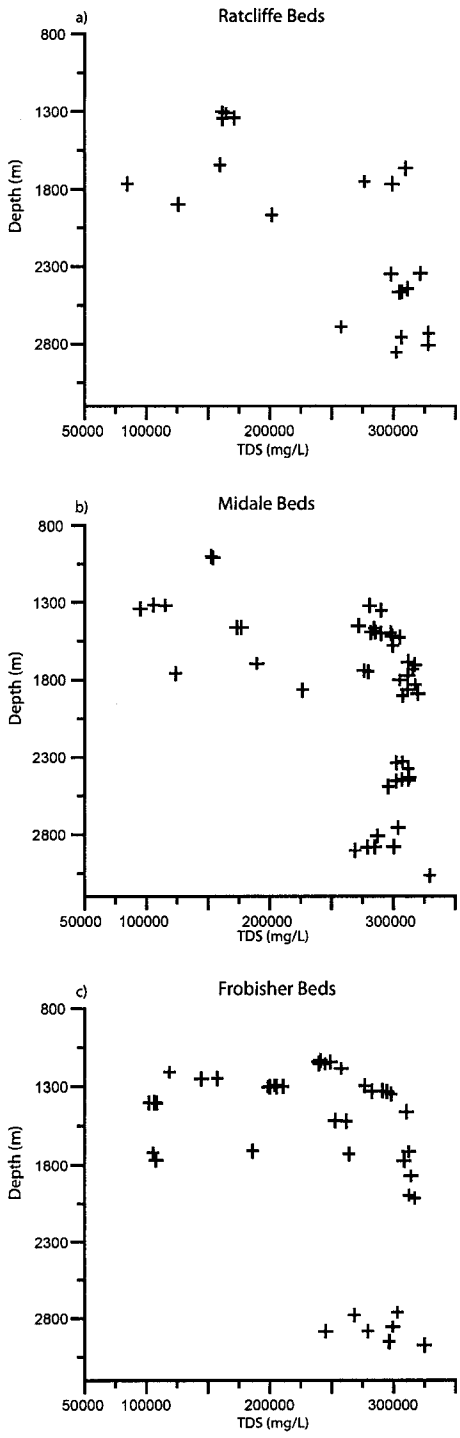

Figure 4.17. Total dissolved solids vs. depth for the three aquifers.
a) Ratcliffe Beds b) Midale Beds c) Frobisher Beds

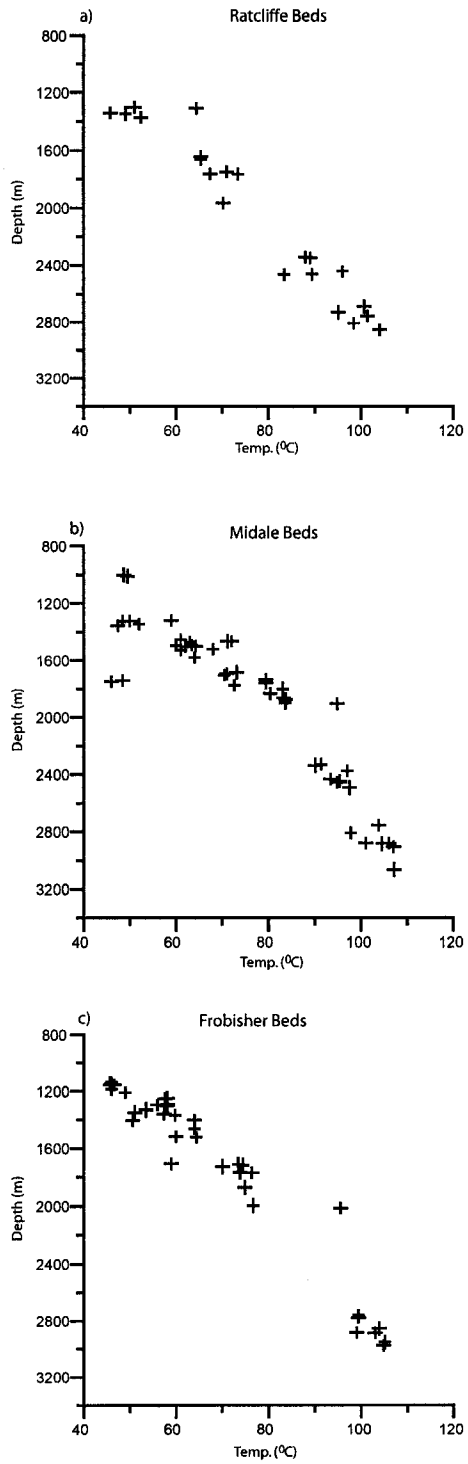

Figure 4.18. Temperature vs. depth for the three aquifers.
a) Ratcliffe Beds b) Midale Beds c) Frobisher Beds

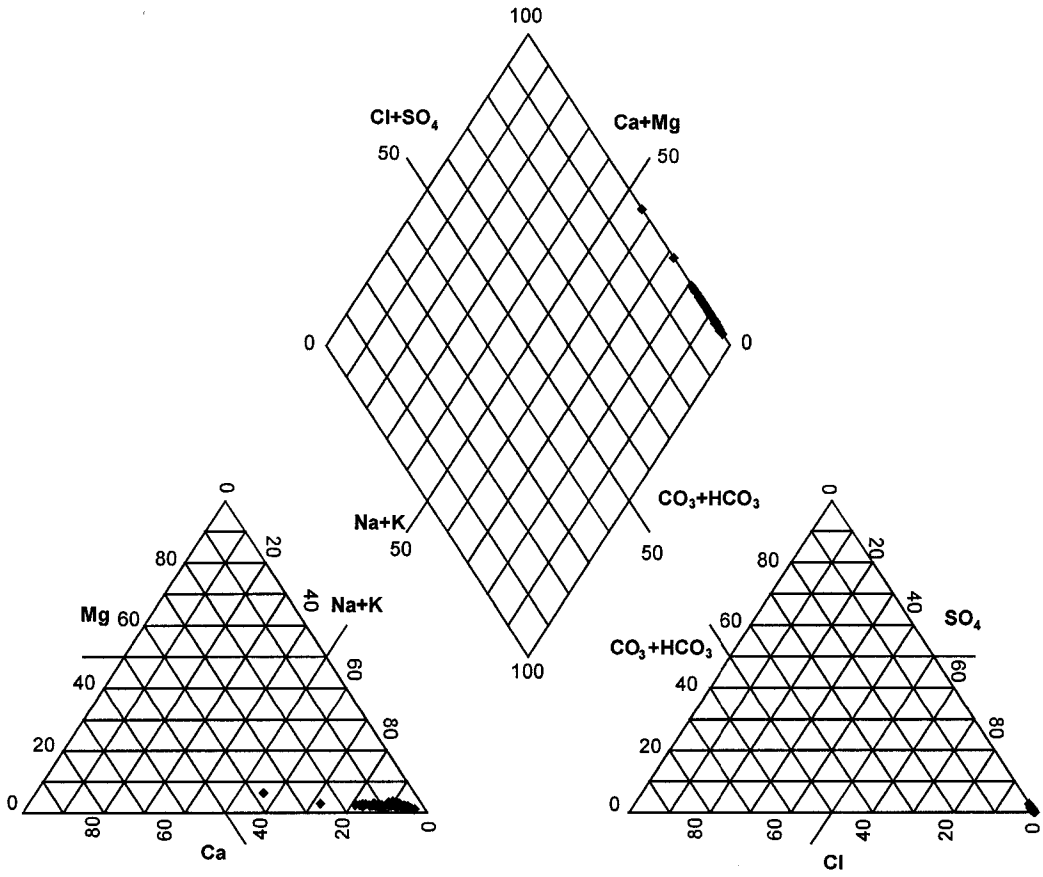

Figure 4.19. Piper plot illustrating the chemical compositions of the samples collected.

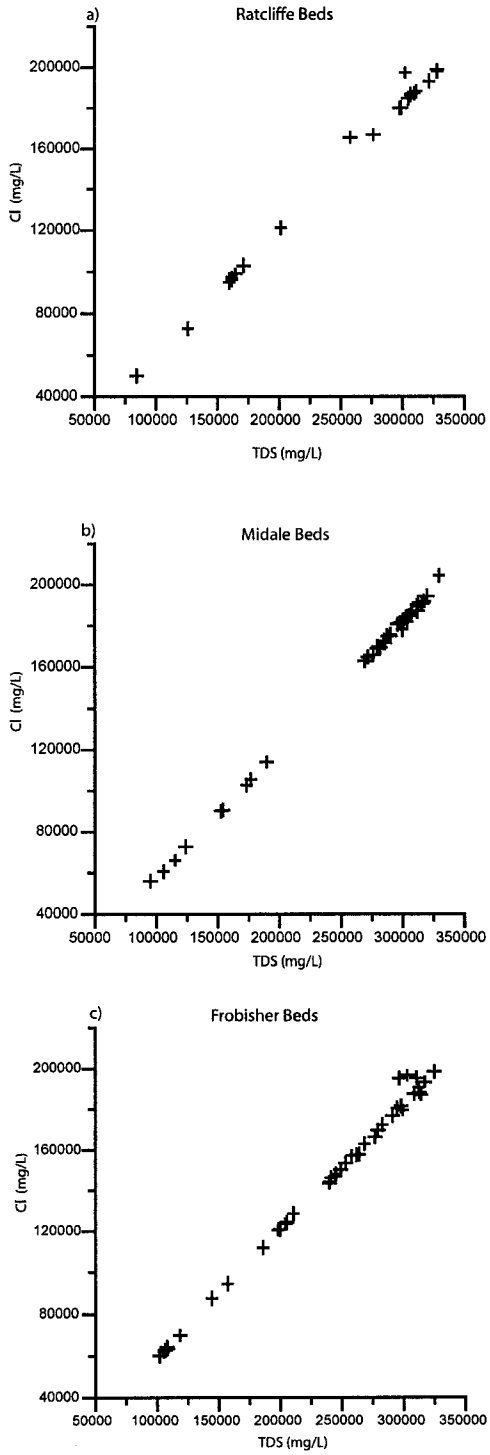

Figure 4.20. Cl vs. TDS for the three aquifers.
a) Ratcliffe Beds b) Midale Beds c) Frobisher Beds

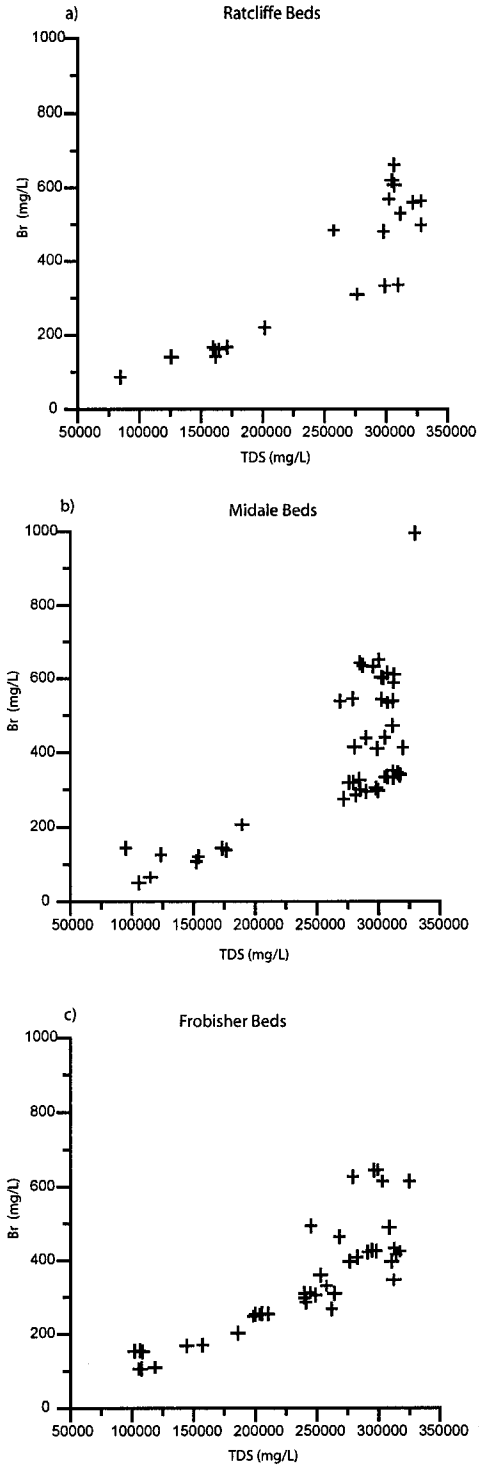

Figure 4.21. Br vs. TDS for the three aquifers.
a) Ratcliffe Beds b) Midale Beds c) Frobisher Beds

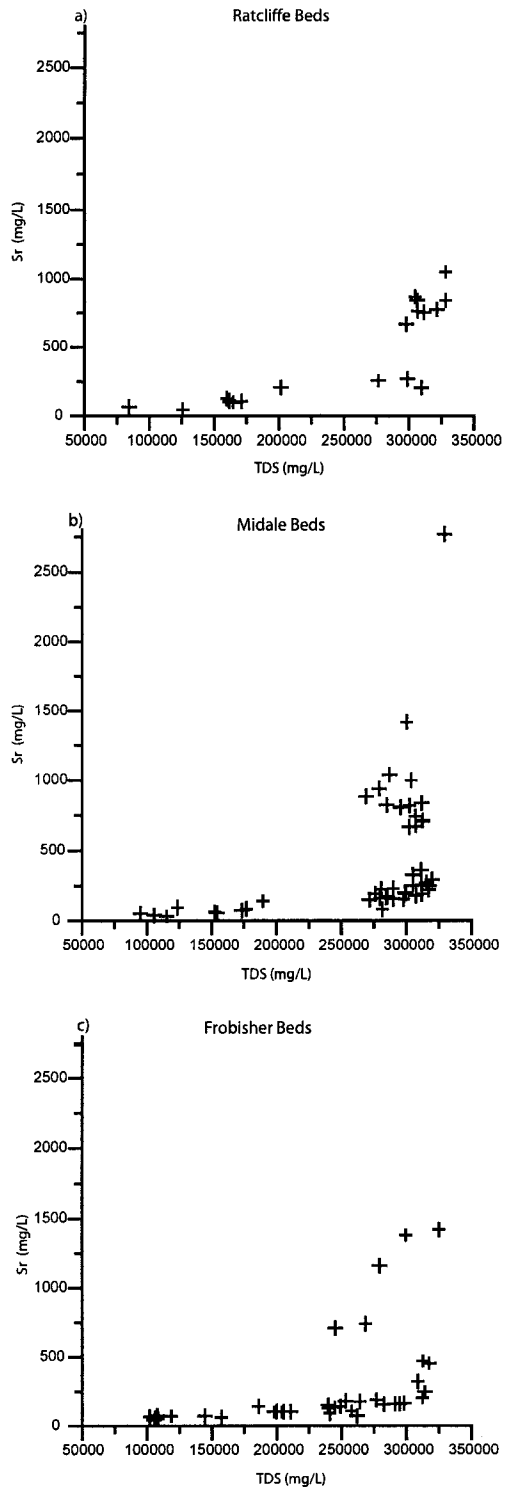

Figure 4.22. Sr vs. TDS for the three aquifers.
a) Ratcliffe Beds b) Midale Beds c) Frobisher Beds

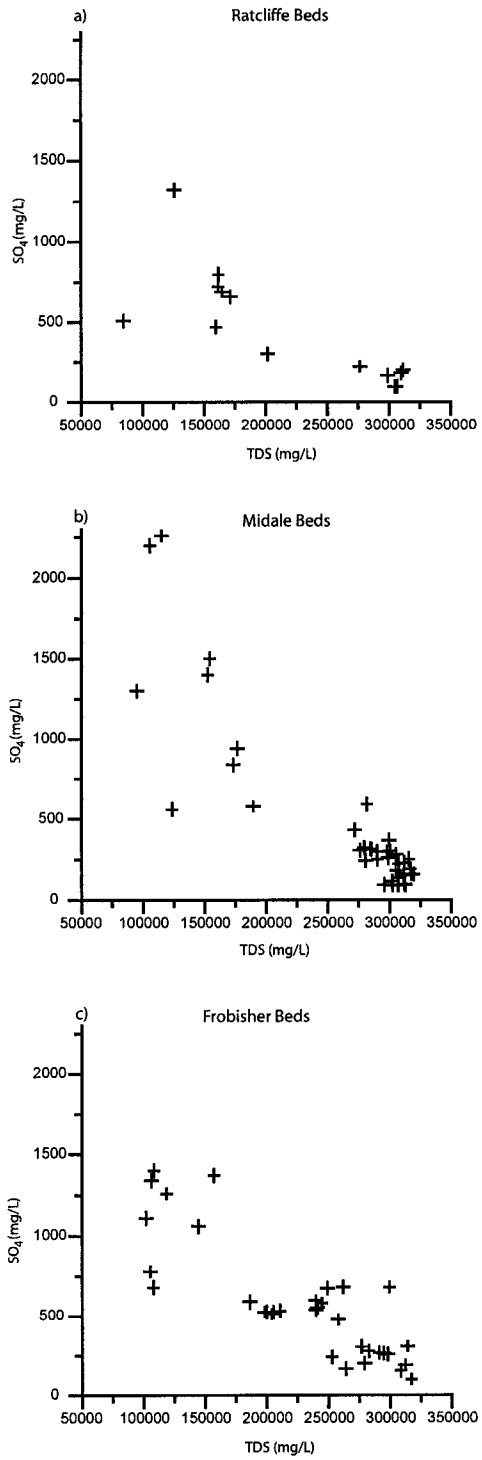

Figure 4.23. SO_4 vs. TDS for the three aquifers.
a) Ratcliffe Beds b) Midale Beds c) Frobisher Beds

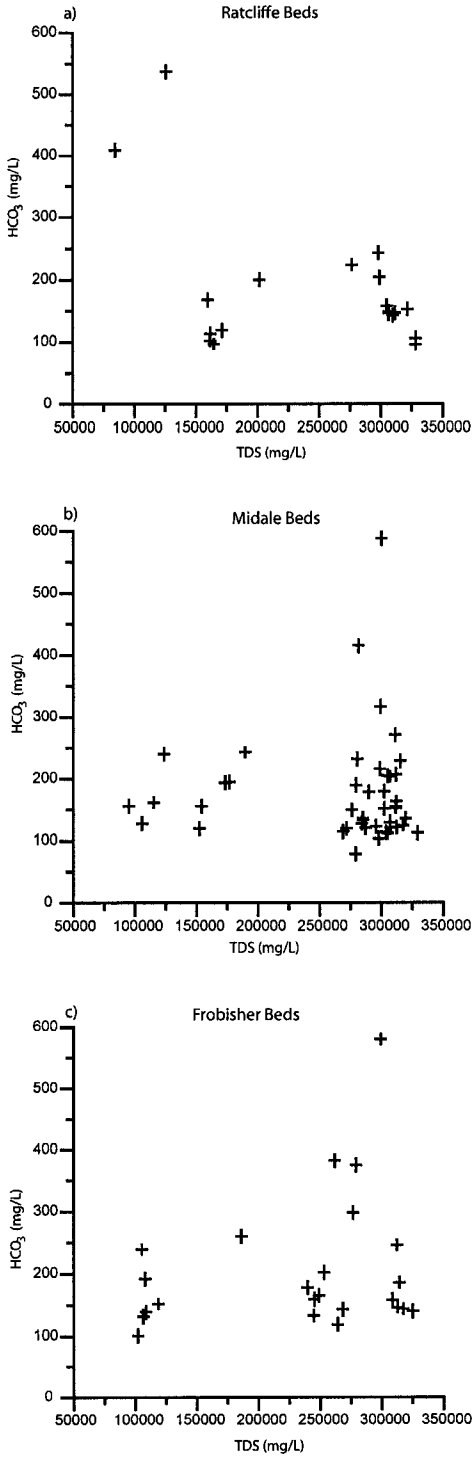

Figure 4.24. HCO_3 vs. TDS for the three aquifers.
a) Ratcliffe Beds b) Midale Beds c) Frobisher Beds

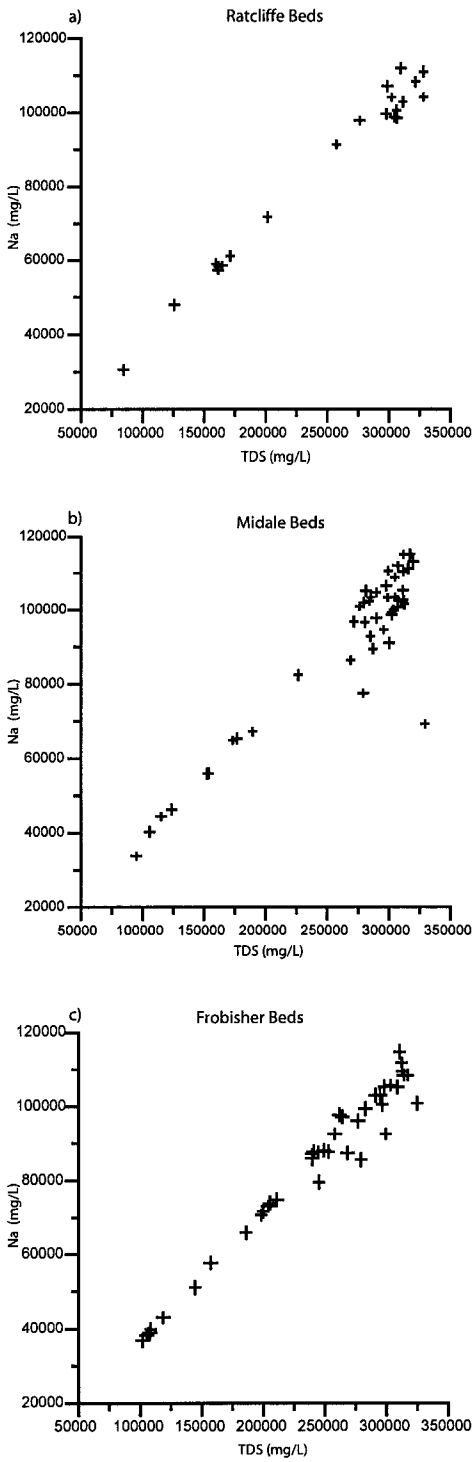

Figure 4.25. Na vs.TDS for the three aquifers.
a) Ratcliffe Beds b) Midale Beds c) Frobisher Beds

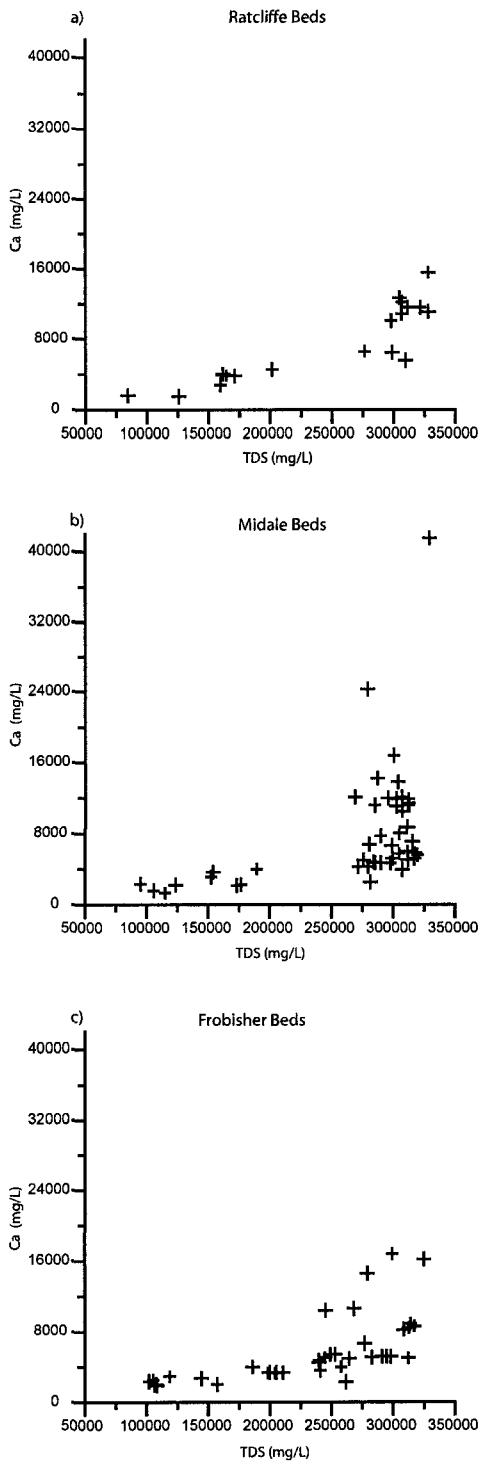

Figure 4.26. Ca vs. TDS for the three aquifers.
a) Ratcliffe Beds b) Midale Beds c) Frobisher Beds

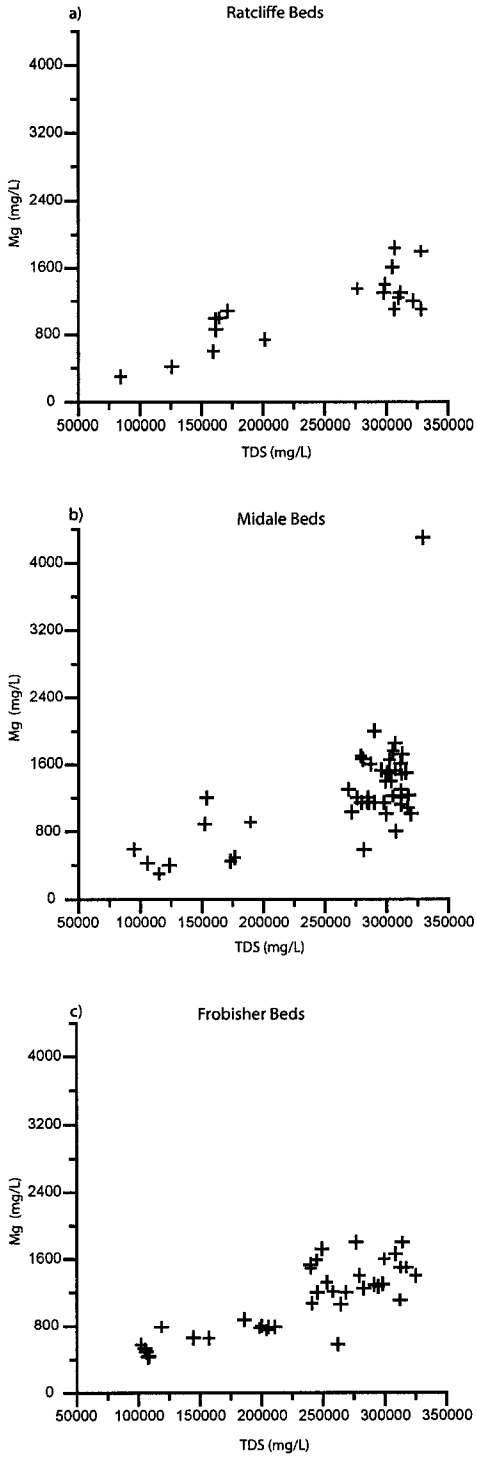

Figure 4.27. Mg vs. TDS for the three aquifers.
a) Ratcliffe Beds b) Midale Beds c) Frobisher Beds

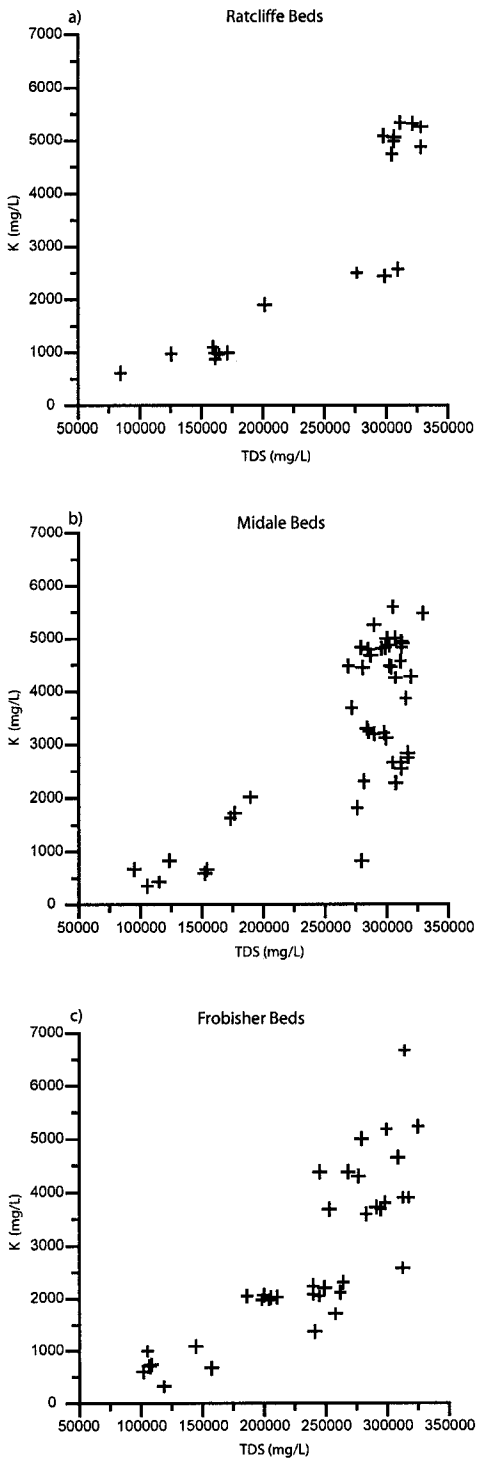

Figure 4.28. K vs. TDS for the three aquifers.
a) Ratcliffe Beds b) Midale Beds c) Frobisher Beds

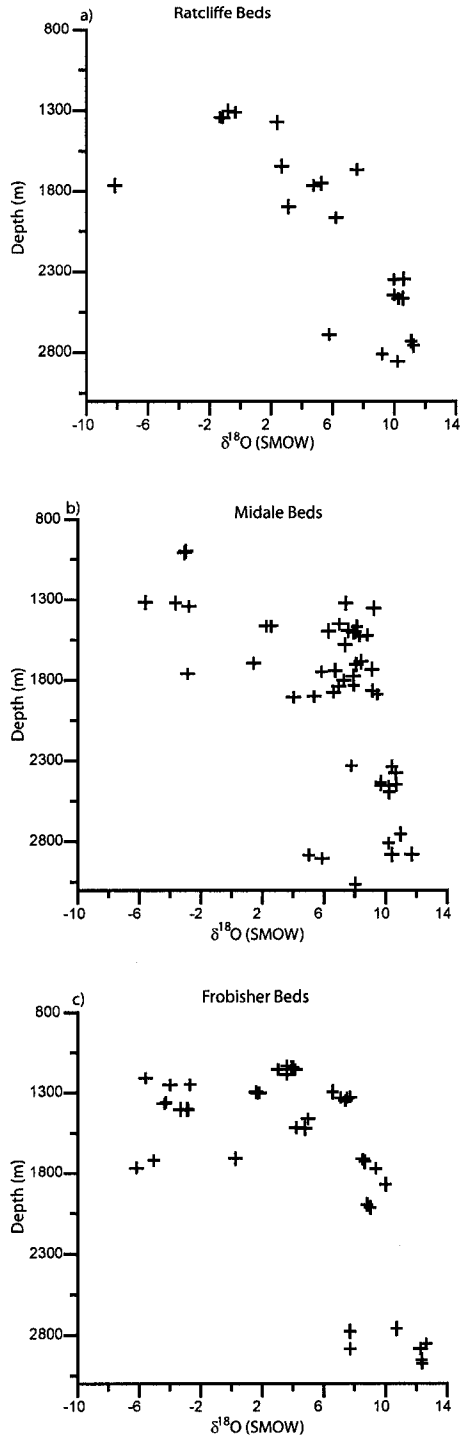

Figure 4.29. $\delta^{18}O$ vs. Depth for the three aquifers.
a) Ratcliffe Beds b) Midale Beds c) Frobisher Beds

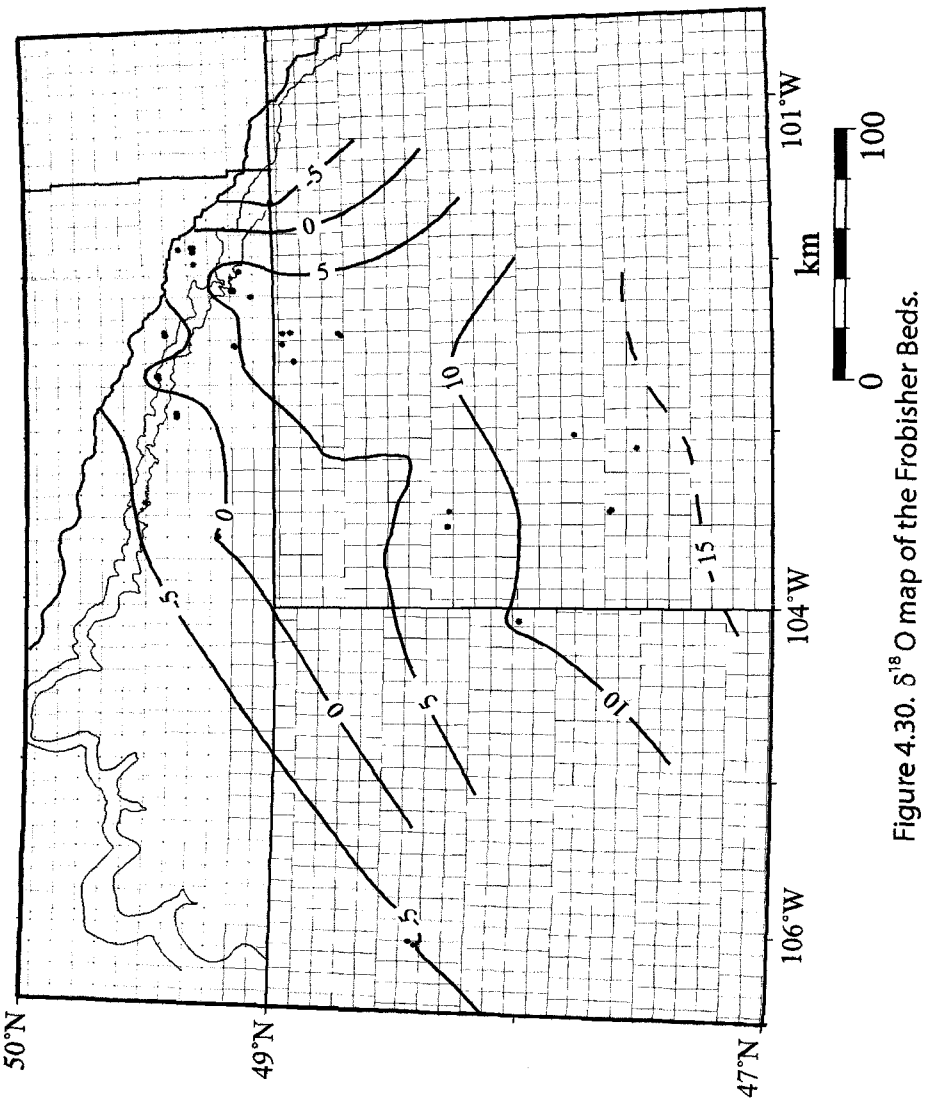

Figure 4.30. $\delta^{18}O$ map of the Frobisher Beds.

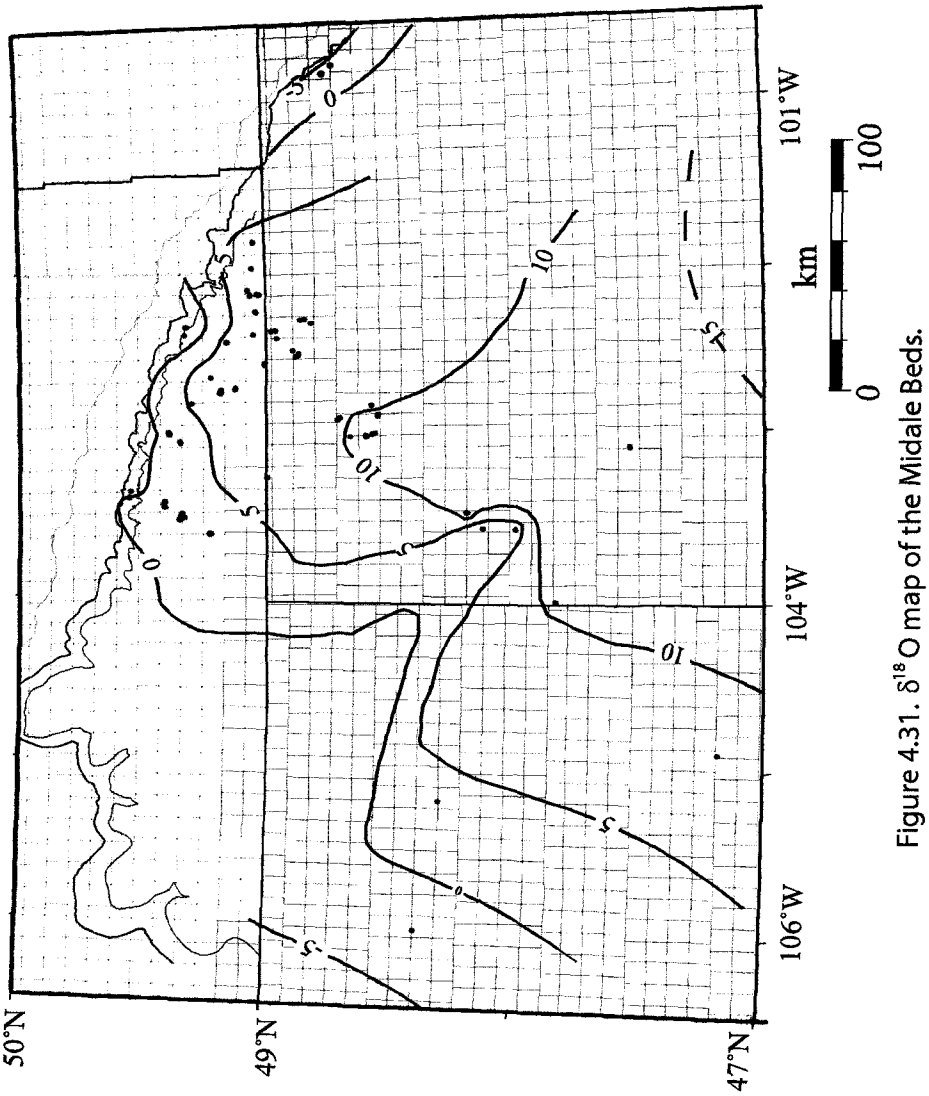

Figure 4.31. $\delta^{18}O$ map of the Midale Beds.

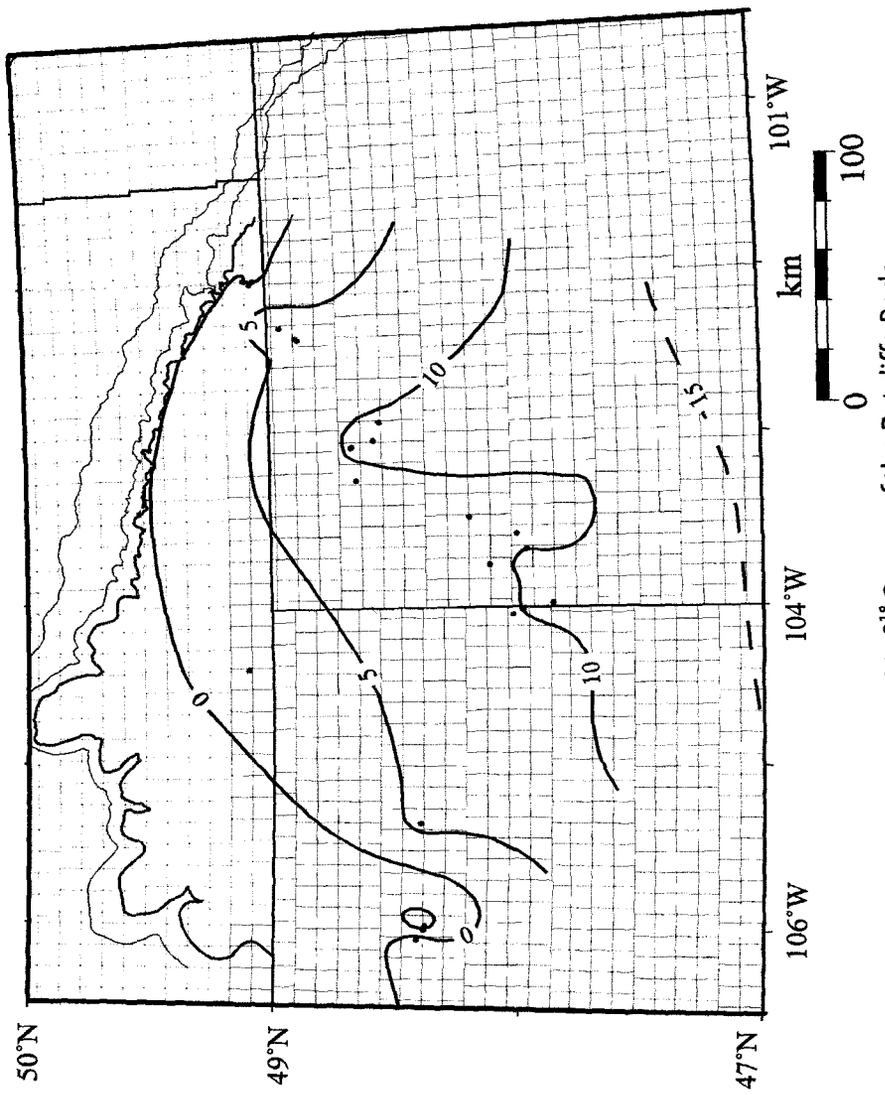

Figure 4.32. $\delta^{18}O$ map of the Ratcliffe Beds.

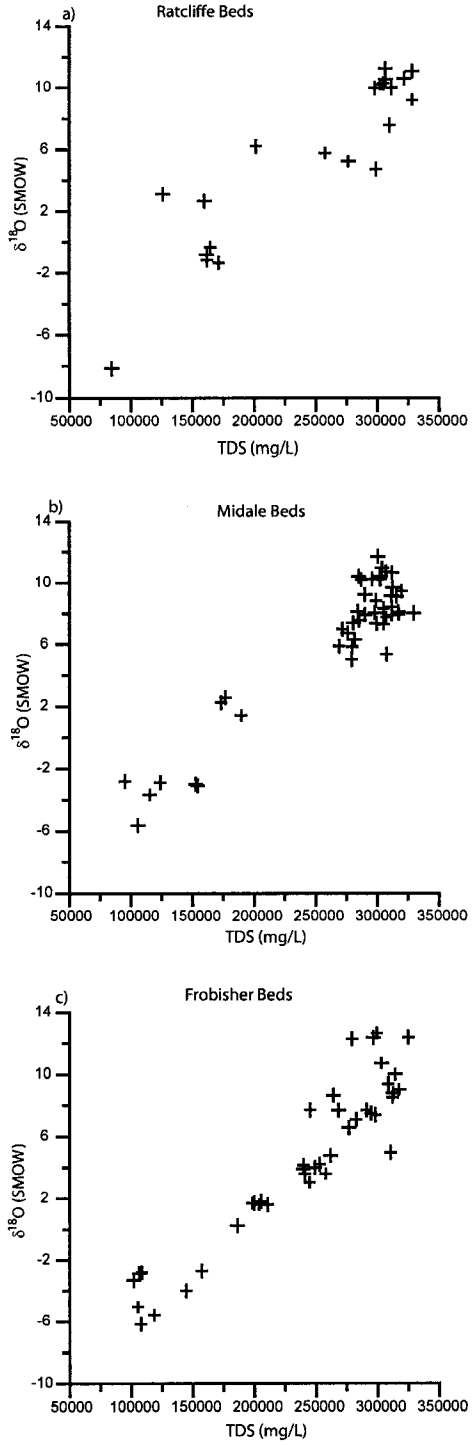

Figure 4.33. $\delta^{18}O$ vs. TDS for the three aquifers.
a) Ratcliffe Beds b) Midale Beds c) Frobisher Beds

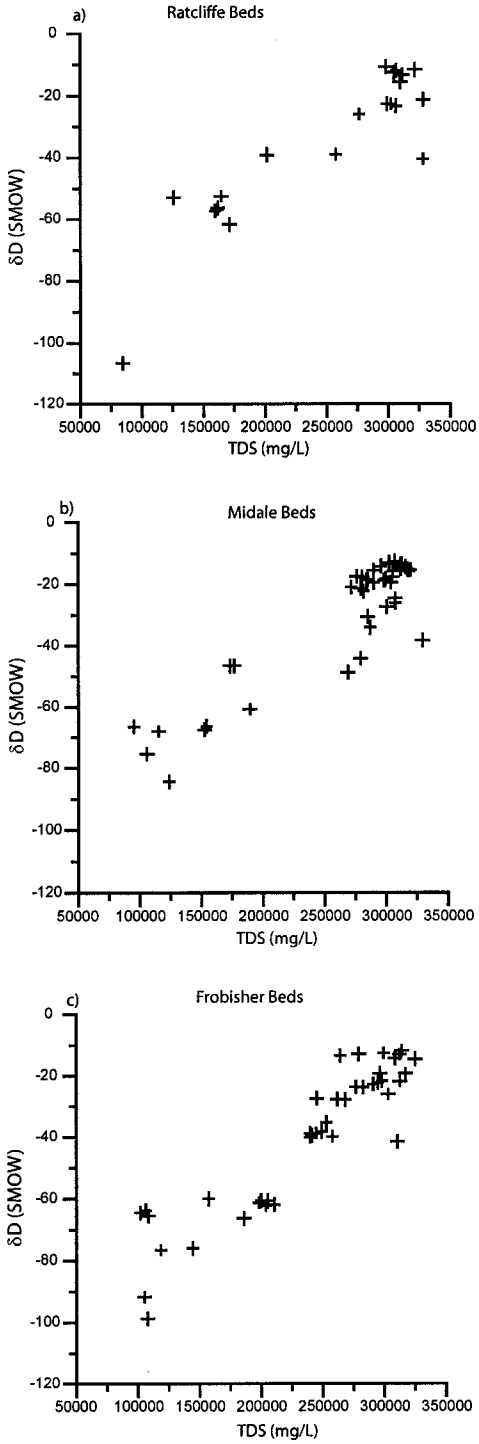

Figure 4.34. δD vs. TDS for the three aquifers.
a) Ratcliffe Beds b) Midale Beds c) Frobisher Beds

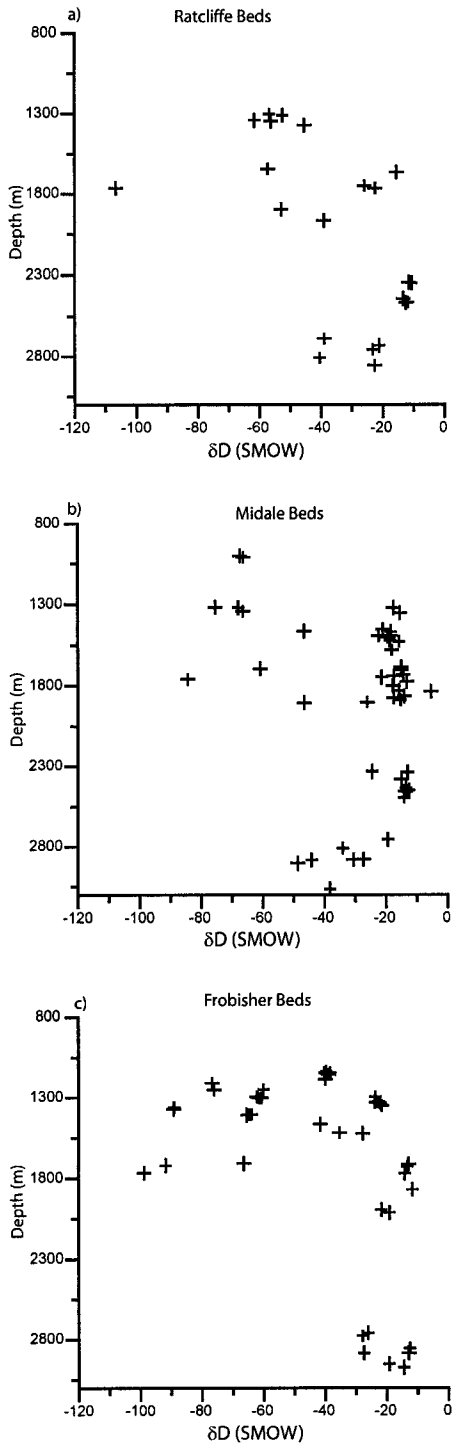

Figure 4.35. δD vs. Depth for the three aquifers.
a) Ratcliffe Beds b) Midale Beds c) Frobisher Beds

Chapter 5 Discussion

5.1. Applications to Petroleum Geology

5.1.1. Fingerprinting Formation Waters

Fingerprinting formation waters using stable isotopes has previously been demonstrated and applied in the potash mining (Wittrup et al., 1987) and oil industries (Rostron et al., 1998; Rostron and Holmden, 2000). Identifying the source of formation waters can lead to safer and more economical operation practices. Rostron et al. (1998), demonstrated that pre-Mississippian aquifers in the Midale area of Saskatchewan possessed unique isotopic compositions, and those could be used to fingerprint sources of contaminated water in hydrocarbon production and drilling activities.

Until now, isotopic fingerprinting has not been possible for Mississippian aquifers in the Williston Basin due to the lack of published stable isotope data from Mississippian aquifers. Data contained in this thesis (e.g., Figures 4.30, 4.31, 4.32) now enables the stable isotopic fingerprinting of Mississippian formation waters. Not only is it possible to fingerprint Mississippian formation waters, but it is feasible to identify the formation water of individual beds within the Mississippian of the Williston Basin (e.g., Jensen and Rostron, 2005).

For example, three water samples were collected during 2003 from three wells (2-35-2-4W2; 3-35-2-4W2; 13-26-2-4W2). Well 3-35-2-4W2 (sample ID 03-252; Table 4.1) produces from a perforated zone of 1515-1518 m and is interpreted to be producing from the Midale Beds (Figure 5.1 a) according to the Accumap database. The second sample (sample ID 03-253; Table 4.1) is from well 2-35-2-4W2 which has a perforated zone of 1495-1496 m. According to the Accumap database production is from the Midale Beds

(Figure 5.1 a). The third sample (sample ID 03-254; Table 4.1) well 13-26-2-4W2 produces from a perforated zone of 1521-1523 m and is listed to produce from the Frobisher Beds according to the Accumap database (Figure 5.1 a). Stable isotopic composition of sample 03-252, 03-253, 03-254 are $\delta^{18}O$ = 4.21‰, 6.29‰, 4.78‰, (Figure 5.1 a) respectively.

Stable isotopic analysis of the produced formation waters contradicts the geologic interpretation of the wells provided by Accumap (Figure 5.1 a), because sample 03-253 is isotopically unique from samples 03-252 and 03-254 (Figure 5.1 a). Using the geological mapping framework herein (i.e., following Kent et al., 2004), a revised geological correlation assisted by stable isotopes of formation waters is shown in Figure 5.1b. Sample 03-252 is now interpreted to be producing from the Frobisher Beds not the Midale Beds as previously thought (Figure 5.1 b). While sample 03-253 is still interpreted to be producing from the Midale Beds and sample 03-254 remains to be producing from the Frobisher Beds (Kent et al., 2004) (Figure 5.1 b). This new geologic interpretation is supported by the isotopic composition of the produced formation waters (Figure 5.1 b). Thus, isotopic fingerprinting within the individual beds of the Mississippian aquifers provides an alternative means for correlating formations (Jensen and Rostron, 2005).

5.1.2. "Out of Zone" Production Water

Produced formation water can have different sources in a well. The ideal situation is to have all produced water from the perforated zone. However, water can also enter a well bore from a casing leak below, or above, the perforation zone. Such leakage

problems can decrease the economic life of an oil well, as the increased cost of disposing of produced water can decrease the profitability of a well. Identifying casing leaks are problematic as typical analyses of produced waters only include TDS and major ions, making the general chemistry of formation waters difficult to distinguish (Rostron and Holmden, 2000). Recently, Rostron et al. (1998) showed that stable isotopes are able to distinguish "out of zone" produced water.

As an example, formation waters from producing wells in the Lignite field (Figure 2.6, Townships 161N-163N, Range 90W-92W) in North Dakota were collected. Two wells (sample 03-233 and sample 03-230) have been producing from the Midale Beds since 1956 (NDIC databases). Typical Midale produced formation waters from samples collected this field have TDS ranging from 270,000 to 311,000 mg/L and $\delta^{18}O$ of 8 to 9 ‰ (S.M.O.W.) (Table 4.1). The first sample (03-231), (Appendix D) has a TDS of 227,000 mg/L and a 77% produced water cut. The second sample (03-230) (Table 4.1) produced water with a TDS of 311,000 mg/L and produced water cut of 46%. Stable isotopic compositions of each sample were measured, with sample 03-231 being $\delta^{18}O$ = 1.99‰, and sample 03-230 being $\delta^{18}O$ = 9.15‰. Produced formation water from sample 03-230 is typical of other Midale producing wells in that area, which is also supported by the higher water cut and TDS. However, sample 03-231 is evidently producing water from a source other than the Midale, possibly leaking into the well bore from another formation. Remedial action on the casing could reduce the water cut and increase the economic life of this well.

5.2. Origin of Mississippian Formation Waters

The origin of subsurface brines has previously been examined by Walter et al. (1990), Hanor (1994) and others. Their conclusions were that brines are formed by one of two processes; 1) subaerial evaporation of seawater at surface or subaerially (Hanor, 1994); alternatively, 2) evaporite dissolution can occur; where fresher water migrates through the rock and increases in TDS, by dissolving halite within the strata and eventually becoming saturated with respect to halite (Walter et al., 1990). Evaporative concentration and evaporite dissolution can be active within the same basin (Stueber and Walter, 1994). Yet, the origin of brines in the Williston Basin has not been studied in detail with wellhead data with the exception of Iampen (2003), who examined the evolution and genesis of pre-Mississippian brines in the Williston Basin. The sections below explore the origin of water in the Mississippian strata in the Williston Basin using various chemical techniques.

The major and minor ionic compositions of subsurface formation waters are typically distinct compared to present-day meteoric water, i.e. seawater and evaporated seawater. As seawater is most likely the precursor to the majority of brines, present-day formation fluids are compared to seawater, by the ratio of components in seawater, or the component of the brines resulting from the evaporation of seawater (Hanor, 1987). There are several hydrochemical tests to distinguish the origin and evolution of formation waters.

5.2.1. Br-Cl-Na relationships in Mississippian Formation Waters

Chloride and bromide concentrations are used as a gauge for the degree of evaporation and halite dissolution in formation waters (Carpenter, 1978). Brines resulting from subaerial evaporation of seawater, and not associated with other chemical reactions or mixed with other fluids, will plot along the seawater evaporation trajectory (SET) (Figure 5.2). During the early stages of seawater evaporation, both Cl and Br increase in the remaining residual brine. Once halite precipitation occurs, Cl is preferentially removed as NaCl, and Br increases in the residual brine. This trend continues until carnallite saturation, then Cl and Br both increase in the residual brine (Figure 5.2).

If halite dissolution occurs, the Cl concentration increases, resulting in a vertical shift upwards from the seawater evaporation trajectory (Figure 5.2; not shown). Conversely, dilution by meteoric water with a brine produces a horizontal shift to the right, therefore plotting below the seawater evaporation trajectory (Carpenter, 1978).

The vast majority of samples plot to the left of the seawater evaporation trajectory representing varying degrees of halite dissolution, then subsequent seawater evaporation (Figure 5.2). A small number of samples have experienced little to no halite dissolution because they plot directly on the seawater evaporation trajectory (Figure 5.2). Samples collected in this study indicate that there is little to no mixing of meteoric water with basinal brines as the samples do not plot below the seawater evaporation trajectory (Carpenter, 1978). There are no differences or groupings in the data between the three formations indicating that all three formations have experienced similar degrees of evaporation and halite dissolution (Figure 5.2).

There are three possible models of evolution (Figure 5.3. a,b,c) to define the formation waters found in the Mississippian aquifers. First, only seawater evaporation can occur resulting in samples which plot directly along the SET (Figure 5.3a). Second, varying degrees of seawater evaporation can occur followed by halite dissolution (Figure 5.3b). Third, halite dissolution could occur followed by seawater evaporation (Figure 5.3c).

5.2.2. Halogen Systematics

In a plot of Na/Br vs. Cl/Br (Figure 5.4) formation waters that have evolved from seawater via halite dissolution or evaporative concentration should define a trend that passes through the composition of seawater and has a slope consistent with equimolar decreases or increases in Cl and Na (Walter et al., 1990). Prior to halite saturation, Na, Cl, and Br ratios are constant during the increasing evaporation of seawater as all three solutes increase in concentration by the same factor. After halite saturation, Na and Cl are removed from solution, excluding Br. Na/Br and Cl/Br ratios in excess of normal seawater plot on a 1:1 line are representative of surface or subsurface dissolution of halite by the fluids (Hanor, 1994). Seawater is plotted on Na/Br vs. Cl/Br plot (Figure 5.4) to distinguish between formation waters derived from halite dissolution and those representing evaporated seawater. Samples which plot above and to the right of seawater derive their salinity from dissolution of halite. Conversely, samples which plot below and to the left of seawater derive their salinity as seawater evaporated past halite saturation (Walter et al., 1990).

The Mississippian data from this study span the spectrum of Na/Br vs. Cl/Br ratios, and all three aquifers encompass the range of ratios (Figure 5.5). All three aquifers display a varying range in their origin of salinity (Figure 5.5). Salinity derived from halite dissolution represents the majority of the data (Figure 5.5). All three formations have samples that derive their salinity as evaporated seawater; this presence of an evaporated end-member brine has not been previous recognized in the Mississippian strata of the Williston Basin.

Mapping the Cl/Br ratios of the samples in plan view produces a trend of decreasing Cl/Br with increasing depth (Figure 5.6, 5.7, 5.8). Samples which derive their salinity from evaporated seawater are located south of the basin center (Figure 5.6, 5.7, 5.8).

5.2.3. Stable Isotope Compositions

Stable isotopes have long been used to study the origin and evolution of formation waters (Clayton et al., 1966; Steuber et al., 1998, and others). Isotopic composition of formation waters can be influenced by the mixing of evolved formation waters and meteoric waters, and the resulting mixing trends can be used to identify a fluid's migration and evolution.

Fractionation of the stable isotopes of hydrogen and oxygen within the surface regime occurs predominantly by changes of state (Hitchon and Friedman, 1969). The temperature at which precipitation occurs generally correlates with latitude and altitude, thus temperature is one of the controlling factors on the fractionation of oxygen and hydrogen isotopes (Dansgaard, 1961). The other main component of isotope fractionation is the depletion ("rain-out") of the heavy isotopes (D, ^{18}O) with each progressive

precipitation event as an air mass migrates inland from the ocean. "Rain-out" depletion has been modelled as a Raleigh fractionation, superimposed on this process is a temperature effect; colder temperatures of condensation deplete the lighter isotopes in the air mass more effectively (Clark and Fritz, 1997). These effects combine to produce a relationship referred to as the global meteoric water line (GMWL) (Craig, 1961). The isotopic composition of precipitation on the Earth produces a straight line trajectory in a $\delta^{18}O$ vs. δD plot, with an equation of $\delta D = [\ 8\ \delta^{18}O] + 10$.

As the precipitation leaves the atmosphere and enters the subsurface its stable isotopes are no longer affected by the Raleigh fractionation and consequently the isotopic value is fixed to the region of precipitation. It was demonstrated that sedimentary basins have individual isotopic lines described by the $\delta^{18}O$ and δD compositions of the basin's formation waters (Figure 5.9). The basin intercept with GMWL represents the current meteoric water for that basin (Clayton et al., 1966). Hydrogen and oxygen isotope relations of formation waters can be used to determine the possibility of two-component mixing between depleted meteoric water and enriched deep basin brines (Stueber et al., 1998). Once in the subsurface hydrogen and oxygen isotopes are primarily affected by rock-water interactions with the host rocks. These reactions are predominantly oxygen isotopes exchanging with the host rocks. Isotopic exchange of hydrogen may occur, however there is very little hydrogen in rock-forming minerals thus, the potential for isotopic exchange is less than for oxygen. Isotope exchange reactions occur on geologic time thus conferring isotopic signatures to formation waters that have remained isolated from the atmosphere (Clark and Fritz, 1997).

Defining the migration history of Mississippian fluids in the Williston Basin will be achieved by the application of stable isotope relations. The depleted D and ^{18}O isotopic compositions of meteoric waters in the Williston Basin provide an excellent indicator for meteoric waters mixing with evolved or connate formation waters (Rostron et al., 1998).

Isotopic compositions of formation waters from the Mississippian aquifers define a basin trend line which intersects the GMWL at a composition not representative of present day meteoric water for the Williston Basin (Figure 5.10). A large spread around the trend of $\delta^{18}O$-δD is observed. This rough trend will be examined below. There is no isotopic differentiation between the three aquifers, demonstrating that all three formations have experienced similar degrees of isotopic exchange with the host rocks (Figure 4.29).

A similarity in oxygen isotopes and TDS patterns suggest that the highest TDS corresponds with the enriched oxygen isotopes, such that samples with TDS > 300,000 mg/L correspond with $\delta^{18}O$ of +10‰ (Figure 5.11). Samples which derive their salinity from evaporitic seawater are located south of the basin center, and these samples generally correspond with $\delta^{18}O$ > +10‰ (Figure 5.12). These preceding observations (Figures 5.11, 5.12) will form the basis for the interpretation of the evolution of Mississippian formation waters in the Williston Basin.

5.3. Implications for Paleohydrogeology

The existing flow model for the Mississippian has formation waters migrating from the south-southwest to the north-northeast across the basin (Downey, 1984; Bachu and Hitchon, 1996). The flow system is proposed to be a continuous system across the entire basin (Downey et al., 1987; Lefever, 1998). This research demonstrates a new variable

flow system which has originated from multiple fluid events across the basin. This is shown by integrating stable isotopes with Na-Cl-Br systematics to further elucidate the formation waters and their evolution and migration history.

As mentioned previously there is a spatial correlation of brines having TDS > 300,000 mg/L, $\delta^{18}O$ > 10 ‰ and, Cl/Br less than seawater (~286). Generally, they are found south of the basin center at approximately 47.2^{0}- 47.8^{0}N (Figure 5.11 and Figure 5.12). By overlying the Cl/Br values relative to seawater with a $\delta^{18}O$-δD plot (Figure 5.13), further classification of the formation waters is observed. Cl/Br ratios are separated by: i) samples which plot below and to the left of seawater (Cl/Br < seawater,); ii) samples which plot relatively equal to seawater (Cl/Br ~seawater); iii) samples that plot above and to the right of seawater (Cl/Br > seawater). At first glance, a pattern emerges with the majority of samples with Cl/Br ≤ seawater being grouped in a region with enriched $\delta^{18}O$ values and relatively depleted δD values (Figure 5.13). The aforementioned samples can be separated further by spatial location in the basin as these samples have TDS > 300,000 mg/L, $\delta^{18}O$ > 10 ‰, and Cl/Br less than seawater (~286), corresponding to the samples that occur south of the basin center. Thus, these samples are interpreted to represent residual waters that have migrated a minimum distance since deposition. This interpretation opposes previous research that believed a continuous flow system is present in the Mississippian and flow was directed to the north and south of a brine slug (TDS > 300,000 mg/L) located in the basin center (Figure 2.5). A pre-Mississippian brine slug with Cl/Br ratio less than seawater was also found in a similar location in the basin (Iampen, 2003).

Further analysis involving spatial location, isotopic composition and Cl/Br ratio in comparison to the GMWL will further define the fluid evolution in the Mississippian aquifers.

5.4. Evidence for Multiple Fluid Pulses in the Williston Basin

By integrating the stable isotopic composition, the Cl/Br ratio, and the spatial location in the basin, it is interpreted that two isotope lines are present in the Mississippian aquifers (Figure 5.13). Waters that have originated from halite dissolution generally plot along what it termed the "upper" basin trend (Figure 5.13). Conversely, waters originating from evaporated seawater plot along what is termed the "lower" basin trend (Figure 5.13). Separate isotopic basin trends have not been previously observed in the Williston Basin. Data presented here provide evidence of two separate fluid events in the Mississippian aquifers and thus the Williston Basin. Separate isotopic trends prompt the postulation of two separate evolutionary pathways within the Mississippian aquifers. To investigate this interpretation, samples were grouped based on spatial location and $\delta^{18}O$-δD composition. This analysis further delineates the samples in the "upper" basin trend, and these samples generally reside along the subcrop trends in the northern portion of the basin. Samples that plot along the "lower" basin trend are found in the western and southern portions of the study area (Figure 5.14).

5.5. Deuterium Shift in Mississippian Waters in the Williston Basin

Numerous factors or mechanisms could account for the scatter in deuterium along a basin line, for a portion of the samples and merits discussion. The isotope data (Figure

5.10) appear to scatter about a basin trend line. However the scatter is larger ($\delta D = 20‰$) than the uncertainty of the measurements ($\delta D = \pm 3‰$) and when considered with other tracers previously discussed (Cl/Br), can be interpreted as evidence for multiple fluid events. It could be suggested that there is scatter on one basin trend line versus two separate basin trend lines present. This postulation is unrealistic as the scatter is defined spatially to separate portions of the basin (Figure 5.14).

Analyzing the isotopic trends in relation to the GMWL, it is evident that the lower trend intersects the GMWL at or near current meteoric water for the Williston Basin (Figure 5.15). Conversely, the upper trend intersects the GMWL at a meteoric water representative of a warmer temperature regime (Dansgaard, 1964);

$$\delta D = 5.6\ T_{annual} - 100‰\ SMOW$$

$$\delta^{18}O = 0.695\ T_{annual} - 13.6‰\ SMOW$$

where T_{annual}: is the annual temperature

One alternative is that the formation waters in the "upper" trend are waters that could have originated from a different paleo-latitude and temperature regime other than what is currently present in the basin. Alternatively, the area in question could have experienced a large scale fluid movement event composed of waters of a warmer temperature. The validity of these hypotheses will be examined. Also, the reason for the enrichment in deuterium of the "upper" basin trend relative to the "lower" basin trend will be investigated.

Firstly, it could be suggested that the error of analysis is responsible for the shift. However the uncertainty in the measurement of δD is $\pm 3‰$ (SMOW), this uncertainty is

smaller than the vertical shift in δD (15-30‰ SMOW) (Figure 5.15). Therefore, the uncertainty of the measurement can not be solely responsible for the shift in deuterium.

Secondly, samples that occur on the upper trend could be a result of a unique geo-thermal temperature regime in separate regions of the basin. This claim is unlikely because temperature does not correspond to the shift in deuterium (Figure 5.16) as the "upper" and "lower" trends are not evident as distinct groups on plots of temperature vs. δD and $\delta^{18}O$.

Thirdly, the possibility of rock water interactions causing the shift in deuterium is not likely as the strata in the Mississippian of the Williston Basin are composed of carbonate rocks interbedded with anhydrite and evaporite layers. These rock units contain little to no hydrogen in their chemical structure and an abundance of oxygen. Therefore, water-rock interactions would conceivably result in enrichment in $\delta^{18}O$ but not δD. This enrichment is evident as $\delta^{18}O$ compositions attain values of +10-12‰ (SMOW).

Further examination of rock water interactions involves the calcite-water equilibrium fractionation equation (O'Neil, 1969), to determine if the formation waters are in equilibrium with the carbonates (Figure 5.17). Mississippian carbonates in the Williston Basin, possess $\delta^{18}O$ values ranging from 22 to 30‰ (SMOW) (Nickel and Qing, 2004). In general, the formation waters are in equilibrium with calcite. Samples which are found above the 30‰ calcite curve are generally found along the "upper" basin trend. This represents further evidence to support the interpretation that a fluid event recently migrated into the Mississippian carbonates from another source, and are not in equilibrium with the calcite. Samples which plot below the 20‰ curve are generally found in Montana, signifying that they are still evolving to calcite equilibrium. There are

two samples that plot below the 20‰ curve and occur on the "upper" basin trend, it is likely that these samples have either not had time to equilibrate with the calcite or the DST temperature is incorrect.

Lastly, the starting composition of the original water could be non-uniform across the basin. This alternative would require either a large scale fluid movement event, composed of waters at a temperature warmer than present-day, or a paleo-geographic temperature regime warmer than present day. If the waters originated from a paleo-latitude closer to the equator the question arises why are all the waters in the basin not affected by this temperature increase? The possibility of only a small portion of the basin being affected by a climatic change is unreasonable. Therefore, the other alternative involves a mass fluid flow event composed of waters at a warmer temperature and such flow events have been documented (Chipley and Kyser, 1989).

Large scale fluid events in the Williston Basin have been recorded as fluid inclusions in halite (Chipley and Kyser, 1989). Three fluid events have been recognized; the first occurred after the deposition of the Devonian Prairie Evaporite, at a temperature of 35^0C and involved water with δD and δ^{18}O near -92 and -8‰ respectively. Then a second fluid event has been recorded with a temperature of 50^0C implying waters with δD near -70‰ and δ^{18}O of -6‰. Finally, a third fluid event occurred having a temperature of 80^0C involving fluids with δD and δ^{18}O near -141 and -15‰, respectively. This event occurred at maximum burial during the end of the Cretaceous (70 mya) (Chipley and Kyser, 1991). This third fluid event has δD and δ^{18}O values that correspond to the intersection of the GMWL and the "upper" basin trend (Figure 5.15). It is interpreted that this fluid event is responsible for the shift in deuterium and creation of the "upper" basin trend. Waters that

are found along the "upper" trend have evolved from this fluid event in much the same fashion as waters that evolved from meteoric water in the "lower" basin trend.

5.6. Implications for Paleo-Flow

Mississippian fluids record two different evolutionary pathways both chemically and spatially. An examination spatially (Figure 5.14) and compositionally (Figure 5.15) provides clues about how the fluids evolved chemically in the basin. These geochemical data demonstrate the migration history of the Mississippian brines, by implementing the isotopic composition and halogen systematics the fluid migration history can be unravelled. As residual seawater is still present in the basin it is interpreted that any pre- or post-Cretaceous fluid flow events were not pervasive enough to flush the residual brine. There are regions surrounding the residual brine that indicate active halite dissolution inferring fluid flow. For evaporated residual seawater to still be present while flushing has occurred in other areas there must be preferential flow around the residual slug to the north. Whether flow is occurring to the south of the residual brine slug is undetermined, further sampling south would be required to indicate if fresher waters are migrating around the brine slug to the south.

The present day chemistry of Mississippian formation waters in the Williston Basin is a result of a four step process: (Figure 5.18 a,b) First, is the deposition of the evaporated seawater in the deepest part of the basin. Through time the evaporated seawater has evolved into a residual brine as a result of little to no migration since deposition. These formation waters are characterized by the heaviest $\delta^{18}O$ compositions (> 10‰), Cl/Br <

seawater and TDS> 300,000 mg/L. These formation waters are present in the study and are located south of 48^0 latitude and between 103^0 and 104^0 longitude.

Second, the upper basin trend along the Mississippian subcrop trend experienced a fluid pulse near the end of the Cretaceous (70 mya) (Chipley and Kyser, 1991). These formation waters occur along the subcrop trend have evolved along the upper basin trend, enriched compositions of δD relative to other Mississippian formation waters. Fluid flow within the upper basin is directed to an area which corresponds to isopach thickening (Figure 2.6) in that area (Figure 5.18 a,b, arrow labelled A), particularly in the Frobisher Beds.

Thirdly, the more recent migration of formation waters have came in from the west and migrated in an eastward direction towards the basin center (Figure 5.18 a,b, arrows labelled 1,2,3,4). These formation waters occur along the lower basin trend, and generally display enrichment in $\delta^{18}O$ along the migration path.

The fourth step is the mixing of the residual brine with the migrating lower basin trend formation waters (Figure 5.18 a,b, labelled "mixing zone"). Migration continues northward towards the Nesson Anticline (Figure 5.18 a,b, arrows labelled 3,4).

5.7. Absence of Ca-Cl waters in Mississippian aquifers

Recent research has found Ca-Cl types in pre-Mississippian brines (Iampen, 2003; Khan, 2006). Khan (2006) also found an absence of Ca-Cl brines in the Mississippian aquifers in the northern portions of the basin, and speculated that they could occur south of his study area in the deep basin (Khan, 2006). With the absence of Ca-Cl waters and

the presence of residual brines in this study it can be postulated that the Mississippian aquifers did not contain Ca-Cl waters.

This presence of residual brines in pre-Mississippian and Mississippian strata both occurring south of the basin center implies that the "connate" waters in the Williston Basin have not been flushed. These findings provide evidence to the hypothesis that global seawater chemistry has a secular variation through geologic time (Lowenstein, 2003). The combination that Ca-Cl brines are found in strata when the global seawater was enriched in Ca (pre-Mississippian) and the absence of Ca-Cl brines when seawater was depleted with Ca (Mississippian), demonstrates the hypothesis of changing seawater with geologic time is viable.

5.8. Summary of Fluid Origin and Evolution

Hydrochemical distribution of the formation waters in the Mississippian aquifers can be described by two brine forming mechanisms, halite dissolution and seawater evaporation. Halogen systematics indicates that the majority of the brines have their salinity derived from halite dissolution. Major ion chemistry and halogen systematics provide evidence that brines south of the basin center have derived their salinity from evaporated seawater and represent residual connate seawater.

Stable isotope compositions display the highest levels of enrichment occurring near the basin center, south of the basin center and along the Nesson Anticline. These compositions are explained by increased residence time resulting from low flow velocities in turn increasing rock-water interactions and enrichment in the heavier

isotope. Isotope relations are interpreted to display two separate basin trends: an upper and lower trend.

This trends are defined by a shift in deuterium, halogen systematics and spatial location (Figure 5.18 a,b). The lower trend represents waters that are typical of present-day meteoric waters that have migrated into the basin then encountered halite and thus evolved to form brines. Infiltrating fresher meteoric waters have flushed the evaporated seawater, first at the basin margins, then further into the basin center subsequently leaving only a residual brine slug south of the basin center. The migration continues mixing with the residual brine present at the basin center and continues to migrate northward; this flow regime is a result of the Laramide uplift.

The upper trend is not typical of present-day meteoric waters that have evolved to form brines. The original water is interpreted to be sourced from a large scale fluid event that occurred during the end of the Cretaceous (70 mya) and is responsible for the shift in deuterium that occurs in the formation waters in that area. Calcite-water equilibrium fractionation further supports this theory as the waters present on the upper trend are not in equilibrium with calcite inferring that the formation waters have not had sufficient time to equilibrate with the strata.

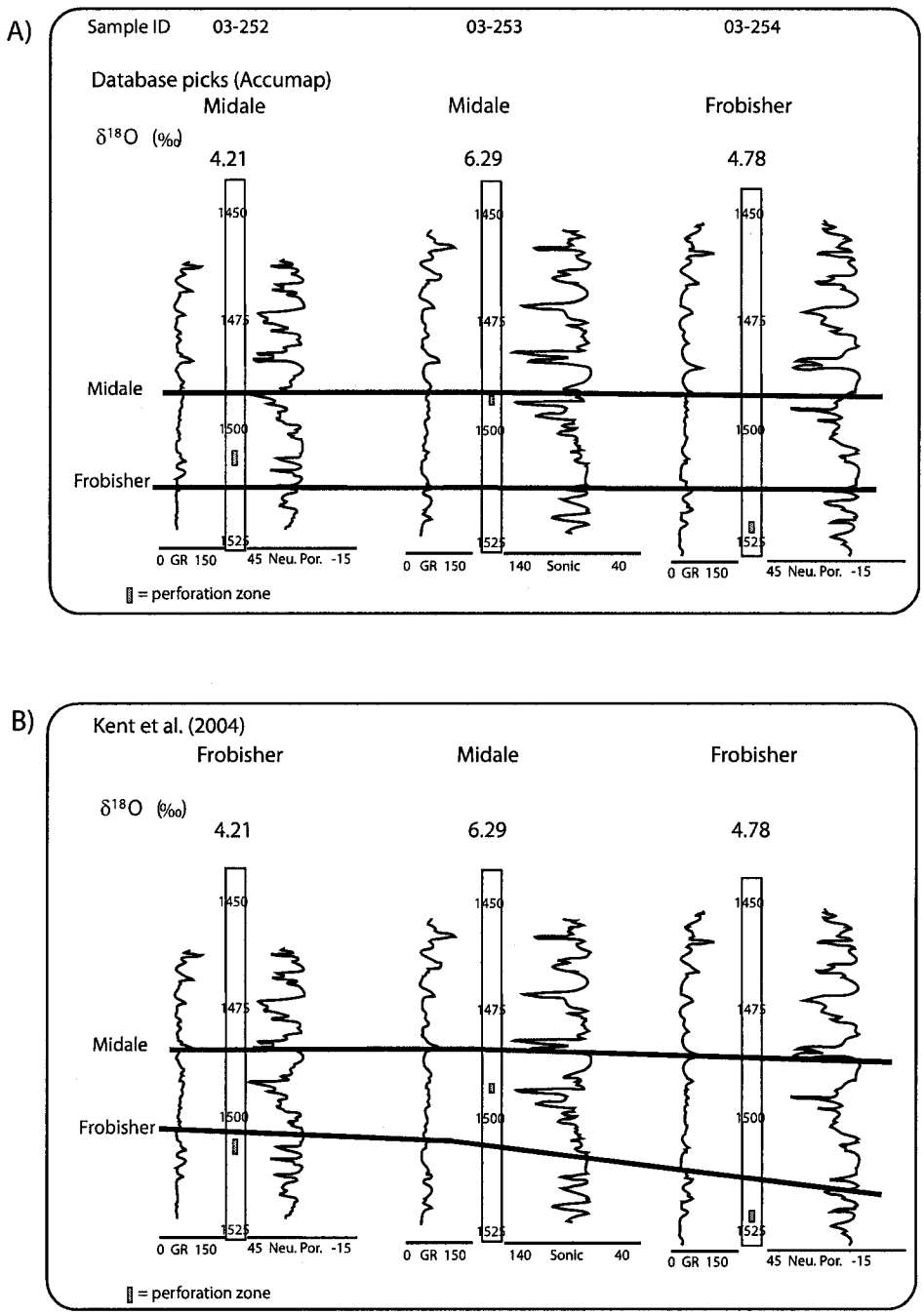

Figure 5.1. Example of isotope hydrostratigraphy. a) Accumap stratigraphy b) Kent et al. (2004) stratigraphy. Isotopic compositions from sampled collected for this study.

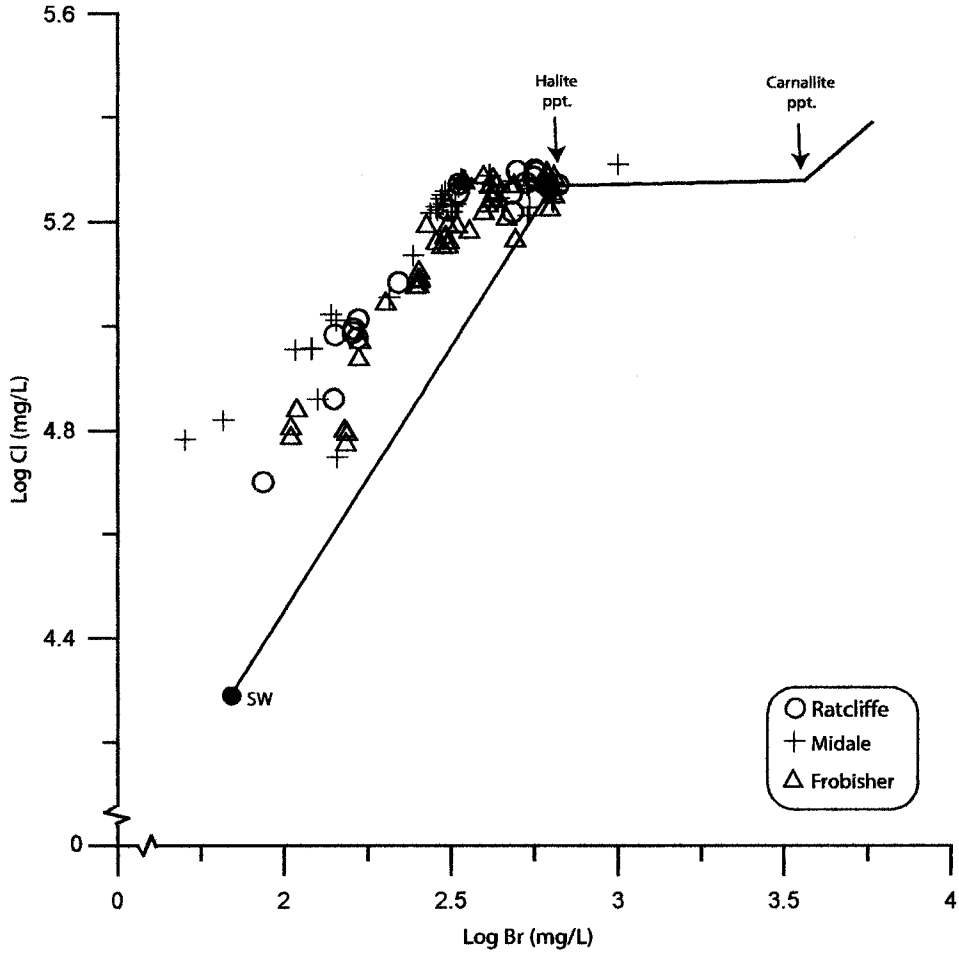

Figure 5.2. Log Br vs. Log Cl, "Carpenter" Diagram for all three Mississippian Aquifers. Seawater evaporation trajectory (SET) from McCaffrey et al. (1987). SW= seawater composition.

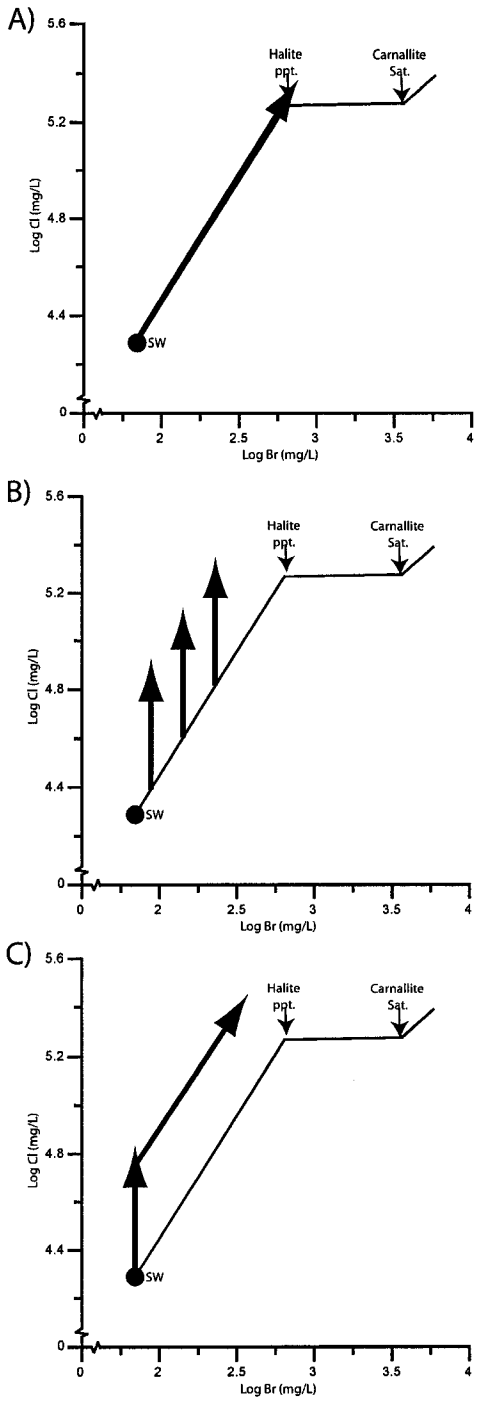

Figure 5.3. "Carpenter" Diagram demonstrating three models of evolution for Mississippian formation waters. a) seawater evaporation b) seawater evaporation followed by halite dissolution c) halite dissolution followed by seawater evaporation

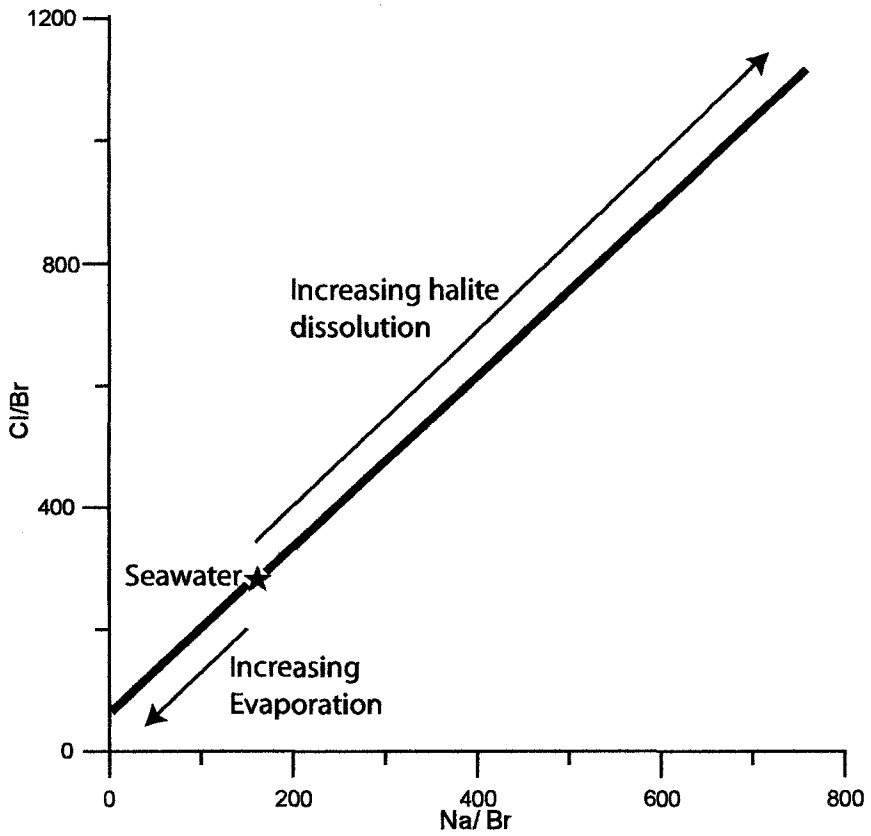

Figure 5.4. Plot of Na/Br vs. Cl/Br depicting the origins of salinity in formation waters. Modified from Walter et al., 1990.

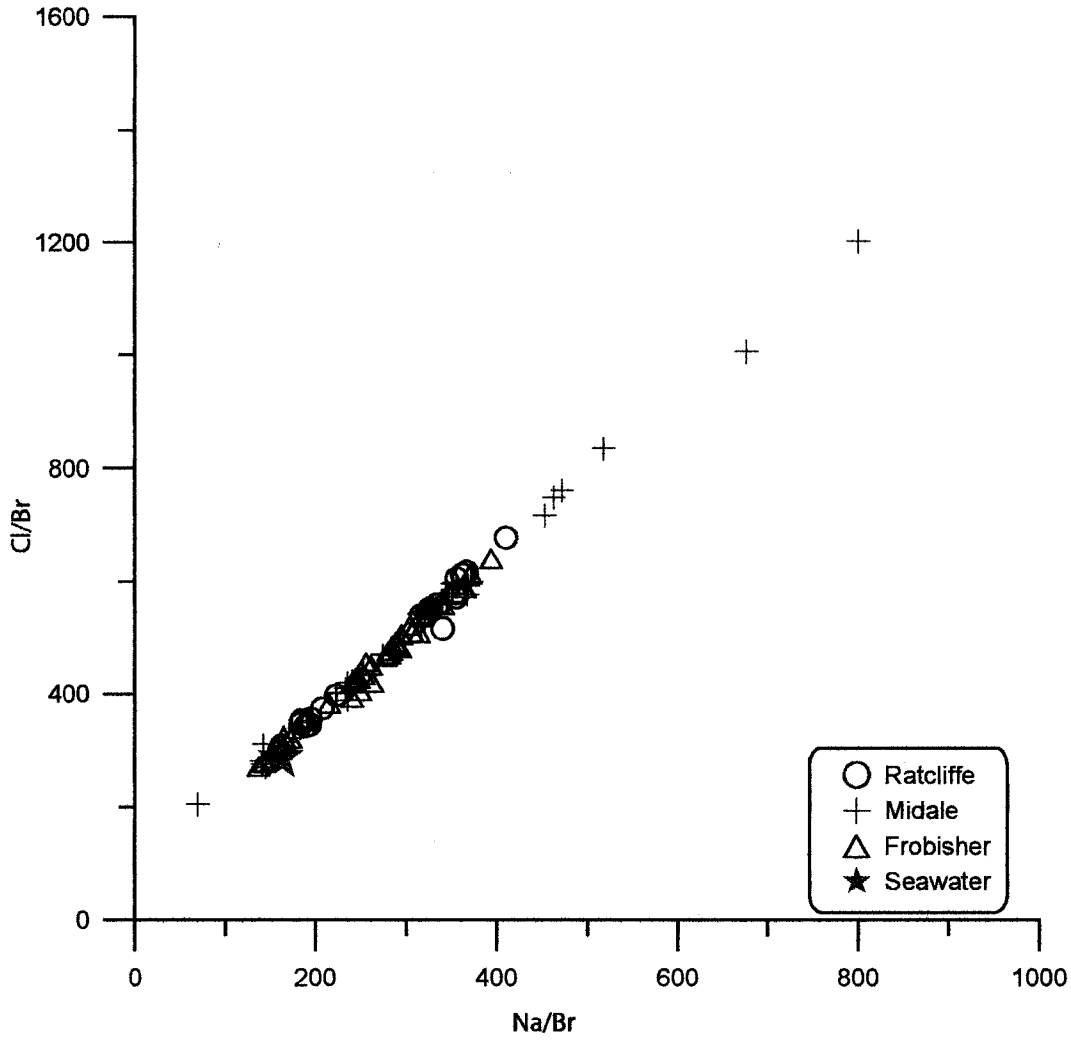

Figure 5.5. Na/Br vs. Cl/Br ratio of the three Mississippian Aquifers. Seawater plotted for a reference.

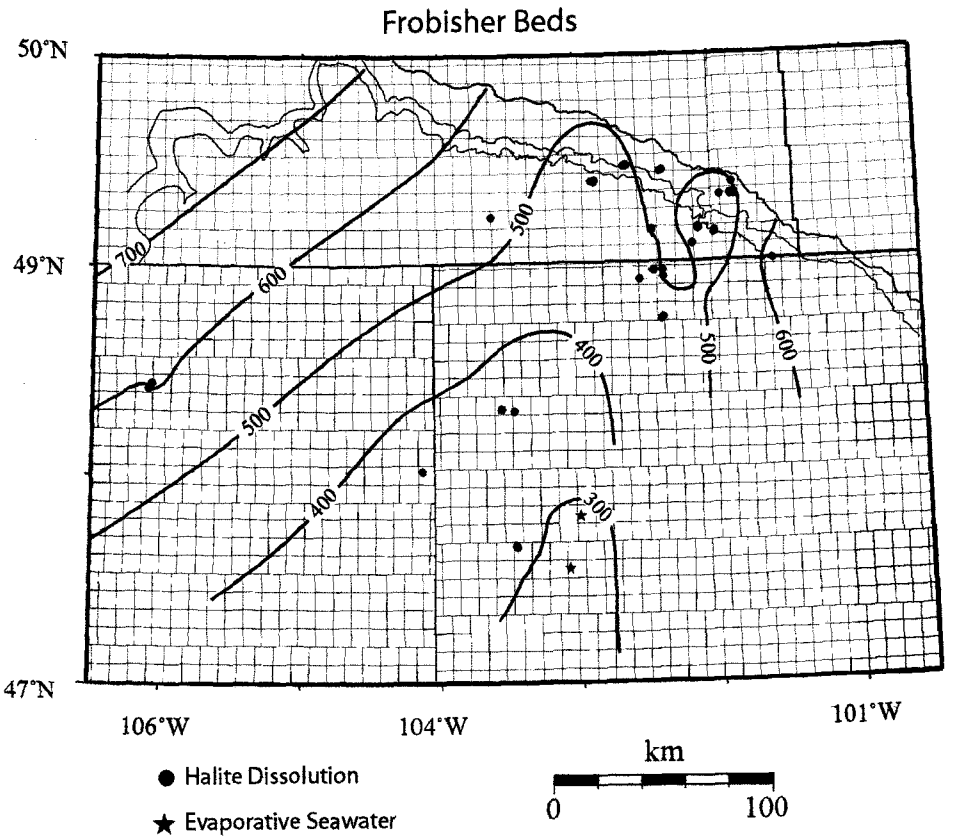

Figure 5.6 Cl/Br ratio map of the Frobisher Beds. Circles represent samples salinity derived from halite dissolution. Stars represent salinity derived from evaporated seawater.

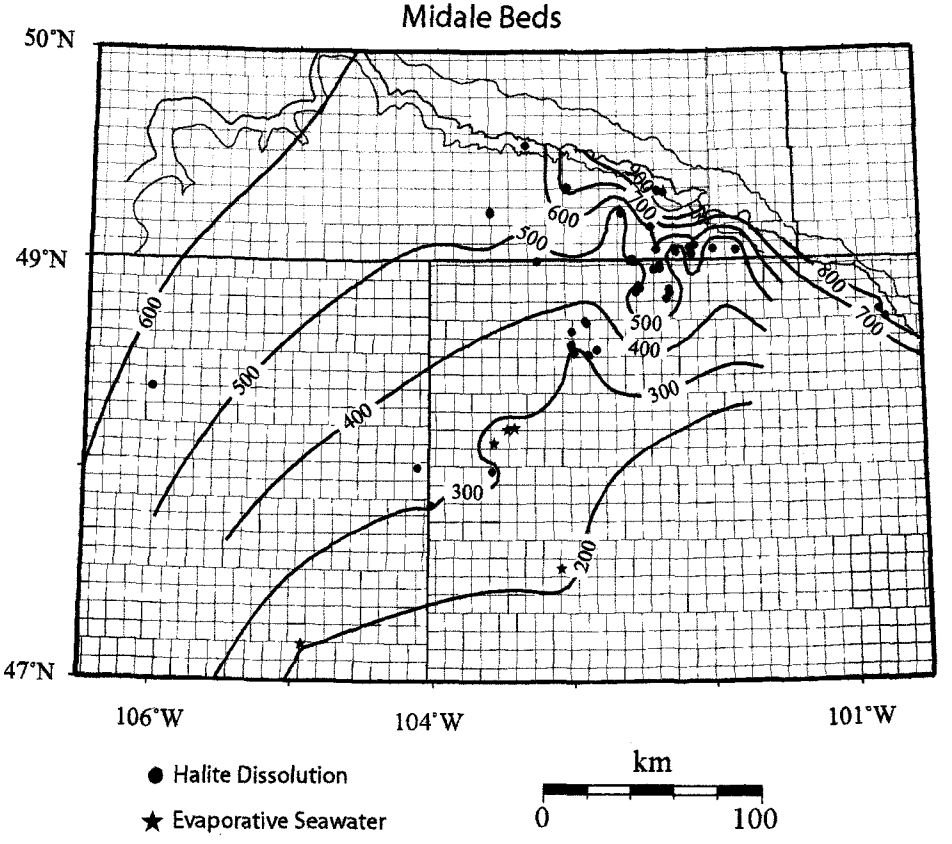

Figure 5.7 Cl/Br ratio map of the Midale Beds. Circles represent samples salinity derived from halite dissolution. Stars represent salinity derived from evaporated seawater.

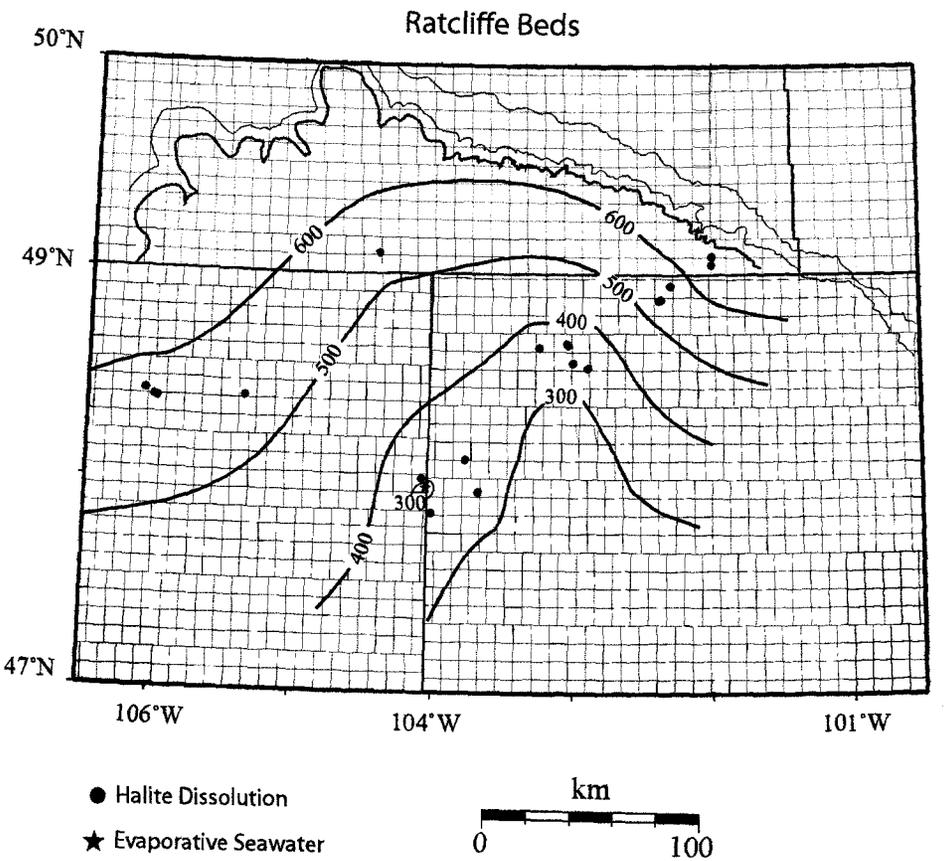

Figure 5.8 Cl/Br ratio map of the Ratcliffe Beds. Circles represent samples salinity derived from halite dissolution. Stars represent salinity derived from evaporated seawater.

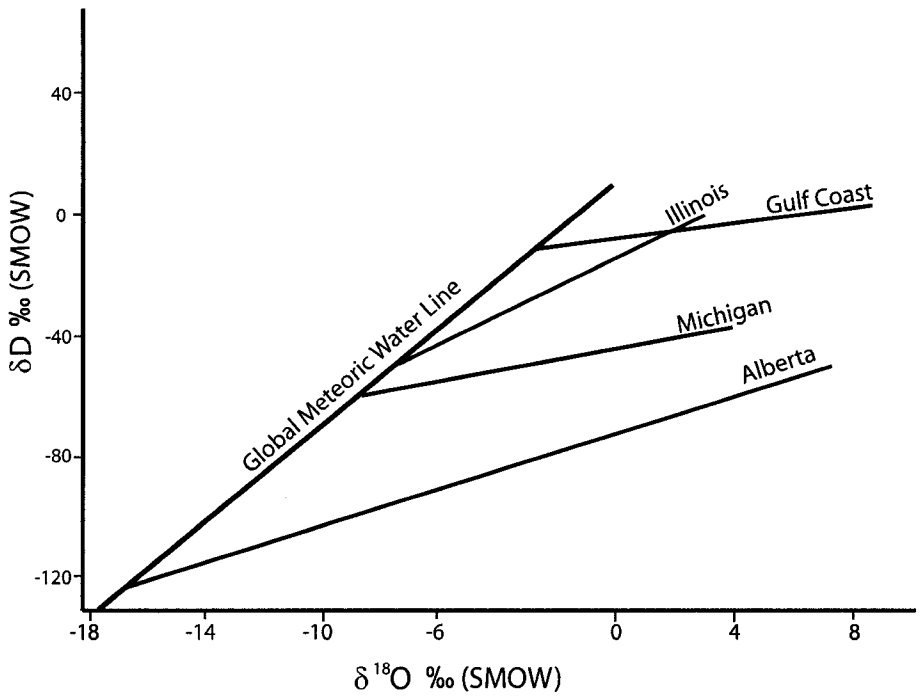

Figure 5.9. Oxygen-hydrogen isotope compositions of sedimentary basins imposed on the Global Meteoric Water Line (Craig, 1961). Modifed from Clayton et al., 1966.

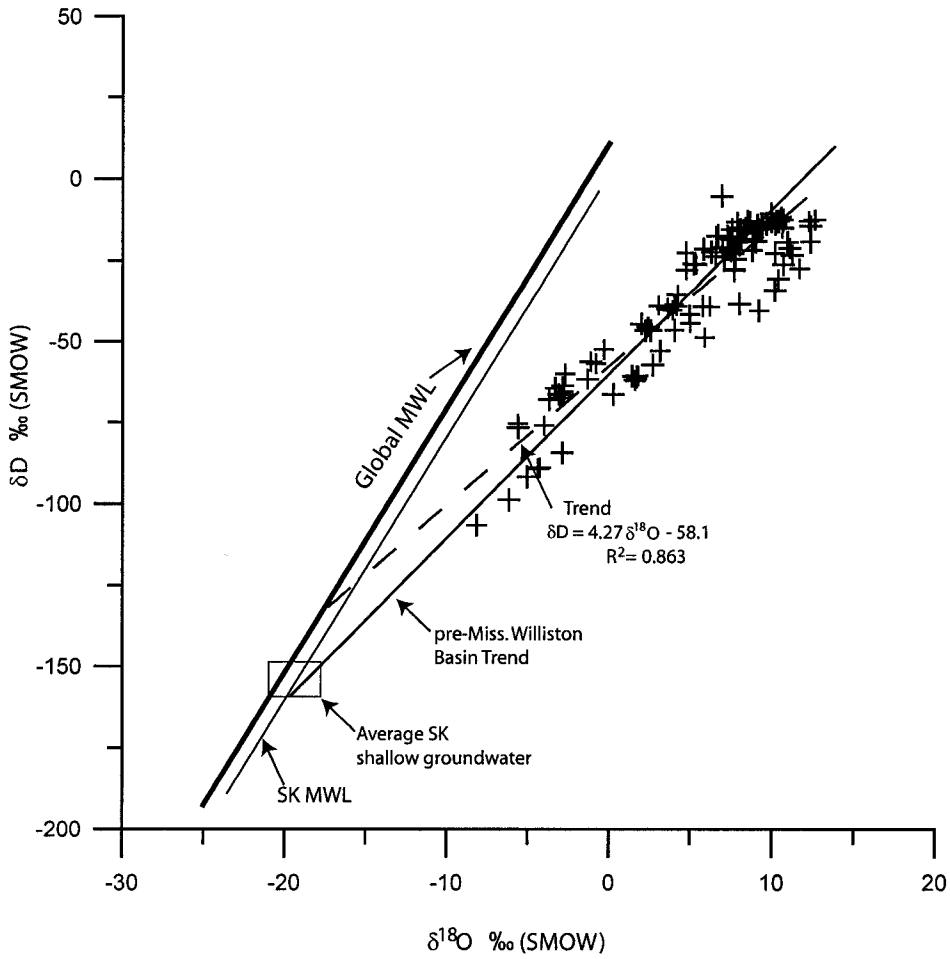

Figure 5.10. δD vs. $\delta^{18}O$ for all three Mississippian aquifers. SK MWL and average SK shallow groundwater modified from McMonagle, 1987. pre-Miss. Williston Basin Trend modified from Rostron et al., 1998.

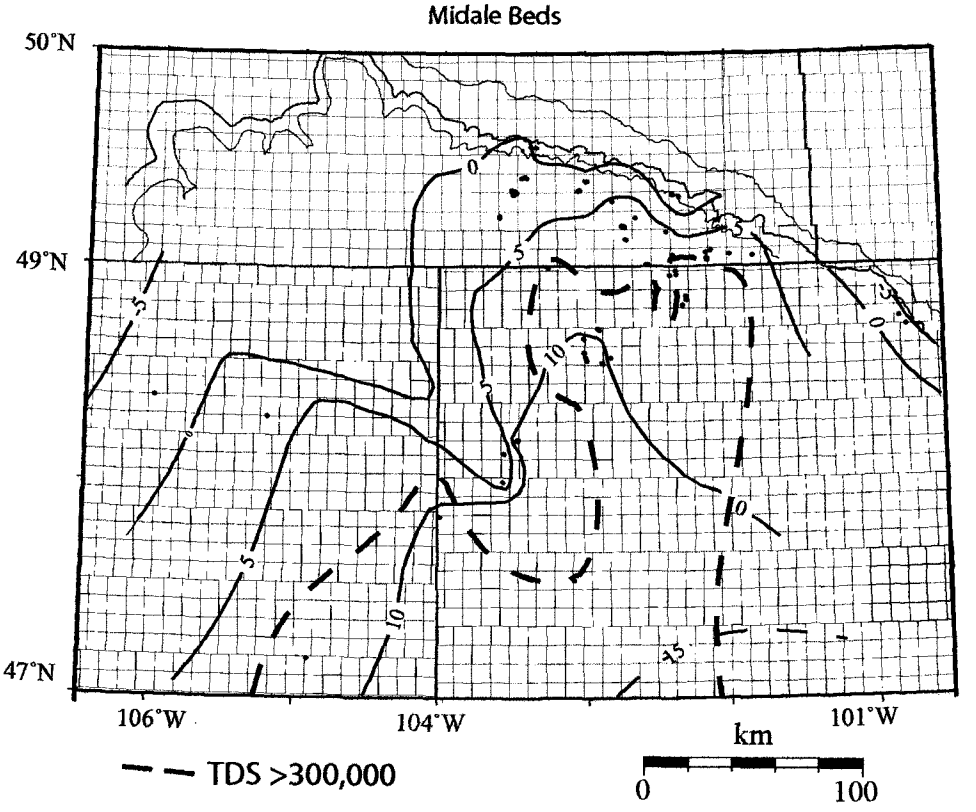

Figure 5.11. Overlay of the 300,000 mg/L TDS contour with the $\delta^{18}O$ composition map of the Midale Beds.

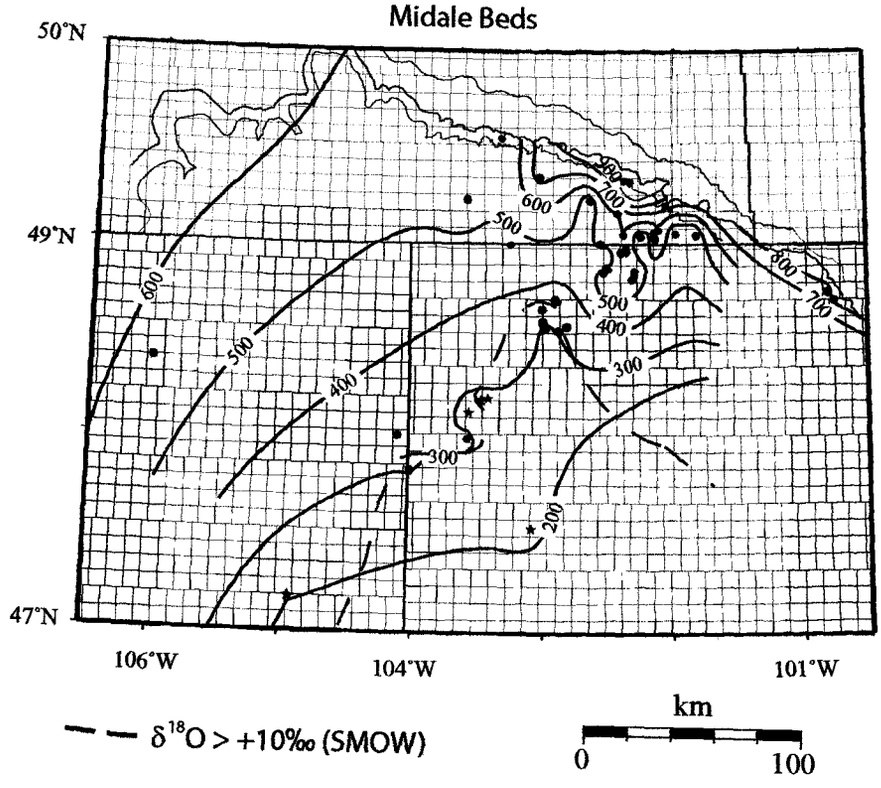

Figure 5.12. Overlay of the +10‰ (SMOW) $\delta^{18}O$ composition contour with the Cl/Br ratio map of the Midale Beds.

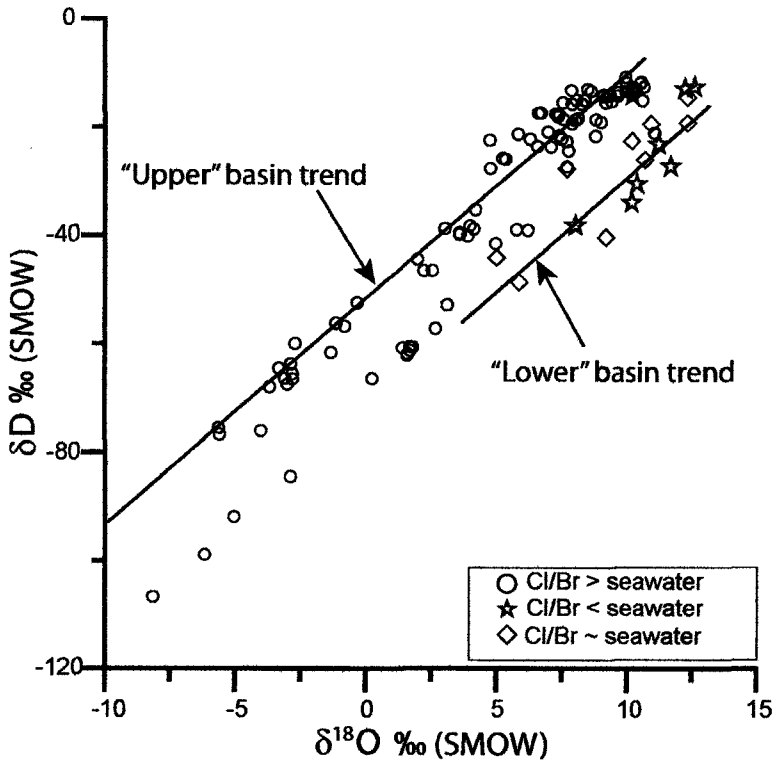

Figure 5.13. $\delta^{18}O$ vrs. δD (SMOW) plot further classified by Cl/Br ratio relative to seawater. Interpreted basin trends based on spatial location, isotopic composition and halogen systematics.

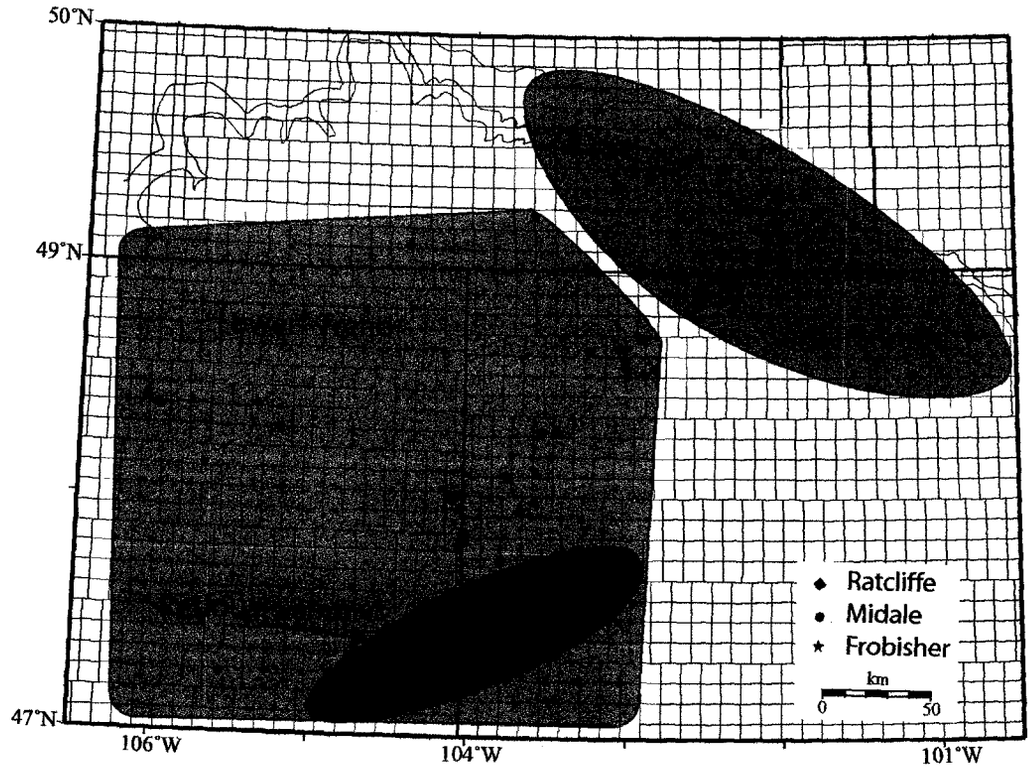

Figure 5.14. Spatial location of "upper" and "lower" basin trends as defined in Figure 5.13. Residual waters have Cl/Br < seawater.

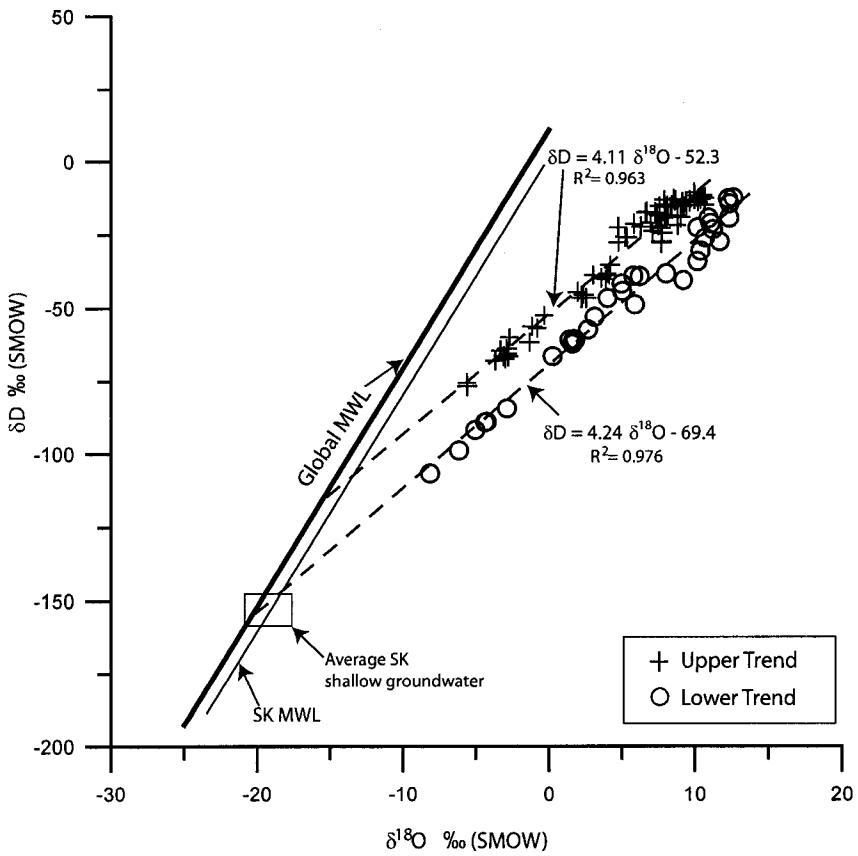

Figure 5.15. δD vs. $\delta^{18}O$ with data separated geographically and isotopically. SK MWL modified from McMonagle, 1987.

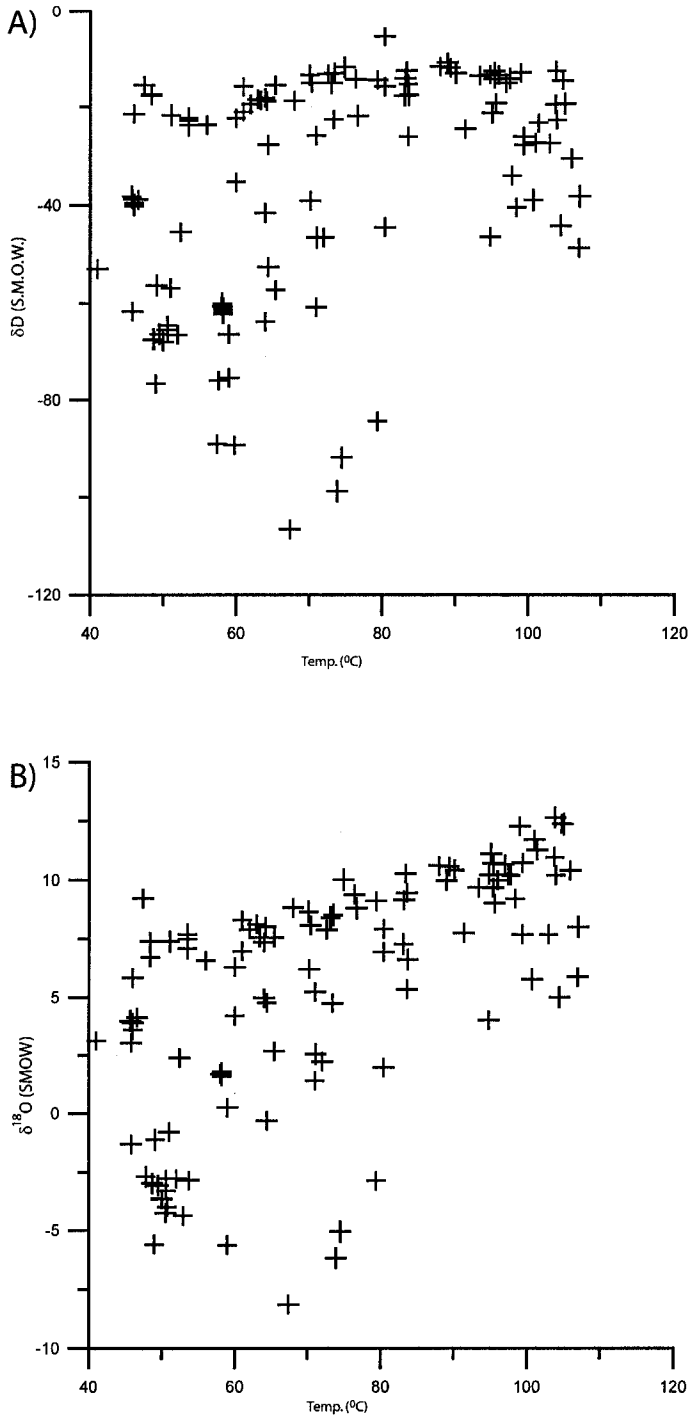

Figure 5.16. δD and δ ^{18}O vs. Temperature (C) for the samples involved in this study

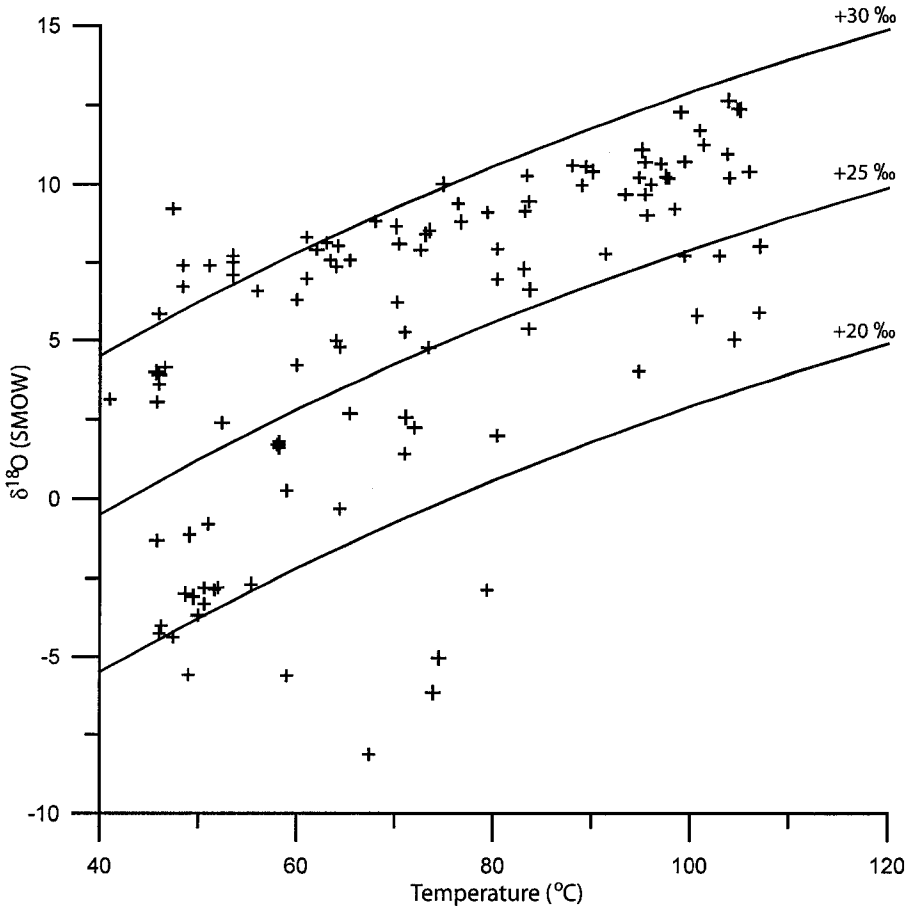

Figure 5.17. Plot of equilibrium isotope fractionation between calcite and water, after O'Neil et al. (1969). Variations of $\delta^{18}O$ compositions with well temperatures taken from bottom hole. Equilibrium curves for calcite at 20, 25 and 30 ‰ (SMOW).

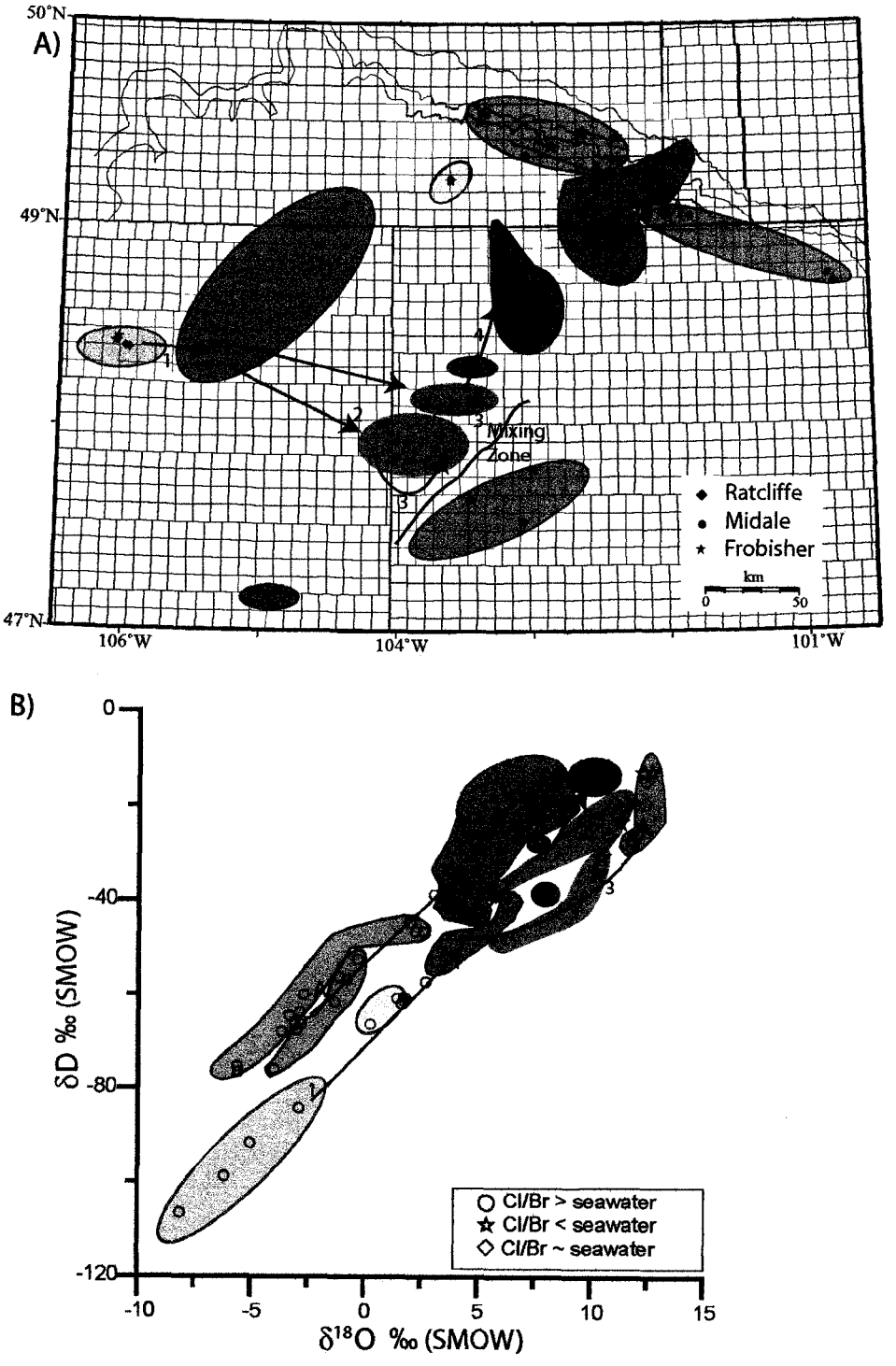

Figure 5.18. Schematic illustration of fluid flow in the Mississippian Aquifers. a) Spatially b) Chemically

Chapter 6 Conclusions

6.1. Thesis Conclusions

1. Using geophysical well logs the Frobisher, Midale, and Ratcliffe Beds within the Mississippian strata can be correlated across the Williston Basin.
2. Results from 114 new samples provide hydrochemistry and stable isotopic compositions that vary within the individual Mississippian Beds and across the Williston Basin.
3. Major ion chemistry and halogen systematics reveal the presence of a residual evaporated seawater slug south of the basin center.
4. Brines surrounding the residual seawater to the north and east originate from evaporite dissolution, therefore implying both brine forming mechanisms of evaporative concentration and evaporite dissolution are occurring in the Mississippian aquifers of the Williston Basin.
5. Two separate flow regimes are interpreted within the Mississippian by integrating halogen systematics and isotopic compositions. One fluid regime originates from present-day meteoric water and then evolves into a saline brine by halite dissolution and subsequent mixing with the residual seawater slug. The other fluid regime originates from a large scale fluid event occurring at the end of the Cretaceous, and then evolves into a saline brine via halite dissolution.
6. Paleo-fluid flow was minimal as a result a residual seawater brine slug still exists in the basin.
7. Conservative tracers indicate that there is little to no mixing of meteoric water with basinal brines in the deep portion of the basin.

8. The present-day flow system resulted from uplifts related to the Laramide Orogeny. Evolved waters are migrating in the basin from the flanks subsequently diluting and flushing the residual seawater through mixing. Due to the large density contrast the migrating waters are diverted to the north and possibly south of the residual seawater slug.
9. Unique isotopic fingerprints are present within the individual beds of the Mississippian strata. These hydrochemical fingerprints can be applied to petroleum exploration and production activities.
10. The absence of Ca-Cl waters within the residual seawater slug in the Mississippian strata and the presence of Ca-Cl waters in the residual seawater slug in the pre-Mississippian possibly provides further evidence of a secular variation in seawater through time.

6.2. Recommendations

To further define the flow system present within the Mississippian aquifers of the Williston Basin, it is recommended to sample wellheads to the south and east of the current study area. This sampling could define the extent of the residual brine slug, as well as to determine if fluid flow is occurring to the south of the brine slug.

References

Bachu, S. and Hitchon, B., 1996. Regional-scale flow of formation waters in the Williston Basin. American Association of Petroleum Geologists Bulletin, v. 80, p. 248-264.

Benn, A. A., and Rostron, B. J., 1997. Regional scale groundwater geochemistry of the Lower Paleozoic formations of the Williston Basin, Canada-USA: Preliminary results. Abstract and poster *in:* Fifth International Williston Basin Horizontal Well Workshop Regina, Saskatchewan.

Benn, A. A., and Rostron, B. J., 1998. Regional hydrochemistry of Cambrian to Devonian aquifers in the Williston basin, Canada-USA. *in*: J. E. Christopher, C. F. Gilboy, D. F. Paterson, and S. L. Bend, eds., Eighth International Williston Basin Symposium: Special Publication: Saskatchewan Geological Society, Regina, p. 238-246.

Bernatsky, R., 1998. Hydrogeochemistry of formation waters in southern Saskatchewan. Unpublished M.Sc. thesis, University of Regina, Regina, 206 p.

Brown, D. L. and Brown, D. L., 1987. Wrench-style deformation and paleostructural influence on sedimentation in and around a cratonic basin. *in*: M. Longman, ed., Williston Basin – Anatomy of a cratonic oil province, Rocky Mountain Association of Geologists, p. 57-70.

Busby, J. F., Kimball, B. A. and Downey, J. S., 1995. Geochemistry of water in aquifers and confining units of the Northern Great Plains in parts of Montana, North Dakota, South Dakota, and Wyoming. U.S. Geological Survey Professional Paper 1402-F, 146 p.

Carlson, C. G. and Anderson, S. B., 1965. Sedimentary and tectonic history of North Dakota part of Williston Basin. American Association of Petroleum Geologists Bulletin, v. 49, p. 1833-1846.

Carlson, C. G., 1967. Cross-section of Paleozoic rocks of western North Dakota. North Dakota Geological Survey, Grand Forks, North Dakota.

Carpenter, A. B., 1978. Origin and Chemical evolution of brines in sedimentary basins. Oklahoma Geological Survey Circular, v. 79, p. 60-77.

Chebotarev, I. I., 1955. Metamorphism of natural waters in the crust of weathering – 1. Geochemica et Cosmochimica Acta, v. 8, p. 22-48.

Chipley, D. and Kyser, T. K., 1989. Fluid inclusion evidence for the deposition and diagenesis of the Patience Lake Member of the Devonian Prairie Evaporate Formation, Saskatchewan, Canada. Sedimentary Geology, v. 64 p. 287-295.

Chipley, D. and Kyser, T. K., 1991. Large scale fluid movement in the Western Canadian Sedimentary Basin as recorded by fluid inclusions in evaporites. *in:* J. E. Christopher, C. F. Gilboy, D. F. Paterson, and S. L. Bend, eds., Sixth International Williston Basin Symposium: Special Publication: Saskatchewan Geological Society, Regina, p. 265-269.

Clark, I., and Frtiz, P., 1997. Environmental Isotopes in Hydrogeology. CRC Press, 328 p.

Clayton, R. N., Friedman, I., Graf, D. L., Mayeda, T. K., Meents, W. F. and Shimp, N. F., 1966. The origin of saline formation waters 1. Isotopic composition. Journal of Geophysical Research, v. 71, p. 3869-3882.

Collins, A. G., 1975. Geochemistry of oilfield waters. Developments in petroleum science, Elsevier Science Publication Company, 496 p.

Craig, H., 1961. Isotopic variations in meteoric waters. Science, v. 133, p. 1702-1703.

Dansgaard, W., 1964. Stable isotopes in precipitation. Tellus, v. 16, p. 436-468.

Downey, J. S., 1984. Geohydrology of the Madison and associated aquifers in parts of Montana, North Dakota, South Dakota, and Wyoming. U.S. Geological Survey Professional Paper 1273-G, 47 p.

Downey, J. S., Busby, J. F. and Dinwiddie, G. A., 1987. Regional aquifers and petroleum in the Williston Basin region of the United States. *in:* Symposium of the Rocky Mountain Association of Geologists, p. 299-312.

Duke, M.J. and Rostron, B.J., in press. Determination of bromine, iodine, chloride and sodium in highly saline formation waters by epithermal Neutron Activation Analysis. Journal of Radioanalytical and Nuclear Chemistry.

Freeze, R. A., and Cherry, J. A., 1979, Groundwater. Prentice-Hall, 604 p.

Fuzesy, L. M., 1983. Correlation and subcrops of the Mississippian strata in southeastern and south-central Saskatchewan. Regina, Saskatchewan Energy and Mines, 63 p.

Gerhard, L. C., Anderson, S. B., Lefever, J. A. and Carlson C.G., 1982. Geological development, origin, and energy mineral resources of Williston Basin, North Dakota. American Association of Petroleum Geologists Bulletin, v. 66, p. 989-1020.

Gerhard, L. C., Anderson, S. B. and Lefever, J. A., 1987. Structural history of the Nesson Anticline, North Dakota. *in:* M. Longman, ed., Williston Basin – Anatomy of a cratonic oil province, Rocky Mountain Association of Geologists, p. 337-353.

Hannon, N., 1987. Subsurface water flow patterns in the Canadian sector of the Williston Basin. *in:* Symposium of the Rocky Mountain Association of Geologists, p. 313-321.

Hanor, J. S., 1987. Origin and migration of subsurface sedimentary brines. SEPM Short Course Notes, Tulsa, OK, v. 21, 247 p.

Hanor, J. S., 1994. Origin of saline fluids in sedimentary basins. Geological Society Special Publication in Parnell, J. ed., 1994, Geofluids: Origin, Migration and Evolution of Fluids in Sedimentary Basins, p. 151-174.

Hitchon, B. and Friedman, I., 1969. Geochemistry and origin of formation waters in the Western Canada Sedimentary Basin - I. Stable isotopes of hydrogen and oxygen. Geochimica et Cosmochimica Acta, v. 33, p. 1321-1349.

Hubbert, M. K., 1953. Entrapment of petroleum under hydrodynamic conditions. American Association of Petroleum Geologists Bulletin, v. 37, p. 1954-2026.

Iampen, H. T., 2003. The genesis and evolution of pre-Mississippian brines in the Williston Basin, Canada-U.S.A. Unpublished M.Sc. thesis, University of Alberta, Edmonton, AB., Canada, 124 p.

Jensen, G. K. S. and Rostron, B. J., 2005. Correlating formation waters using stable isotopes in Mississippian aquifers, Williston Basin, Canada-USA. abstr. *in*: American Association of Petroleum Geologists Annual Convention: Calgary, Alberta, June 19-22.

Kent, D. M., 1984. Depositional setting of the Mississippian strata in southeastern Saskatchewan: A conceptual model for hydrocarbon accumulations. *in:* Lorsong, J.A. and Wilson, M.A. (eds), Oil and Gas in Saskatchewan, Sask. Geol. Soc., Regina, Spec. Publ. no. 7, p. 19-30.

Kent, D. M., 1987. Mississippian facies, depositional history and oil occurrences in Williston Basin, Manitoba and Saskatchewan. *in:* M. Longman, eds., Williston Basin – Anatomy of a cratonic oil province, Rocky Mountain Association of Geologists, p. 157-170.

Kent, D.M., 1999. A re-examination of the processes of formation and diagenesis of coated-grain accumulations and contiguous facies in the Mississippian of southeastern Saskatchewan. Summary of Investigations 1999, v. 1: SK, Canada, Saskatchewan Industry and Resources, Regina, 10 p.

Kent, D.M., 2001. A regressive discontinuity in the Midale Beds succession: a cause for two diagentic events. In: Ninth Williston Basin Horizontal Well and Petroleum Conference, North Dakota Geological Survey. extented abstract.

Kent, D.M. and Nimegeers, A.R., 2002. Intrastratal deposition breaks in the Mississippian Midale Beds of southern Saskatchewan; their roles in reservoir rock creation and hydrocarbon accumulation. Canadian Society of Petroleum Geologists, core convention, abstract, p. 47.

Kent, D. M., Thomas, P. and Heck, T., 2004. Geological mapping of the Mississippian strata in southeastern Saskatchewan, northwestern North Dakota, and northeastern Montana. Summary of Investigations 2004, v. 1: Regina, SK, Canada, Saskatchewan Industry and Resources, 22 p.

Khan, D.K., 2006. Hydrogeological characterization of the Weyburn CO_2 project area and gradient-free inverse conditioning of heterogeneous aquifer models to hydraulic head data. Unpublished Ph.D. thesis, University of Alberta, Edmonton, AB., Canada, 238 p.

Kreis, L. K., Gent, M. and Vigrass, L. W., 1991. Subsurface brines in southern Saskatchewan. *in:* J. E. Christopher, C. F. Gilboy, D. F. Paterson, and S. L. Bend, eds., Sixth Annual Williston Basin Symposium: Special Publication: Regina, Saskatchewan Geological Society, p. 283-292.

Laird, W.M., 1952. Geology of the Williston Basin in North Dakota. World Petroleum, v. 23, p. 42-44.

Lefever, R. D., 1998. Hydrodynamics of formation waters in the North Dakota Williston Basin. *in:* J. E. Christopher, C. F. Gilboy, D. F. Paterson, and S. L. Bend, eds., Eighth Annual Williston Basin Symposium: Special Publication: Regina, Saskatchewan Geological Society, p. 229-237.

Lico, M. S., Kharaka, Y. K. Carothers, W. W. and Wright, V. A., 1982. Methods for collection and analysis of geopressured geothermal and oilfield waters. United States Geological Survey Water Supply Paper 2194.

Lowenstein, T. K., Hardie, L. A., Timofeeff, M. N. and Demicco, R. V., 2003. Secular variation in seawater chemistry and the origin of calcium chloride basinal brines. Geology, v. 31, p. 857-860.

MacCaffrey, M. A., Lazar, B. and Holland, H. D., 1987. The evaporation path of seawater and the coprecipitation of Br- and K+ with halite. Journal of Sedimentary Petrology, v. 57, p. 928-937.

McMonagle, L., 1987. Stable isotopic and chemical compositions of surface and subsurface waters in Saskatchewan. Unpublished M.Sc. thesis. University of Saskatchewan, Saskatoon, SK, Canada, 108 p.

Mossop, G. and Shetsen, I. eds., 1994. Geological Atlas of the Western Canada Sedimentary Basin. Alberta Research Council, 510 p.

Nickel, E. and Qing, H., 2004. Geochemical and petrographic characterization of the unconformity-related seal in the weyburn Midale pool, southeastern Saskatchewan. *in:* Summary of Investigations 2004, v. 1: Regina, SK, Canada, Saskatchewan Industry and Resources, 10 p.

Nimegeers, A.R. and Qing, H., 2002. Depositional model of Midale Beds, steelman field, southwestern Saskatchewan. *in:*Summary of Investigations 2002, v. 1: Regina, SK, Canada, Saskatchewan Industry and Resources, 11 p.

O'Neil, J.R., Clayton, R.N. and Mayeda, T.K., 1969. Oxygen isotope fractionation in divalent metal carbonates. Journal of Chemical Physics, v. 51, no. 12 p. 5547-5558.

Peterson, J. A. and MacCary, L.M., 1987. Regional stratigraphy and general petroleum geology, Williston Basin, United States and adjacent area, *in*: M. Longman, eds., Wiliston Basin – Anatomy of a cratonic oil province. Rocky Mountain Association of Geologists, p. 9-44.

Rostron, B. J., Holmden, C. and Kreis, L. K., 1998. Hydrogen and oxygen isotope compositions of Cambrian to Devonian formation waters, Midale area, Saskatchewan. *in:* J. E. Christopher, C. F. Gilboy, D. F. Paterson, and S. L. Bend, eds., Eighth International Williston Basin Symposium: Special Publication: Saskatchewan Geological Society, Regina, p. 267-273.

Rostron, B. J., Kreis, L.K. and Holmden, C., 1999. The Saskatchewan brine sampling program. Summary of Investigations 1999, v. 1: Regina, SK, Canada, Saskatchewan Industry and Resources, p. 85-86.

Rostron, B. J. and Holmden, C., 2000. Fingerprinting formation-waters using stable isotopes, Midale Area, Williston Basin, Canada. Journal of Geochemical Exploration, v. 69-70, p. 219-223.

Sloss, L. L., 1987. The Williston Basin in the family of cratonic basins. *in:* M. Longman, ed., Williston Basin – Anatomy of a cratonic oil province, Rocky Mountain Association of Geologists, p. 1-8.

Stueber, A.M. and Walter, L.M., 1994. Glacial recharge and paleohydrodrologic flow systems in the Illinois basin: Evidence from chemistry of Ordovician carbonate (Galena) formation waters. Geological Society of America Bulletin, v. 106, p. 1430-1439.

Stueber, A. M., Saller, A. H. and Ishida, H., 1998. Origin, migration and mixing of brines in the Permian Basin: Geochemical evidence from the eastern central basin platform, Texas. American Association of Petroleum Geologists Bulletin, v. 82, p. 1652-1672.

Tóth, J., 1980. Cross-formational gravity-flow of groundwater: A mechanism of the transport and accumulation of petroleum (The generalized hydraulic theory of petroleum migration). *in:* W. H. Roberts III, and R. J. Cordell, eds., Problems of Petroleum Migration, v. Studies in Geology Number 10: Tulsa, American Association of Petroleum Geologists Bulletin, p. 121-167.

Tóth, J., 1984. The role of gravity flow in the chemical and thermal evolution of ground water. *in:* First Canadian/American Conference on Hydrogeology; Practical Applications of Groundwater Geochemistry, p. 3-39.

Walter, L. M., Stueber, A. M. and Huston, T. J., 1990. Br-Cl-Na systematics in Illinois basin fluids: constraints on fluid origin and evolution. Geology, v. 18, p. 315-318.

Wittrup, M. B., Kyser, T. K. and Danyluk, T. 1987. The use of stable isotopes to determine the source of brines in Saskatchewan potash mines. Economic Minerals of Saskatchewan, p. 159-165.

Wittrup, M. B. and Kyser, T. K., 1990. The petrogenesis of brines in Devonian potash deposits of western Canada. Chemical Geology, v. 82, p. 103-128.

Appendix A. Well Location, API, Well Name, Date Sampled

Sample ID		LSD	Sec	TWP	RNG	Mer	Latitude	Longitude	API	Well Name	Date Sampled
03-201	1	5	5	5	8	2	49.3536	-103.0569			Aug. 4/03
03-203	31	6	5	5	8	2	49.3542	-103.0514			Aug. 4/03
03-206	11	9	28	4	3	2	49.3276	-102.3444			Aug. 5/03
03-207	1	1	19	1	2	2	49.0451	-102.2552			Aug. 5/03
03-208	21	16	2	1	5	2	49.0113	-102.5695			Aug. 5/03
03-209	41	16	19	3	5	2	49.2304	-102.6584			Aug. 5/03
03-210	1	14	2	1	5	2	49.0119	-102.5796			Aug. 6/03
03-211	2	1	31	4	3	2	49.3356	-102.3900			Aug. 6/03
03-213	11	8	31	1	1	2	49.0774	-102.1206			Aug. 7/03
03-216	1	5	30	3	12	2	49.2371	-103.6173			Aug. 8/03
03-217	91	15	30	1	3	2	49.0562	-102.3950			Aug.8/03
03-218	91	9	13	1	2	2	49.0382	-102.1454			Aug.8/03
03-219	11	15	13	1	2	2	49.0410	-102.1478			Aug. 9/03
03-220	41	11	25	1	2	2	49.0673	-102.1533			Aug. 9/03
03-221	91	8	13	1	2	2	49.0326	-102.1438			Aug. 9/03
03-222	11	11	22	1	33	1	49.0520	-101.8227			Aug. 9/03
03-230	NW	SE	6	162	91		48.8851	-102.5322	33013000820000	Bunting 2-B	Aug. 11/03
03-232	NE	SE	13	162	92		48.8562	-102.5484	33013008440000	Hermanson 1	Aug. 11/03
03-234	NW	NW	2	160	95		48.7186	-102.9263	33023000460000	Louis Holte 1	Aug. 12/03
03-235	SE	SE	2	160	95		48.7075	-102.9109	33023004090000	Kjelshus 1	Aug. 12/03
03-238	SE	SE	32	164	90		48.9822	-102.3725	33013013040000	Wilson 44-32H	Aug. 12/03
03-241	SE	SE	11	162	90		48.8663	-102.3069	33013012910000	Pederson 44-11H	Aug.13/03
03-242	SE	SE	27	162	90		48.8228	-102.3288	33013012850000	Mertes 44-27H	Aug.13/03
03-243	NW	NW	24	162	90		48.8489	-102.3025	33013012750000	Durward et al 11-24	Aug. 14/03
03-244	SE	NE	36	159	95		48.5550	-102.8886	33105008200000	Carlson 8-36	Aug. 14/03
03-245	NW	NW	9	163	90		48.9655	-102.3693	33013013030000	Mcclaflin 11-9H	Aug. 14/03
03-246	NW	SE	30	159	95		48.5663	-103.0023	33105005020000	F. E. Mccoy 1	Aug.15/03
03-249	1	4	3	1	10	2	49.0012	-103.2720			Aug.15/03
03-250	NW	NE	13	159	96		48.6021	-103.0233	33105005940000	E. L. GUDVANGEN 1	Aug.16/03
03-251	SE	SE	12	159	96		48.6062	-103.0179	33105006360000	E. Goetz 1	Aug.16/03
03-253	31	2	35	2	4	2	49.1636	-102.4406			Aug. 17/03
03-258	NE	SW	21	159	94		48.5807	-102.8340	33013000520000	August Moberg 1 P-6	Aug. 18/03
04-101	31	3	18	7	10	2	49.5543	-103.3534			May 20/04
04-105		10-28	4-28	1	34	1	49.0592	-101.9852			May 21 /04
04-110	SE	NE	12	163	91		48.9612	-102.4166			May 23/04
04-114	SE	SW	33	163	91		48.8960	-102.4936			May 23/04

Appendix A. Well Location, API, Well Name, Date Sampled

Sample ID		LSD	Sec	TWP	RNG	Mer	Latitude	Longitude	API	Well Name	Date Sampled
04-	115	SE	NW	8	162	91		48.8742	-102.5158			May 23/04
04-	117	SW	NE	20	161	78		48.7571	-100.8050			May 23/04
04-	118	NE	NE	5	160	78		48.7184	-100.7587			May 23/04
05-	103	SE	NE	30	154	100		48.1357	-103.5842	33105010790000	Brakken 24-30	Aug. 2/05
05-	104	NE	SW	36	155	100		48.2017	-103.4876	33105013080000	State 23-36	Aug. 2/05
05-	107	NE	NW	1	154	100		48.1965	-103.4879	33105013330000	Sudderth 21-1	Aug. 2/05
05-	110	SW	NW	19	147	97		47.5403	-103.0949	33025004680000	Bob Creek Federal 4-19-1D-R	Aug. 4/05
05-	115	SW	NW	10	152	101		48.0024	-103.5917	33053019180000	Anderson 32 -1	Aug. 4/05
05-	117	NW	SW	5	150	104		47.8392	-104.0297	33053025640000	Karst 13-5	Aug. 4/05
05-	124	SW	NE	6	16	54		47.1757	-104.9294	25021051350000	Elpel 1	Aug. 7/05
05-	138	NE	NE	5	30	44		48.3908	-106.0239	25105212660000	J. Reddig 1	Aug. 10/05
05-	140	NW	SE	24	160	96		48.6681	-103.0240	33023002620000	Vatne 24-1	Aug. 10/05
05-	144	SW	SW	33	30	50		48.3044	-105.2329	25085214450000	Long Creek 333 #1	Aug. 10/05
03-	202	30	5	22	5	7	2	49.3972	-102.8785			Aug.4/03
03-	204	1	5	23	5	7	2	49.3972	-102.8552			Aug.4/03
03-	205	1	1	22	5	7	2	49.3936	-102.8610			Aug.5/03
03-	212	1	9	4	1	31	1	49.0083	-101.5663			Aug.7/03
03-	215	1	13	19	3	12	2	49.2297	-103.6173			Aug.7/03
03-	223	41	9	20	2	34	1	49.1411	-101.9908			Aug. 9/03
03-	229	1	7	1	2	2	2	49.0926	-102.1489			Aug. 11/03
03-	239	SE	SE	5	163	90		48.9676	-102.3725	33013012900000	Iverson 45-5H	Aug.13/03
03-	240	NW	NW	21	163	90		48.9365	-102.3692	33013001770000	Larson 11-21H	Aug.13/03
03-	252	11	3	35	2	4	2	49.1624	-102.4443			Aug.16/03
03-	254	41	13	26	2	4	2	49.1598	-102.4497			Aug. 17/03
03-	255	SE	SE	2	163	91		48.9684	-102.4387	33013009530000	Stierle 1	Aug. 17/03
04-	109	SW	SW	19	163	91		48.9250	-102.5428	33013010520000	Probst 2	May 23/04
05-	101	SW	NE	29	161	90		48.7447	-102.3779	33013010830000	Opseth 29-7	Aug. 1/05
05-	102	NW	NW	32	161	90		48.7333	-102.3905	33013011330000	Hermanson 32-4	Aug. 1/05
05-	112	SW	SE	18	147	97		47.5468	-103.0840	33025002470000	Carus Unit "A" 1	Aug. 4/05
05-	114	SW	NW	20	150	96		47.7985	-103.0023	33053008610000	Lillibridge 3	Aug. 4/05
05-	116	SE	SW	8	148	100		47.6495	-103.4521	33053016080000	Ceynar 1	Aug. 4/05
05-	118	SW	SE	30	156	99		48.3009	-103.4611	33105012800000	Strang Trust 34-30	Aug. 4/05
05-	119	SE	NW	28	156	100		48.3089	-103.5540	33105011570000	Arthur Smith 22-28	Aug. 4/05
05-	128	SE	NE	7	148	100		47.6558	-103.4634	33053005980000	Stevens 1	Aug. 7/05
05-	129	NW	SE	8	26	59		48.0168	-104.1249	25083218090000	Burgess 1-8	Aug. 7/05
05-	133	SW	NE	26	31	43		48.4157	-106.0940	25105213060000	Sylvia Roberts 1	Aug. 10/05
05-	137	SW	SE	13	31	43		48.4379	-106.0720	25105213070000	Iron Bear Heirs 2	Aug. 10/05
00-	181	1	2	32	2	1	2	49.1634	-102.1036			Summer 2000
00-	182	1	3	32	2	1	2	49.1630	-102.1094			Summer 2000
00-	183	21	7	32	2	1	2	49.1663	-102.1045			Summer 2000

Appendix A. Well Location, API, Well Name, Date Sampled

Sample ID		LSD	Sec	TWP	RNG	Mer	Latitude	Longitude	API	Well Name	Date Sampled
00-184	1	11	32	2	1	2	49.1703	-102.1094			Summer 2000
00-169	31	5	16	6	5	2	49.4705	-102.6320			Summer 2000
00-170	91	2	17	6	5	2	49.4665	-102.6424		2C5-16-4C2-17-6-5W2	Summer 2000
00-171	91	6	16	6	5	2	49.4702	-102.6255		4B5-16-2D6-16-6-5W2	Summer 2000
00-172	41	7	16	6	5	2	49.4702	-102.6191			Summer 2000
00-173	41	11	16	6	5	2	49.4743	-102.6255			Summer 2000
99-102	1	6	5	6	3	2	49.4411	-102.3788			Summer 1999
99-104	1	12	4	6	3	2	49.4451	-102.3626			Summer 1999
03-009	91	1	3	7	11	2	49.5250	-103.4077		8B9-3/2D1-3-7-11W2	June 13/03
03-011	91	1	3	7	11	2	49.5250	-103.4077		8B9-3/2D1-3-7-11W2	June 13/03
00-164	1	16	24	4	34	1	49.3218	-101.9373			Aug. 1/03
00-161	1	16	10	5	33	1	49.3820	-101.8470			Aug. 1/03
03-129	1	4	27	4	33	1	49.3268	-101.8634			July 30/03
03-130	31	14	23	4	33	1	49.3237	-101.8355			July 30/03
03-145	31	14	22	4	33	1	49.3231	-101.8590			July 31/03
03-146	1	6	26	4	33	1	49.3311	-101.8354			July 31/03
03-224	41	14	1	2	19	2	49.1000	-104.4228			Aug. 9/03
03-225	81	3	5	2	34	1	49.0913	-102.0028		3B5-3-4C3-2-34W1	Aug. 9/03
03-226	92	3	28	1	34	1	49.0605	101.9822		2B15-28-2C3-1-34W1	Aug. 9/03
03-227	91	3	5	2	34	1	49.0888	-102.0008		3B10-5-4A3-5-2-34W1	Aug. 9/03
03-237	NW	NW	13	163	90		48.9510	-102.3032	33013012890000	Sorum 11-13H	Aug. 12/03
03-247	NE	SW	19	159	95		48.5808	-103.0096	33105009690000	F. E. Mccoy 2	Aug.15/03
03-248	SE	NW	36	159	95		48.5554	-102.8988	33105010830000	State 1-36	Aug.15/03
03-256	NE	SE	5	162	90		48.8856	-102.3731	33013013170000	E.M. Kalmbach 5-9	Aug. 18/03
03-259	NE	NW	8	162	90		48.8783	-102.3839	33013013180000	E.J. 8-3	Aug. 18/03
04-103	92	9	26	1	1	2	49.0665	-102.0301		1B2-35-3A9-26-1-1W2	May 21 /04
04-104	91	9	26	1	1	2	49.0529	-102.0081		3D15-26-7A9-26-1-1W2	May 21 /04
05-106	NW	NW	25	152	102		47.9626	-103.6859	33053016740000	Novak 25-11	Aug. 2/05
05-109	SW	NE	32	151	104		47.8578	-104.0186	33053024800000		Aug. 4/05
05-111	SE	SE	34	154	102		48.1144	-103.7811	33105012390000	Hansen 16-34	Aug. 4/05
05-121	NW	SW	29	160	97		48.6532	-103.2520	33023004530000	Rosten 29-1	Aug. 5/05
05-122	SE	NW	23	160	96		48.6713	-103.0505	33023000650000	Sullivan 23-1	Aug. 5/05
05-123	NW	SE	23	160	96		48.6677	-103.0451	33023001420000	Nygaard 33-23	Aug. 5/05
05-127	SW	NE	26	26	59		47.9783	-104.0611	25083217920000	Filler 26-32	Aug. 7/05
05-130	SE	NW	10	26	59		48.0221	-104.0889	25085215680000	Berry 1-10	Aug. 7/05
05-131	NE	NE	26	31	43		48.4190	-106.0890	25105213680000	Sylvia Robert 2	Aug. 10/05
05-135	NE	NE	32	31	49		48.4020	-105.3690	25085211010000	Longee 1	Aug. 10/05
05-136	SW	NW	3	30	44		48.3870	-105.9960	25105212720000	Tieszen-Toews 3-3	Aug. 10/05

Appendix B. Open Hole Depth, Operator, Well Type, KB, Perf. Interval, Sample Point, Temp.

Sample ID	Open Hole Depth	Operator	Type	KB (m)	Perf. Interval (m)	Sample Point (m)	Temp. (°C)	Temp Comment
03- 201		Duce Oil	V	599	1464-1465.5	1465	71.1	DST nearby
03- 203		Duce Oil	V	599	1464.5-1466	1465	72	DST nearby
03- 206		Duce Oil	V	589.5	1317-1319	1318	59	DST nearby
03- 207		Arc Energy Trust	V	566.7	1527-1529	1528	61	DST this well
03- 208		Athena Oil & Gas	V	602.7	1721-1762	1741	48.4	DST nearby
03- 209		Advantage Oil	V	585.4	1521-1522	1521	68	DST this well
03- 210		Athena Oil & Gas	V	603	1735-1760	1748	46	DST this well
03- 211		Athena Oil & Gas	V	590	1318-1324	1321	50	DST nearby
03- 213		Zargon	V	570.7	1449-1455	1453	61	DST nearby
03- 216		Arc Sask Trust	V	599	1695-1696	1695	71	DST nearby
03- 217		Husky	H	564	1572-1589	1580	64	DST nearby
03- 218		Acclaim	H	567	1490-1493	1492	63.4	DST nearby
03- 219		Acclaim	V	574.5	1500.5-1504	1502	62	DST nearby
03- 220		Midale Petroleum	V	581	1465-1475	1470	63	DST nearby
03- 221		Acclaim	H	577	1492-1506	1500	64.2	DST nearby
03- 222		Acclaim	V	528	1322.5-1324	1323	48.4	DST nearby
03- 230		Condor Petroleum	V	598	1862-1867	1865	83.2	
03- 232		Condor Petroleum	V	595.5	1897-1906	1902	83.6	
03- 234		Condor Petroleum	V	719	2330-2331	2331	91.4	
03- 235		Condor Petroleum	V	728.4	2334.5-2340.5	2338	90.1	
03- 238	5800-11634	Nance Petroleum	H	589	1677-1692	1685	73.1	
03- 241	6085-11540	Nance Petroleum	H	597.5	1767-1783	1775	72.6	
03- 242	6455-11211	Nance Petroleum	H	600.5	1826-1837	1832	80.4	
03- 243		Nance Petroleum	V	601	1787-1814	1801	83.1	
03- 244		Condor Petroleum	V	708	2441-2450.5	2446	95.4	
03- 245	5759-11009	Nance Petroleum	H	592	1698-1707	1703	70.4	
03- 246		Condor Petroleum	V	723.5	2488-2495	2492	97.5	
03- 249		APF Energy	V	586	1886-1892	1889	83.6	
03- 250		Eagle Operating	V	702	2451-2455	2453	95.4	
03- 251		Eagle Operating	V	706	2454-2457	2456	94.8	
03- 253		Simoil	V	571.8	1495-1496	1496	60	DST nearby
03- 258		Eagle Operating	V	692	2428-2438.5	2433	93.4	
04- 101		Bison	V	610.6	1340-1345	1343	52	
04- 105		NorthRock	H	535.2	1344-1364	1354	47.4	DST nearby
04- 110		Condor Petroleum	V	591	1728-1740	1734	79.4	
04- 114		Condor Petroleum	V	596.5	1832-1842	1837	80.4	

Appendix B. Open Hole Depth, Operator, Well Type, KB, Perf. Interval. Sample Point, Temp.

Sample ID	Open Hole Depth	Operator	Well Type	KB (m)	Perf. Interval (m)	Sample Point (m)	Temp. (^{0}C)	Temp Comment
04- 115		Condor Petroleum	V	728.5	1873-1881.5	1877	83.7	DST nearby
04- 117		Eagle Operating	V	449.5	1003-1016	1009	49.5	DST nearby
04- 118		Eagle Operating	V	449.3	997-1002	1000	48.7	DST nearby
05- 103		Prospective Oil	V	570.5	2806-2813	2809	97.8	DST this well
05- 104		Prospective Oil	V	640	2879-2883	2881	106	DST this well
05- 107		Prospective Oil	V	660.5	2902-2906	2904	107	DST this well
05- 110		Citation Oil & Gas	V	686.5	2878-2880	2879	101	DST this well
05- 115		Westport Oil & Gas	V	651	2877-2888	2883	104.5	DST nearby
05- 117		Bill Barrett Corp.	V	582.5	2751-2758	2755	103.8	DST nearby
05- 124		Wesco Operating, Inc.	V	823.5	3047-3081	3064	107.1	DST nearby
05- 138		Helis Oil	V	854.9	1739-1780	1760	79.4	DST nearby
05- 140		Prospective Oil	V	701.5	2374-2378	2376	97	DST this well
05- 144		Journey Operating	V	732.4	1904-1908	1906	94.8	DST nearby
03- 202		Duce Oil	V	597.4	1403.6-1404.5	1404	50.6	DST nearby
03- 204		Duce Oil	V	596.8	1402-1404.5	1403	51	DST nearby
03- 205		Duce Oil	V	597	1406.7-1407.6	1406	50.6	DST nearby
03- 212		Arc Resources	V	500.5	1208-1211	1210	49	DST nearby
03- 215		Arc energy trust	V	596	1722-1724	1708	59	DST this well
03- 223		Husky	V	533	1295-1297	1296	56	DST nearby
03- 229		Advantage	V	574.5	1461-1464.5	1463	64	DST nearby
03- 239		Nance Petroleum	V	590.5	1710-1716	1713	73.5	DST nearby
03- 240		Nance Petroleum	V	594	1720-1736	1728	70.1	DST nearby
03- 252		Simoil	V	571.8	1515-1518	1517	60	DST nearby
03- 254		Simoil	V	572.5	1521-1522.5	1522	64.4	DST nearby
03- 255		Eagle Operating	V	591.5	1764.5-1776.5	1771	76.4	DST nearby
04- 109		Eagle Operating	V	594.6	1870.5-1872	1871	74.9	DST nearby
05- 101		Ballantyne Oil	V	629	1993-1999	1996	76.7	DST this well
05- 102		Ballantyne Oil	V	637	2003-2025	2014	95.6	DST this well
05- 112		Citation Oil & Gas	V	615.5	2849-2860	2855	103.9	DST nearby
05- 114		Nance Petroleum	V	709	2879-2888	2884	99	DST this well
05- 116		Westport Oil & Gas	V	704.5	2972-2977	2975	104.8	DST nearby
05- 118		Citation Oil & Gas	V	692.5	2880-2889	2885	103	DST this well
05- 119		Citation Oil & Gas	V	592	2776-2780	2778	99.4	DST nearby
05- 128		Westport Oil & Gas	V	683	2947-2957	2952	105.1	DST nearby
05- 129		Nance Petroleum	V	577.3	2674-2845	2760	99.4	DST nearby
05- 133		Helis Oil	V	814.1	1714-1726	1720	74.5	DST nearby
05- 137		Helis Oil	V	827.5	1755-1779	1767	73.9	DST nearby
00- 181		Wascana Energy	V	536.7	1325-1331	1328	53.5	DST nearby
00- 182		Wascana Energy	V	542.2	1330-1336	1333	53.5	DST nearby
00- 183		Wascana Energy	V	541	1330-1333	1332	53.5	DST nearby

Appendix B. Open Hole Depth, Operator, Well Type, KB, Perf. Interval. Sample Point, Temp.

Sample ID	Open Hole Depth	Operator	Well Type	KB (m)	Perf. Interval (m)	Sample Point (m)	Temp. (^{0}C)	Temp Comment
00-184		Wascana Energy	V	556.6	1347-1353	1350	51.11	DST this well
00-169		Wascana Energy	V	600.9	1298-1303	1300	58.2	DST this well
00-170	1409-2040	Wascana Energy	H	600.6	1303-1305	1304	58.2	DST nearby
00-171	1440-1783	Wascana Energy	H	601.2	1300-1305	1302	58.2	DST nearby
00-172		Wascana Energy	V	599.7	1301-1306	1303	58	DST this well
00-173		Wascana Energy	V	602.1	1292-1299	1295	58.2	DST nearby
99-102		Wascana Energy	V	596.2	1251-1256	1253	47.6	DST nearby
99-104		Wascana Energy	V	597.1	1247-1253	1250	48.1	DST nearby
03-009	1323-1676	Anadarko	V		1369-1372	1360	47.4	DST nearby
03-011	1323-2044	Anadarko	V		1368-1370	1369	45.8	DST nearby
00-164		Wascana Energy	V	559.3	1185-1189	1187	46	DST nearby
00-161		Wascana Energy	V	570	1131-1137	1135	46	DST nearby
03-129		Nexen	V	557.3	1152-1161	1156	45.8	DST nearby
03-130		Nexen	V	555.4	1144-1148	1145	45.7	DST nearby
03-145		Nexen	V	557.1	1152-1159	1156	46.6	DST nearby
03-146		Nexen	V	556.5	1142-1147	1145	46	DST nearby
03-224		NorthRock	V	736	1892-1905	1897	41	DST this well
03-225	1303-1319	NorthRock	H	520.3	1303-1319	1311	64.4	DST nearby
03-226	1436-2389	NorthRock	H	537.6	1335-1349	1342	45.8	DST nearby
03-227	1480-2020	NorthRock	H	515.2	1295-1310.5	1303	51	DST nearby
03-237	5705-11139	Nance Petroleum	H	589.5	1660-1670	1665	65.4	DST nearby
03-247		Condor Petroleum	V	720.8	2451.5-2484.5	2467	83.4	DST nearby
03-248		Condor Petroleum	V	727.5	2449-2479.5	2464	89.4	DST nearby
03-256		Eagle Operating	V	596.5	1738-1761	1750	71	DST this well
03-259		Eagle Operating	V	593	1762-1767	1765	73.4	DST nearby
04-103	1470-2331	NorthRock	H	557.8	1363-1383	1373	52.4	DST nearby
04-104	1506-2228	NorthRock	H	552.7	1301-1391	1346	49.1	DST nearby
05-106		Headington Oil	V	676	2845-2866	2856	104	DST this well
05-109		Nance Petroleum	V	583	2723-2741	2732	95.1	DST nearby
05-111		Citation Oil & Gas	V	642	2802-2817	2809	98.4	DST nearby
05-121		Armstrong Operating	V	696.5	2443-2445	2444	96	DST this well
05-122		Marsha Azar Oil	V	707	2345-2353	2349	89	DST this well
05-123		Nance Petroleum	V	703.5	2342-2348	2345	88	DST nearby
05-127		Nance Petroleum	V	577.3	2741-2774	2758	101.4	DST nearby
05-130		Nance Petroleum	V	576.7	2684-2695	2690	100.7	DST nearby
05-131		Helis Oil	V	790.6	1640-1649	1644	65.4	DST nearby
05-135		Helis Oil	V	784.3	1959-1973	1966	70.2	DST nearby
05-136		Helis Oil	V	871.7	1759-1768	1764	67.4	DST nearby

Appendix C. Minor Elements

Sample ID	Al	Sb	As	Ba	Be	Bi	Cd	Cr	Co	Cu	I	Fe	Pb	Li	pH	Temp	Density
03- 201	<1	<0.04	0.11	<0.2	<0.02	<0.1	<0.002	<0.1	<0.1	<0.02	n.d.	<0.2	<0.02	46.9	n.d.	n.d.	n.d.
03- 203	<1	<0.04	0.25	<0.2	<0.02	<0.1	<0.002	<0.1	0.1	<0.02	n.d.	<0.2	<0.02	40.7	n.d.	n.d.	n.d.
03- 206	<1	<0.04	0.065	<0.2	<0.02	<0.1	<0.002	<0.1	<0.1	<0.02	4.9	3.6	<0.02	6.11	7.41	28.7	1.0720
03- 207	<1	<0.04	0.11	<0.2	<0.02	<0.1	<0.002	0.11	<0.1	<0.02	n.d.	<0.2	<0.02	46.2	6.47	33.7	1.1910
03- 208	<1	<0.04	0.11	<0.2	<0.02	<0.1	<0.002	<0.1	0.11	<0.02	n.d.	<0.2	<0.02	211	n.d.	n.d.	n.d.
03- 209	<1	<0.04	0.13	<0.2	<0.02	<0.1	<0.002	0.11	0.11	<0.02	48.7	<0.2	<0.02	44.1	6.21	35.2	1.1855
03- 210	<1	<0.04	0.11	0.23	<0.02	<0.1	<0.002	<0.1	0.11	<0.02	n.d.	<0.2	<0.02	305	n.d.	n.d.	n.d.
03- 211	<1	<0.04	<0.04	<0.2	<0.02	<0.1	<0.002	<0.1	0.11	<0.02	n.d.	<0.2	<0.02	7.29	n.d.	n.d.	n.d.
03- 213	<1	<0.04	0.1	<0.2	<0.02	<0.1	<0.002	<0.1	0.11	<0.02	22.7	7.2	<0.02	31.4	5.87	28.5	1.1750
03- 216	<1	<0.04	0.11	<0.2	<0.02	<0.1	<0.002	<0.1	0.11	<0.02	22.8	<0.2	<0.02	29.3	n.d.	n.d.	n.d.
03- 217	<1	<0.04	0.15	0.33	<0.02	<0.1	<0.002	0.15	0.11	<0.02	n.d.	<0.2	<0.02	19.8	7.05	26.1	1.1965
03- 218	<1	<0.04	0.26	<0.2	<0.02	<0.1	<0.002	<0.1	0.11	1.6	n.d.	<0.2	<0.02	32	6.81	27.9	1.1865
03- 219	<1	<0.04	0.39	<0.2	<0.02	<0.1	<0.002	<0.1	0.11	<0.2	n.d.	<0.2	<0.02	29	6.76	30.9	1.1855
03- 220	<1	<0.04	0.418	<0.2	<0.02	<0.1	<0.002	<0.1	0.11	<0.2	n.d.	<0.2	<0.02	25	6.56	32.1	1.1855
03- 221	<1	<0.04	0.4	<0.2	<0.02	<0.1	<0.002	<0.1	0.11	<0.2	23.7	<0.2	<0.02	28.2	6.64	36.3	1.1835
03- 222	<1	<0.04	0.38	<0.2	<0.02	<0.1	<0.002	<0.1	0.11	<0.2	n.d.	<0.2	<0.02	36.1	n.d.	n.d.	n.d.
03- 230	<1	<0.04	0.28	0.25	<0.02	<0.1	<0.002	<0.1	0.11	<0.2	n.d.	<0.2	<0.02	63.2	6.38	30.3	1.2005
03- 231	<1	<0.04	0.21	<0.2	<0.02	<0.1	<0.002	<0.1	0.11	<0.2	n.d.	<0.2	<0.02	104	6.72	30.4	1.1445
03- 232	<1	<0.04	0.3	0.26	<0.02	<0.1	<0.002	<0.1	0.11	<0.2	n.d.	<0.2	<0.02	59.4	6.43	32.3	1.1770
03- 234	<1	<0.04	0.053	0.38	<0.02	<0.1	<0.002	<0.1	0.11	<0.2	57.0	<0.2	<0.02	46.7	6.28	37.5	1.1600
03- 235	<1	0.077	0.13	0.46	<0.02	<0.1	<0.002	<0.1	0.11	<0.2	54.2	<0.2	<0.02	56.1	6.15	36.9	1.1935
03- 238	<1	<0.04	0.2	<0.2	<0.02	<0.1	<0.002	<0.1	0.11	<0.2	n.d.	<0.2	<0.02	21.6	6.87	31.8	1.1995
03- 241	<1	<0.04	0.22	<0.2	<0.02	<0.1	<0.002	<0.1	0.11	<0.2	n.d.	<0.2	<0.02	53.9	6.74	35.5	1.2010
03- 242	<1	<0.04	0.2	<0.2	<0.02	<0.1	<0.002	<0.1	0.11	<0.2	n.d.	<0.2	<0.02	27.5	6.25	35.9	1.1980
03- 243	<1	<0.04	0.2	<0.2	<0.02	<0.1	<0.002	<0.1	0.11	<0.2	18.8	<0.2	<0.02	43.4	6.19	35.9	1.1955
03- 244	<1	<0.04	0.17	0.32	<0.02	<0.1	<0.002	<0.1	0.11	<0.2	60.9	<0.2	<0.02	47.6	6.13	40.1	1.1970
03- 245	<1	<0.04	<0.040	0.53	<0.02	<0.1	<0.002	<0.1	0.11	<0.2	n.d.	<0.2	<0.02	21.1	n.d.	n.d.	n.d.
03- 246	<1	<0.04	0.2	0.9	<0.02	<0.1	<0.002	<0.1	0.11	<0.2	67.8	<0.2	<0.02	42.3	6.06	33.5	1.1915
03- 249	<1	<0.04	<0.040	<0.2	<0.02	<0.1	<0.002	<0.1	0.11	<0.2	n.d.	<0.2	<0.02	33.7	n.d.	n.d.	n.d.
03- 250	<1	<0.04	<0.040	1.6	<0.02	<0.1	<0.002	<0.1	0.11	<0.2	n.d.	<0.2	<0.02	61.1	6.19	34.3	1.2005
03- 251	<1	<0.04	<0.04	1.8	<0.02	<0.1	<0.002	<0.1	0.11	<0.2	n.d.	<0.2	<0.02	52.7	6.12	32.9	1.1970
03- 253	<1	<0.04	0.048	<0.2	<0.02	<0.1	<0.002	<0.1	0.11	<0.2	n.d.	<0.2	<0.02	10.9	7.51	35.7	1.1815
03- 258	<1	<0.04	0.065	0.65	<0.02	<0.1	<0.002	<0.1	0.11	<0.2	60.9	<0.2	<0.02	50.1	n.d.	n.d.	n.d.
04- 101	<1	<0.04	0.27	<0.2	<0.02	<0.02	<0.002	<0.1	0.11	<0.2	13.6	<0.2	<0.02	7.8	n.d.	n.d.	n.d.
04- 105	<1	<0.04	0.82	<0.2	<0.02	<0.02	<0.002	<0.1	0.11	<0.2	59.5	<0.2	<0.02	28.3	6.31	25	1.1900
04- 110	<1	<0.04	0.69	0.3	<0.02	<0.02	<0.002	<0.1	0.11	<0.2	27.8	<0.2	<0.02	22.7	6.6	25	n.d.
04- 114	n.d.	n.d.	n.d.	n.d.	n.d.	n.d.	n.d.	n.d.	0.11	n.d.	n.d.	n.d.	n.d.	n.d.	n.d.	n.d.	n.d.

Ti, Sn, U, V, Se, Ni, Ag, Mo, Th, Bi, Cd, Be, CO_3: all measured and below detection limit
05-122 Mn level 2.4 mg/L, all other samples below Mn detection limit
(mg/L) n.d. = not determined, Temp. during filtering.

05-124 Zn level 6 mg/L, 03-180 Zn level 0.39 mg/L, all other samples below Zn detection limit
03-235 Sb level 0.077 mg/L, all other samples below Sb detection limit

Appendix C. Minor Elements

Sample ID	Al	Sb	As	Ba	Be	Bi	Cd	Cr	Co	Cu	I	Fe	Pb	Li	pH	Temp	Density
04- 115	n.d.	n.d.	n.d.	n.d.	n.d.	n.d.	n.d.	n.d.	0.11	n.d.	23	n.d.	n.d.	n.d.	n.d.	n.d.	n.d.
04- 117	<1	<0.04	0.23	<0.2	<0.02	<0.02	<0.002	<0.1	0.11	<0.2	7.87	<0.2	<0.02	7.5	7.36	25	n.d.
04- 118	<1	<0.04	0.21	<0.2	<0.02	<0.02	<0.002	<0.1	0.11	<0.2	7.58	<0.2	<0.02	8.3	6.78	25	n.d.
05- 103	<2	<0.08	0.93	2	<0.04	<0.2	<0.004	<0.20	0.11	<0.4	86.8	<0.2	<0.02	49.9	n.d.	n.d.	n.d.
05- 104	<2	<0.08	1.1	1	<0.04	<0.2	<0.004	<0.20	0.11	<0.4	89.6	<0.2	<0.02	45.2	n.d.	n.d.	n.d.
05- 107	<2	<0.08	0.83	2	<0.04	<0.2	<0.004	<0.20	0.11	<0.4	67.7	<0.2	<0.02	54.5	n.d.	n.d.	n.d.
05- 110	<2	<0.08	0.98	3	<0.04	<0.2	<0.004	<0.20	0.11	<0.4	93.8	<0.2	<0.02	57	n.d.	n.d.	n.d.
05- 115	<2	<0.08	0.84	8.7	<0.04	<0.2	<0.004	<0.20	0.11	<0.4	59.3	<0.2	<0.02	60.7	n.d.	n.d.	n.d.
05- 117	<2	<0.08	1	3	<0.04	<0.2	<0.004	<0.20	0.11	<0.4	97.6	<0.2	<0.02	49	6.11	35.1	n.d.
05- 124	<2	<0.08	1.4	2	<0.04	<0.2	0.056	<0.20	0.11	<0.4	45.3	13	<0.02	40.4	n.d.	n.d.	n.d.
05- 138	<2	<0.08	0.2	<0.4	<0.04	<0.2	<0.004	<0.20	0.11	9.3	17.8	<0.2	<0.02	12	7.13	28.4	n.d.
05- 140	<2	<0.08	0.84	0.9	<0.04	<0.2	<0.004	<0.20	0.11	<0.4	60.6	<0.2	<0.02	69	6.36	28.5	n.d.
05- 144	n.d.	n.d.	n.d.	n.d.	n.d.	n.d.	n.d.	n.d.	0.11	n.d.	n.d.	n.d.	n.d.	n.d.	n.d.	n.d.	n.d.
03- 202	<1	<0.04	0.041	<0.2	<0.02	<0.1	<0.002	<0.1	0.11	<0.2	n.d.	<0.2	<0.02	10.4	7.23	27	1.0695
03- 204	<1	<0.04	<0.04	<0.2	<0.02	<0.1	0.002	<0.1	0.11	<0.2	13.5	<0.2	<0.02	17.4	7.15	31	1.0715
03- 205	<1	<0.04	<0.04	<0.2	<0.02	<0.1	<0.002	<0.1	0.11	<0.2	n.d.	<0.2	<0.02	19.3	7.32	29.7	1.0715
03- 212	<1	<0.04	<0.04	<0.2	<0.02	<0.1	<0.002	<0.1	0.11	<0.2	n.d.	<0.2	<0.02	5.77	7.29	28.4	1.0825
03- 215	<1	<0.04	0.14	<0.2	<0.02	<0.1	<0.002	<0.1	0.11	<0.2	n.d.	<0.2	<0.02	28.6	n.d.	n.d.	n.d.
03- 223	<1	<0.04	0.33	<0.2	<0.02	<0.1	<0.002	<0.1	0.11	<0.2	44.0	<0.2	<0.02	34	6.15	39.7	1.1735
03- 229	n.d	n.d.	n.d	n.d.	n.d	n.d.	n.d	n.d.	0.11	n.d.	12.7	n.d.	n.d	n.d.	n.d.	n.d.	n.d.
03- 239	<1	<0.04	0.2	<0.2	<0.02	<0.1	<0.002	<0.1	0.11	<0.2	n.d.	<0.2	<0.02	24.5	7.07	33	1.1975
03- 240	<1	<0.04	0.21	<0.2	<0.02	<0.1	<0.002	<0.1	0.11	<0.2	n.d.	<0.2	<0.02	17.9	6.78	34.9	1.1685
03- 252	<1	<0.04	<0.04	<0.2	<0.02	<0.1	<0.002	<0.1	0.11	<0.2	39.6	<0.2	<0.02	31.8	6.65	37.9	1.1590
03- 254	<1	<0.04	<0.04	<0.2	<0.02	<0.1	<0.002	<0.1	0.11	<0.2	n.d.	<0.2	<0.02	10.7	n.d.	n.d.	n.d.
03- 255	<1	<0.04	0.048	<0.2	<0.02	<0.1	<0.002	<0.1	0.11	<0.2	n.d.	<0.2	<0.02	49.6	6.22	37.2	1.1950
04- 109	<1	<0.04	0.76	<0.2	<0.02	<0.1	<0.002	<0.1	0.11	<0.2	44.3	<0.2	<0.02	60.1	6.07	25	1.2065
05- 101	<2	<0.08	0.77	<0.4	<0.04	<0.2	<0.20	<0.04	0.11	<0.4	39.6	<0.2	<0.02	45.9	n.d.	n.d.	n.d.
05- 102	<2	<0.08	0.69	<0.4	<0.04	<0.2	<0.004	<0.20	0.11	<0.4	40.7	<0.2	<0.02	44.5	n.d.	n.d.	n.d.
05- 112	<2	<0.08	0.96	3	<0.04	<0.2	<0.004	<0.20	0.11	<0.4	93.9	<0.2	<0.02	54.4	n.d.	n.d.	n.d.
05- 114	<2	<0.08	1	2	<0.04	<0.2	<0.004	<0.20	0.11	<0.4	97.3	<0.2	<0.02	50.6	6.52	32.7	n.d.
05- 116	<2	<0.08	0.96	4	<0.04	<0.2	<0.004	<0.20	0.11	<0.4	90.2	<0.2	<0.02	56.9	n.d.	n.d.	n.d.
05- 118	<2	<0.08	0.76	2	<0.04	<0.2	<0.004	<0.20	0.11	<0.4	56.4	<0.2	<0.02	53.9	n.d.	n.d.	n.d.
05- 119	<2	<0.08	0.68	1	<0.04	<0.2	<0.004	<0.20	0.11	<0.4	54.3	<0.2	<0.02	52.1	6.45	32.5	n.d.
05- 128	n.d	n.d.	n.d	n.d.	n.d	n.d.	n.d	n.d.	0.11	n.d.	89.5	n.d.	n.d	n.d.	n.d.	n.d.	n.d.
05- 129	n.d	n.d.	n.d	n.d.	n.d	n.d.	n.d	n.d.	0.11	n.d.	81.3	n.d.	n.d	n.d.	n.d.	n.d.	n.d.
05- 133	<2	<0.08	<0.08	<0.4	<0.04	<0.2	<0.004	<0.2	0.11	<0.4	15.4	2.6	<0.2	4	7.07	27.8	n.d.
05- 137	<2	<0.08	0.2	<0.4	<0.04	<0.2	<0.004	<0.20	0.11	<0.4	14.7	1.1	<0.2	12	7.12	27.8	n.d.
00- 181	1.2	<0.5	<1.0	0.03	<0.05	<0.7	<0.05	<0.08	0.11	<0.1	44.7	0.25	0.25	30.5	6.47	20.1	1.1815
00- 182	1.6	<0.5	<1.0	0.03	<0.05	<0.7	<0.05	<0.08	0.11	<0.1	45.5	<0.2	<0.2	30.3	6.48	20.7	1.1810
00- 183	1.5	<0.5	<1.0	0.04	<0.05	<0.7	<0.05	<0.08	0.11	<0.1	42.9	<0.2	<0.2	29.7	6.42	17.5	1.1805

Ti, Sn, U, V, Se, Ni, Ag, Mo, Th, Bi, Cd, Be, CO_3: all measured and below detection limit
05-122 Mn level 2.4 mg/L, all other samples below Mn detection limit
(mg/L) n.d. = not determined, Temp. during filtering.

05-124 Zn level 6 mg/L, 03-180 Zn level 0.39 mg/L, all other samples below Zn detection limit
03-235 Sb level 0.077 mg/L, all other samples below Sb detection limit

Appendix C. Minor Elements

Sample ID	Al	Sb	As	Ba	Be	Bi	Cd	Cr	Co	Cu	I	Fe	Pb	Li	pH	Temp	Density
00- 184	1.8	<0.5	<1.0	0.05	<0.05	<0.7	<0.05	<0.08	0.11	<0.1	45.6	5.43	<0.2	31.4	6.3	16.6	1.1830
00- 169	2	<0.5	<1.0	<0.02	<0.05	<0.7	<0.05	<0.08	0.11	<0.1	28.6	7.85	<0.2	29.9	6.63	22.6	1.1245
00- 170	1.8	<0.5	<1.0	<0.02	<0.05	<0.7	<0.05	<0.08	0.11	0.62	28.6	7.03	<0.2	29.2	6.61	20.6	1.1250
00- 171	1.9	<0.5	<1.0	0.02	<0.05	<0.7	<0.05	<0.08	0.11	<0.1	27.8	2.8	0.2	29.7	6.83	22.9	1.1250
00- 172	1.7	<0.5	<1.0	<0.02	<0.05	<0.7	<0.05	<0.08	0.11	<0.1	28.7	2.5	<0.2	30.3	6.48	22.2	1.1245
00- 173	2	<0.50	<1.0	0.02	<0.05	<0.7	<0.05	<0.08	0.11	<0.1	29.9	2.4	<0.2	29	6.52	21.3	1.1250
99- 102	6.8	<1	<2	0.05	<0.1	<2	<0.05	<0.1	0.11	0.25	<0.3	1.4	<0.5	17.5	6.82	27.8	1.0931
99- 104	5.8	<1	<2	0.13	<0.1	<2	<0.05	<0.1	0.11	0.38	<0.3	1.4	0.57	13.9	6.55	23.1	1.1062
03- 9	n.d.	n.d.	n.d.	n.d.	n.d.	n.d.	n.d.	n.d.	0.11	n.d.	n.d.	n.d.	n.d.	n.d.	n.d.	n.d.	n.d.
03- 11	n.d.	n.d.	n.d.	n.d.	n.d.	n.d.	n.d.	n.d.	0.11	n.d.	n.d.	n.d.	n.d.	n.d.	n.d.	n.d.	n.d.
00- 164	1.6	<0.5	<1.0	0.03	<0.05	<0.7	<0.05	<0.08	0.11	0.12	35.6	1.6	1.7	24.8	6.57	33.7	1.1535
00- 161	1.6	<0.5	<1.0	<0.02	<0.05	<0.7	<0.05	<0.08	0.11	<0.1	31.6	1.7	<0.2	19.8	6.59	31.8	1.1480
03- 129	<1	<0.04	0.599	<0.2	<0.02	<0.1	<0.05	0.13	0.11	<0.2	42.6	<0.2	<0.2	34	6.68	27.8	1.1562
03- 130	<1	<0.04	0.699	<0.2	<0.02	<0.1	<0.05	0.13	0.11	<0.2	43.2	<0.2	<0.2	40.4	6.29	25.5	1.1580
03- 145	<1	<0.04	0.599	<0.2	<0.02	<0.1	<0.05	0.12	0.11	<0.2	34.7	<0.2	<0.2	36.9	6.45	22.7	1.1605
03- 146	<1	<0.04	0.533	<0.2	<0.02	<0.1	<0.05	0.13	0.11	<0.2	32.2	<0.2	<0.2	31.9	6.51	25.4	1.1555
03- 224	<1	<0.04	0.18	<0.2	<0.02	<0.1	<0.002	<0.1	0.11	<0.2	n.d.	<2	<0.02	22.9	6.85	28.6	1.0850
03- 225	<1	<0.04	0.2	<0.2	<0.02	<0.1	<0.002	<0.1	0.11	<0.2	n.d	<2	<0.02	14.4	6.71	28.3	1.1105
03- 226	<1	<0.04	0.18	<0.2	<0.02	<0.1	<0.002	<0.1	0.11	<0.2	n.d	2.5	<0.02	17.6	6.8	28.5	1.1135
03- 227	<1	<0.04	0.16	<0.2	<0.02	<0.1	<0.002	<0.1	0.11	<0.2	n.d.	2.8	<0.02	13.9	n.d.	n.d.	n.d.
03- 237	<1	<0.04	0.17		<0.02	<0.1	<0.002	<0.1	0.11	<0.2	16.5	4.6	<0.02	19.2	6.53	29.2	1.2015
03- 247	<1	<0.04	0.21	1.5	<0.02	<0.1	<0.002	<0.1	0.11	<0.2	n.d.	<2	<0.02	48.5	6.16	27.8	1.2015
03- 248	<1	<0.04	<0.040	0.4	<0.02	<0.1	<0.002	<0.1	0.11	<0.2	61.2	<2	<0.02	52.3	6.08	29.4	1.2005
03- 256	<1	<0.04	0.061	0.49	<0.02	<0.1	<0.002	<0.1	0.11	<0.2	18.8	<2	<0.02	25.8	6.77	36.5	1.1790
03- 259	<1	<0.04	0.09	0.33	<0.02	<0.1	<0.002	<0.1	0.11	<0.2	n.d.	<2	<0.02	35.7	n.d.	n.d.	n.d.
04- 103	n.d	n.d.	n.d	n.d.	n.d	n.d.	n.d	n.d.	0.11	n.d.	n.d	n.d.	n.d	n.d.	n.d.	n.d.	n.d.
04- 104	<1	<0.04	0.25	0.3	<0.04	<0.2	<0.004	<0.20	0.11	<0.4	10.2	<2	<0.02	10	n.d.	n.d.	n.d.
05- 106	<2	<0.08	0.94	2	<0.04	<0.2	<0.004	<0.20	0.11	<0.4	75.9	10	<0.02	58	n.d.	n.d.	n.d.
05- 109	<2	<0.08	0.73	6.2	<0.04	<0.2	<0.004	<0.20	0.11	<0.4	63	<2	<0.02	59.6	6.07	25	1.2065
05- 111	<2	<0.08	0.85	1	<0.04	<0.2	0.005	<0.20	0.11	<0.4	75.6	34	<0.02	60.6	n.d.	n.d.	n.d.
05- 121	<2	<0.08	0.79	0.7	<0.04	<0.2	<0.004	<0.20	0.11	<0.4	59.9	<2	<0.02	68.6	n.d.	n.d.	n.d.
05- 122	<2	<0.08	0.72	1	<0.04	<0.2	<0.004	<0.20	0.11	<0.4	49.7	29	<0.02	78.2	n.d.	n.d.	n.d.
05- 123	<2	<0.08	0.85	1	<0.04	<0.2	<0.004	<0.20	0.11	<0.4	62.1	<2	<0.02	58.6	n.d.	n.d.	n.d.
05- 127	<2	<0.08	0.99	1	<0.04	<0.2	<0.004	<0.20	0.11	<0.4	108.3	<2	<0.02	63.6	6.13	38.2	n.d.
05- 130	n.d.	n.d.	n.d.	n.d.	n.d.	n.d.	n.d.	n.d.	0.11	n.d.	61.7	n.d.	n.d.	n.d.	n.d.	n.d.	n.d.
05- 131	<2	<0.08	0.3	<0.4	<0.04	<0.2	<0.004	<0.20	0.11	<0.4	24	<2	<0.02	9.6	6.96	28.8	n.d.
05- 135	<2	<0.08	0.3	<0.4	<0.04	<0.2	0.005	<0.20	0.11	1	30.6	<2	<0.02	25	7.06	26.3	n.d.
05- 136	<2	<0.08	0.1	<0.4	<0.04	<0.2	<0.004	<0.20	0.11	<0.4	12.8	<2	<0.02	8	7.58	27.3	n.d.

Ti, Sn, U, V, Se, Ni, Ag, Mo, Th, Bi, Cd, Be, CO_3: all measured and below detection limit
05-122 Mn level 2.4 mg/L, all other samples below Mn detection limit
(mg/L) n.d. = not determined, Temp. during filtering.

05-124 Zn level 6 mg/L, 03-180 Zn level 0.39 mg/L, all other samples below Zn detection limit
03-235 Sb level 0.077 mg/L, all other samples below Sb detection limit